University of South Africa

Second Symposium of the

Astronomical Society of Southern Africa (ASSA)

F6.2
BC 1506
ASTRONOMICAL
ASSOCIATION SA

Astronomical Society of Southern Africa

ASSA

Walter F Wargau
Barbara Cunow
Editors

SECOND SYMPOSIUM
OF THE
ASTRONOMICAL SOCIETY OF SOUTHERN AFRICA

Proceedings of a Symposium

held at the
University of South Africa
Muckleneukrand, Pretoria, South Africa
27-29 September 1993

Editors

Walter F. Wargau

Barbara Cunow

UNISA, Dept. of Mathematics, Applied Mathematics and Astronomy

Editorial Board

N.T. Bishop	(UNISA, Department of Mathematics, Applied Mathematics and Astronomy)
G. Nicolson	(Hartebeesthoek Radio Astronomy Observatory)
M.D. Overbeek	(Astronomical Society of Southern Africa)
B.C. Raubenheimer	(Potchefstroom University, Department of Physics)
R.S. Stobie	(South African Astronomical Observatory)
W.F. Wargau	(UNISA, Department of Mathematics, Applied Mathematics and Astronomy)

UNIVERSITY OF SOUTH AFRICA
1994

© 1994 University of South Africa
First edition, first impression

ISBN 0 86981 898 8

Printed and published by the
University of South Africa
P O Box 329
0001 Pretoria

CONTENTS

Group Photograph iv
Participants vi
Preface ix

Contributions

1. Quasi Steady State Cosmology - J V Narlikar 1
2. Magnitude Calibration for Statistical Measurements of Faint Galaxies - Barbara Cunow and W F Wargau 12
3. Amateur Seismography - M D Overbeek 25
4. Singularity Free Cosmology and the Chaotic Model - S Mukherjee and N Dadhich. 26
5. Visual Observations and Evolution of Meteor Streams - T Cooper 37
6. TeV Gamma-Ray Astronomy in South Africa - B C Raubenheimer 42
7. Gravitational Wave Calculations on Null Cones - N T Bishop 49
8. The Large Number Hypothesis Re-visited - A Beesham 55
9. Finding Density at Large Scales - P Haines 61
10. Nearby Large-scale Structures in the Universe - A P Fairall 71
11. Dynamical Symmetries in Relativistic Kinetic Theory - R Maartens and D R Taylor 78
12. Anisotropic Cosmology with Conformal Symmetry - R Maartens and C M Mellin 99
13. Radio Emission from Infrared Regions - D P Smits 104
14. The South African Large Telescope - R S Stobie 111
15. Metallicity in Globular Clusters - V Pieters and W F Wargau 119
16. The Solar Eclipse of June 1992 - what did we do? The Solar Eclipse of 1994 - what will we do? - J Knight 126

STERREWAG OBSERVATORY

GROUP PHOTOGRAPH

Participants in front of the Observatory of the University of South Africa in Pretoria

Back row from left to right:

1. M Hannibal
2. A Beesham
3. M Poll
4. J Wiesner
5. H Calitz
6. A S Hilton
7. M Leigh
8. M D Overbeek
9. J Smit
10. J de Villiers
11. P Haines
12. D P Smits
13. P de Weerdt
14. C Kauffmann
15. S Stanley-Adams
16. P Lourens
17. P v d Westhuizen
18. F le Roux
19. C C Smith
20. J da Silva

Middle row from left to right:

1. E Carey
2. T Viljoen
3. A Kemball
4. D Schmieder
5. V Pieters
6. M Gerner
7. U Huyssen
8. R Karberg
9. N Thomas
10. N Kriek
11. L Higgs
12. W P Uys
13. T Cooper
14. J E van Zyl
15. H Lund
16. G Jacobs
17. A Greyvensteyn
18. W Biemond
19. C L de Coning
20. M Bamping

Front row from left to right:

1. J Dean
2. L Fouche
3. A Snell
4. M Schoch
5. A P Fairall
6. J Bondietti
7. S Enke
8. N T Bishop
9. J V Narlikar
10. B Warner
11. W F Wargau
12. G Nicolson
13. R S Stobie
14. R Schneider
15. R Sarracino
16. S Mukherjee
17. P van Blommestein
18. K Wain
19. P Ntsoele

ASSA SYMPOSIUM PARTICIPANTS

Mr M Bamping	Box 32576, Braamfontein, 2017
Prof A Beesham	Dept Applied Maths, University of Zululand, P/Bag X1001, Kwa-Dlan Gezwa, 3886
Mr W Biemond	Box 815, Ellisras, 0555
Prof N T Bishop	Department of Mathematics, Unisa, Box 392, Pretoria, 0001
Mr J Bondietti	5 Bath St, Gardens, 8001
Mr H Calitz	Box 11233, Universitas, 9321
Rev E Carey	8 Edge Road, Beacon Bay, 5241
Mr L Collier	Box 289, Chrissiefontein, 1963
Mr T Cooper	56 Tenth Ave, Northmead, Benoni, 1501
Mr J da Silva	305 Kelvin Court, 625 Pretorius St, 0083
Dr J Dean	15 Craig Ave, Malanshof, Randburg
Miss M de Boom	11 Villa Marija, Marija St 173, 0182
Mr C L de Coning	Box 25933, Langenhoven Park, 9322
Mr J de Villiers	35 Galena Ave, Helderkruin, Roodepoort, 1725
Mr P de Weerdt	22 Matumie Ave, Weltevreden Park, 1709
Mr C Engelbrecht	Department of Physics, Unisa, Box 392, Pretoria, 0001
Mrs. S Enke	Box 5198, Windhoek, Namibia
Mrs L Fouche	24 Westfort Road, Northshore, Hout Bay, 7800
Mr A Greyvensteyn	Box 79403, Senderwood, 2145
Dr P Haines	Department of Mathematics, Applied Mathematics and Astronomy, Unisa, Box 392, Pretoria, 0001
Mr M Hannibal	Box 8777, Johannesburg, 2000
Mrs L Higgs	21 Helgaard St, Kilner Park, Pretoria, 0186
Mr A S Hilton	Box 68846, Bryanston, 2021
Mrs U Huyssen	417 Mackenzie St, Menlo Park, Pretoria, 0081
Mr G Jacobs	P/Bag X7, Parkview, 2122
Mrs R Karberg	Box 2016, Kuruman, 8460
Mr C Kauffmann	Abtsberg 12, D - 96049 Bamberg, Germany
Dr A Kemball	Box 443, Krugersdorp, 1740
Mr J Knight	17 Mars St, Atlasville, 1459
Dr N Kriek	Box 17, Britstown, 8970
Mr M Leigh	Box 218, WITS, 2050
Prof G Lemmer	Department of Mathematics, Applied Mathematics and Astronomy, Unisa, Box 392, Pretoria, 0001
Mr F le Roux	Box 25621, Monument Park, 0105
Dr P Lourens	185 Jonk Ave, Clubview East, Verwoerdburg
Mr H Lund	118 Seventeenth St, Parkhurst, 2193
Dr R Maartens	University of the Witwatersrand, 2050
Dr S Maharaj	Department of Mathematics, University Natal, Durban, 4001
Prof S Mukherjee	Dept Applied Maths, University of Zululand, P/Bag X1001, Kwa-Dlan Gezwa, 3886
Prof J V Narlikar	IUCAA, P/B4, Ganeshkhind, Pune 411007, India
Dr G Nicolson	Box 443, Krugersdorp, 1740
Mr P Ntsoele	S1130 Dubula St, P.O. Sharpeville, 1933
Mr M D Overbeek	Box 212, Edenvale, 1610
Mr M Poll	Box 125, Medunsa, 0204

Prof C Raubenheimer	Space Research Unit, Potchefstroom University, 2520
Dr R Sarracino	Box 262, Kelvin, 2054
Dr D Schmieder	AEROTEK, CSIR, Box 395, Pretoria, 0001
Mr R Schneider	Computer Services, Unisa, Box 392, Pretoria, 0001
Mrs M Schoch	Education Centre, 31 Deale Rd, Bloemfontein
Dr J Smit	1183 Dickenson Ave, Waverley, 0186
Mr C C Smith	Box 6178, Ansfrere, 1711
Mr A Snell	Box 70225, Wilgers, Pretoria, 0041
Mr S Stanley-Adams	Box 820, Olivedale, 2158
Dr R S Stobie	SAAO, Box 9, Observatory 7935, Cape
Mr D R Taylor	Dept Comp & Appl Maths, University of the Witwatersrand, 2050
Mr N Thomas	32 Lilaron Flats, 684 Pretorius St, Pretoria
Mr W P Uys	Box 1286, Faerie Glen, 0043
Mr P van Blommestein	4 Belmont Road, Simon's Town, 7995
Mr P van der Westhuizen	Box 252, Pinetown, 3600
Mr J E van Zyl	51 16th St, Welverdiend, 2700
Mrs K Wain	Box 73579, Fairland, 2030
Prof W F Wargau	Department of Mathematics, Applied Mathematics and Astronomy, Unisa, Box 392, Pretoria, 0001
Mr J Wiesner	110 Umtata Ave, Doringkloof, Verwoerdburg

Preface

The Astronomical Society of Southern Africa has a longstanding tradition of promoting Astronomy in Southern Africa by bringing together professionals and amateurs. The Society was formed in 1922 by the amalgamation of the Cape Astronomical Association, which was founded in 1912, and the Johannesburg Astronomical Association, which was founded in 1918. Membership of the Society is open to all interested persons, regardless of knowledge or experience. The Society publishes its own journal, the *Monthly Notes of the Astronomical Society of Southern Africa (MNASSA)* on a bi-monthly basis and an annual *Handbook*. Members also receive *Sky and Telescope*, the leading popular astronomy magazine published in the USA.

Autonomous local Centres of the Society exist at Bloemfontein, Cape Town, Durban, Harare, Johannesburg, Pietermaritzburg, Pretoria and Somerset West.

On the initiative of Jose Campos, former President of ASSA, the first ASSA Symposium was held at the South African Museum in Cape Town in April 1992. Due to its great success and the unprecedented response received from all over the country, the Council of ASSA decided to make this a regular event. Although it is intended to be a bi-annual occurrence, Council decided to hold this second Symposium in 1993 already. Henceforth symposia will be organized every second year.

In the past Pretoria played a major role in professional optical astronomy in South Africa. That is, until the seventies, when the Radcliffe Observatory's 1,9m reflecting telescope was moved to the South African Astronomical Observatory at Sutherland. In amateur astronomy circles, Pretoria was also well known as the home of the famous comet hunter and supernova discoverer, Jack Caister Benett.

The Transvaal is also home to a number of excellent amateur astronomers who are internationally acknowledged for their valuable contribution to astronomy: Danie Overbeek, director of the national Occultation Section and a foremost star observer; Tim Cooper, director of the Comet and Meteor Section, and Jim Knight, director of the Solar Section, to mention but a few.

Delegates had the opportunity to visit the newly erected Unisa Observatory on campus. It houses a 35cm computer-controlled reflecting telescope, backed up by sophisticated electronics and systems for photometry, spectroscopy, photography, micrometry and solar observation.

A visit to the Radio Astronomy Observatory at Hartebeesthoek was organized. The delegates had the opportunity to see the facilities, and a one- hour lecture on the history of Radio Astronomy in South Africa was presented. The tour was rounded off by a braai. The trip was thoroughly enjoyed by all the delegates. Our special thanks go to George Nicolson, director of HartRAO, Derck Smits and Claire Flanagan.

The talks delivered at the Symposium covered a wide range of topics, from the Sun and the solar system to the Galaxy and beyond, even to the latest theories in cosmology. As a special guest from India we were privileged to have world-famous cosmologist Professor Jayant V Narlikar amongst us.

As fas as observational techniques are concerned, we heard from speakers working in various regions of the electromagnetic regime, all the way from gamma ray to the radio regime.

I should like to express my gratitude to members of the Department of Mathematics, Applied Mathematics an Astronomy and other staff of the University, who provided help in so many ways. To mention just a few: Nigel T Bishop, Paul Haines and Rudi Schneider. And Willie de Beer who did the Symposium photograph for us.

My special thanks go to Marlene Gerner. Without her organising talent, the Symposium could not have been such a success. And to Barbara Cunow, who finally managed to get these Proceedings to the publisher.

I thank the Council of ASSA for their vote of confidence in allowing us in Pretoria to host this Symposium.

I thank the University of South Africa for its generous financial support in preparing the Symposium, for publishing the proceedings and making the Senate Hall and lecture facilities available to us.

And I would like to thank all the speakers and other participants who helped to make the conference a really successful and enjoyable event. I am particularly pleased that we have received manuscripts for most of the presentations.

I conclude by expressing the hope that there may be many such Symposia to come.

Walter F Wargau
President of ASSA

Quasi Steady State Cosmology

Jayant V Narlikar
Inter-University Centre for Astronomy and Astrophysics
Post Bag 4, Ganeshkhind, Pune 411007, India

Abstract

Because of a number of unsatisfactory features of the standard hot big bang cosmology, it is argued that there is a case for exploring alternative approaches to cosmology. The approach described here attempts to relate the large scale features of the universe to the basic phenomenon of creation of matter.

This theory, called the quasi steady state cosmology (QSSC), begins with a field theoretic description of matter creation within the framework of general relativity. A scalar field C of zero restmass but negative energy and stresses interacts with matter at the instants of creation thereby preserving the law of conservation of the universe expanding at an overall exponential rate along with cycles of expansion and contraction with shorter time scales.

It is argued that such a solution arises from mini-creation events taking place near the event horizons of highly collapsed massive objects. The now familiar phenomena like QSOs, AGN, radio sources, etc. are the manifestations of matter creation in such events. These events are cophased and the oscillations occur because of feedback between the creation process and the expansion of space. In this way the cosmology is seen to be related to high energy astrophysics in a very direct way.

The QSSC can explain the abundances of light nuclei and the microwave background, the observed large scale features of the universe like the $m-z$ relation, the source count, the angular size-redshift relation, as well as the observed distribution of the ages of galaxies. This work gives a brief review of these properties of the quasi steady state cosmology.

1 Introduction

The standard big bang cosmology has the universe created out of a primeval explosion that not only created matter and radiation but also spacetime itself. The big bang event itself cannot be discussed within the framework of a physical theory but the events following it are in principle considered within the scope of science. The recent developments on the frontier between particle physics and cosmology highlight the attemps to chart the history of the very early universe.

Exciting though these studies are, they have failed to resolve some of the basic issues of cosmology. These issues can be stated briefly as follows:

1. The microwave background radiation (MBR) is considered a fundamental proof of the big bang cosmology. Yet, cosmological considerations so far have failed to deduce its present temperature of *2,73*K.

2. While the Planckian spectrum of the MBR is deduced from its relic interpretation, its small scale anisotropy has not been successfully related to the observed large scale inhomogeneity of matter distribution in the universe, the recent findings of the satellite COBE notwithstanding.

3. There is no consistent theory of structure formation that takes in a reasonable hypothesis of dark matter and can reproduce the observed large scale structure and motions from primordial seed fluctuations.

4. The claims of explaining the large scale features of the universe in terms of discrete source populations inevitably require epicyclic hypotheses of evolution of physical properties of these sources that are post-facto rather than having any predictive power.

5. The age distribution of galaxies poses many problems for the canonical big bang model. How to accommodate globular clusters of ages *15-18 Gyrs* in a big bang universe with $k = 0$, that is required by inflations in the very early phase? Equally difficult it is to understand the existence of very young galaxies at the present epoch, for, galaxy formation is supposed to have taken place in the early universe.

6. The phenomena in high energy astrophysics like the QSOs, AGN, radio sources, etc. show big outpourings of matter and energy from compact regions. However these events have no relation to the primordial big bang which is totally isolated from this relatively recent activity.

7. Finally, on a theoretical issue the big bang itself is an inconsistency. Its existence is deduced from the equations of general relativity which are derived from an action principle. Yet, the big bang itself is seen as a spacetime singularity arising from these very equations and at the singularity the action principle breaks down. Thus the cycle of reasoning is self-contradictory and the question of the origin of matter remains not only unsolved but is declared unsolvable.

For details of these points see earlier work of Arp et al (1990) and Hoyle et al (1993). At a nontechnical level I have discussed these ideas in the New Scientist (Narlikar 1991, 1993). My main purpose here is to argue that despite the popularity enjoyed by the big bang cosmology today, the above list is sufficient to motivate an alternative approach to cosmology.

Any alternative to big bang cosmology should fulfill a few minimum conditions. First it must do at least as well as the big bang cosmology in explaining the MBR and light nuclear abundances and in describing the observed features of discrete source surveys. Next it must try to do better than the big bang model on some of the abovementioned fronts. Finally, as a scientific theory it must make a few disprovable predictions that distinguish it from the standard model.

In the remaining part of this work I will describe a model that claims to do just that. This is the quasi steady state cosmology (QSSC) proposed by Fred Hoyle, Geoffrey Burbidge and myself. The first paper in the series on this topic is referred to above (viz. Hoyle et al 1993) while others are in various stages towards publication. Further details of the present concise account may be found there.

2 Creation of matter

In 1948 Bondi and Gold (1948) and Hoyle (1948) had independently proposed the steady state theory as an alternative to the big bang cosmology. Bondi and Gold had adopted the Perfect Cosmological Principle as the starting point of their approach while Hoyle had taken the phenomenon of matter creation as the main motivation. Here we will follow the second approach but with some significant modification.

As mentioned in Point 7 against the big bang, a scientific theory of cosmology should provide a consistent description of matter creation; eg., a theory in which the phenomenon is described within the action principle formulation which has proved so universally useful in theoretical physics. Point 6 further provides a clue that the creation should occur in small bursts rather than in one big bang. The steady state theory on the other hand met these objections only half way. While it did provide a field theory for matter creation, it assumed that creation takes place in a homogeneous and isotropic way. The resulting steady state model was too simple and constrained to explain the variety of cosmological observations and was thus disproved.

The QSSC, however, introduces an important modification of the above simple steady state concept by arguing that creation takes place only in the vicinity of collapsed massive objects. The feedback of creation on the geometry of spacetime then determines the expansion of the universe which is no longer the de Sitter expansion of the old steady state model. To see this we look at the field equations that govern the large scale structure of the universe.

The field equations are derived from an action principle. Although Hoyle et al (op. cit.) considered a direct particle interaction approach motivated by Mach's Principle, the following simplified derivation essentially reproduces their equations in the more familiar field theory format. Thus the classical Hilbert action leading to the Einstein equations is modified by the inclusion of a scalar field C whose derivatives with respect to the spacetime coordinates x^i are denoted by C_i. The notation followed here is that of my textbook on cosmology (Narlikar 1993) where further details may be found. The action is given by

$$\mathcal{A} = \sum_a \int_{\Gamma a} m_a c ds_a + \int_v \frac{c^3}{16\pi G} R\sqrt{-g} d^4x - \frac{1}{2c} f \int_v C_i C^i \sqrt{-g} d^4x + \sum_a \int_{\Gamma a} C_i da^i \qquad (1)$$

where C is a scalar field and $C_i = \partial C/\partial x^i$. f is a coupling constant. The last term of (1) is manifestly path-independent and so, at first sight it appears to contribute no new physics. The first impression, however, turns out to be false if we admit the existence of broken worldlines.

Thus, if the worldline of particle a begins at point A, then the variation of A with respect to that worldline gives

$$m_a \frac{da^i}{ds_a} = g^{ik} C_k \tag{2}$$

at A. In other words, the C-field balances the energy-momentim of the created particle. The field equations likewise get modified to

$$R_{ik} - \frac{1}{2} g_{ik} R = -\frac{8\pi G}{c^4} \left[\underset{m}{T_{ik}} + \underset{c}{T_{ik}} \right] \tag{3}$$

where

$$\underset{c}{T_{ik}} = -f \left\{ C_i C_k - \frac{1}{2} g_{ik} C^l C_l \right\}. \tag{4}$$

Thus the energy conservation law is

$$\underset{m}{T_{ik}}{}_{;k} = - \underset{c}{T_{ik}}{}_{;k} = f C^i C^i_{;k}. \tag{5}$$

That is, matter creation via a nonzero left hand side of (5) is possible while conserving the overall energy and momentum.

The C-field tensor has negative stresses which lead to the expansion of spacetime, as in the case of inflation. The formalism described here is essentially that used by Hoyle and Narlikar (1962, 1966 a,b) in the 1960s to produce inflation type solution (which, of course predated Guth's inflationary cosmology by 15 years!).

From (2) we therefore get a necessary condition for creation as

$$C_i C^i = m_a^2 c^4; \tag{6}$$

This is the "creation threshold" which must be crossed for particle creation. How this can happen near a massive object, can be seen from the following simple example.

The Schwarzschild solution for a massive object M of radius $R > 2GM/c^2$ is

$$ds^2 = c^2 dt^2 \left(1 - \frac{2GM}{c^2 r}\right) - \frac{dr^2}{1 - \frac{2GM}{c^2 r}} - r^2 \left(d\theta^2 + \sin^2\theta d\phi^2\right), \tag{7}$$

for $r \geq R$. Now if the C-field does not seriously change the geometry, we would have at $r \gg R$,

$$\dot{C} \approx \alpha, C' \equiv \frac{\partial C}{\partial r} \cong 0. \tag{8}$$

If we continue this solution closer to $r \approx R$, we find that

$$C^i C_i \equiv \left(1 - \frac{2GM}{c^2 r}\right)^{-1} \frac{\alpha^2}{c^2}. \tag{9}$$

In other words $C_i C^i$ increases towards the object and can become arbitrarily large if $r \approx 2GM/c^2$. So it is possible for the creation threshold to be reached *near* a massive

collapsed object even if it C_iC^i is *below* the threshold far away from the object. In this way massive collapsed objects can provide new sites for matter creation. Thus, instead of a single big bang event of creation, we have mini-creation events (MCEs) near collapsed massive objects.

3 A Cosmological Solution

Since the C-field is a global cosmological field, we expect the creation phenomenon to be globally cophased. Thus, there will be phases when the creation activity is large, leading to the generation of the C-field strength in large quantities. However, the C-field growth because of its large negative stresses leads to a rapid expansion of the universe and a consequent drop in its background strength. When that happens creation is reduced and takes place only near the most collapsed massive objects thus leading to a drop in the intensity of the C-field. The reduction in C-field slows down the expansion, even leading to local contraction and so to a build-up of the C-field strength. And so on!

We can describe this up and down type of activity as an oscillatory solution superposed on a steadily expanding de Sitter type solution of the field equations as follows. For the Robertson-Walker line element the equations (3)-(5) give

$$3\frac{S^2+kc^2}{S^2} = 8\pi G\left(\rho - \frac{1}{2}f\dot{C}^2\right), \tag{10}$$

$$2\frac{\ddot{S}^2}{S} + \frac{\dot{S}^2kc^2}{S^2} = 4\pi Gf\dot{C}^2, \tag{11}$$

where $S(t)$ is the scale factor and k the curvature parameter (=0,±1). The cosmic time is given by t. These equations have a de Sitter type solution given by

$$S \propto \exp(t/P), k = 0, \dot{C} = \text{constant}, \rho = \text{constant}$$

The oscillatory solution is given by

$$k = +1, \dot{C} \propto 1/S^3, \rho \propto 1/S^3. \tag{12}$$

Thus (10) becomes, in the latter case

$$\dot{S}^2 = -c^2 + \frac{A}{S} - \frac{B}{S^4}, A, B = \text{constant}. \tag{13}$$

Here the oscillatory cycle will typically have a period $Q \ll P$.

Although the exact solution of (14) will be difficult to obtain, we can use the following approximate solution of (13) and (14) to describe the short-term and long-term cosmological behaviour:

$$S(t) = \exp\left(\frac{t}{P}\right)\left\{1 + \alpha\cos\frac{2\pi t}{Q}\right\}. \tag{14}$$

Note that the universe has a long term secular expanding trend, but because $|\alpha| < 1$, it also executes non-singular oscillations around it. We can determine α and our present

epoch $t = t_0$ by the observations of the present state of the universe. Thus an acceptable set of parameters is

$$\alpha = 0.75, t = 0.85Q, Q = 4 \times 10^{10}\,\text{yr.}, P = 20Q. \tag{15}$$

Although the set is not unique and there will be a *range* of acceptable values, we will work with this set to illustrate the performance of the model.

4 The Origin of Nuclei and the Microwave Background

We have as yet not said what particle is being created by the C-field. The answer is, the Planck particle whose mass is

$$m_P = \sqrt{\frac{3h}{4\pi G}} \sim 10^{-5} g \tag{16}$$

This particle, however, has a very short lifetime

$$\tau_P \sim \sqrt{\frac{Gh}{c^5}} \sim 5 \times 10^{-44} s. \tag{17}$$

It decays ultimately into the baryon octet and radiation. Most members of the octet except n and p are also short-lived and decay into protons. Only the neutron and the proton live long enough to combine into helium nuclei. Thus approximately 25% by mass (2 out of 8 baryons) combine to form helium.

A more careful calculation gives the helium mass fraction to be around 23%, with a tiny fraction of 1-2% in the form of metals. This type of nucleosynthesis also generates ^{2}H, ^{3}H, ^{3}He, ^{6}Li, ^{7}Li, ^{9}Be, ^{10}B etc. in small amounts that are in agreement with the observations. In fact, the light nuclear abundances in this cosmology lead to a better agreement with observations than in the big bang model.

There is one further important consequence. In the big bang model the required production of deuterium imposes a stringent upper limit on the present day baryon density. This limit forces us to assume that the dark matter component of the universe must be largely nonbaryonic. In the QSSC, there is no such density limit from deuterium abundance and thus the dark matter component *can be baryonic.* We will discuss this point further in the following section.

What about the microwave background? The QSSC obtains it in the following way. First, each Planck particle decay is like a fireball: it produces a lot of energy, including baryons ($\sim 10^{19}$ per Planck particle) and radiation. More than the hot big bang, the Planck fireball can provide several interesting and realistic studies in astroparticle physics. Further, since the Planck fireballs are repeated phenomena, rather than the "once only" type situation of the hot big bang cosmology, they are amenable to a more exhaustive scientific study.

Bulk of the fireball energy goes into expansion. However, some radiation remains as relic of the fireball. Toghether with the starlight generated in the preceding oscillatory

cycles this energy is to be thermalized to provide the microwave background. Does it provide enough radiant energy to give a 2.7 K background? Is the background thoroughly thermalized to produce a black body spectrum? Also, is it homogeneous to the extent given by COBE (Smoot, et al 1992) and other measurements?

The answer to all these questions is in the affirmative as we shall now demonstrate.

Let us consider the present day energy density of intergalactic starlight which comes largely from old star populations. Taking into consideration the usual estimates of 10^{-14} erg cm^{-3} for starlight in the visible spectral region, we get the total (in all wavelengths) starlight energy density as $\sim 2\times 10^{14}$erg cm^{-3}. Using (16) we estimate the average starlight production rate per unit volume per unit time as

$$\epsilon = 1.14 \times 10^{-13}\,\mathrm{erg\,cm^{-3}Q^{-1}}. \tag{18}$$

Thus the total amount of starlight produces from the previous oscillatory minimum at $t = -0.5Q$ to $t = 0.5Q$ (the last minimum) is

$$\epsilon \int_{-0.5Q}^{0.5Q} \frac{dt}{1+z} \approx 4.56 \times 10^{-13}\,\mathrm{erg\,cm^{-3}}. \tag{19}$$

Now the weakening [due to the expansion factor (exp t/P) in each cycle] of energy density $W_{\min}$ at the oscillatory minimum is $4Q/P \times W_{\min}$. This must be replenished by fresh thermalization of starlight produced. Thus in the steady state we get for $P = 20Q$,

$$W_{\min} = 1.14 \times 10^{-13} \times \frac{P}{Q} = 2.28 \times 10^{-12}\,\mathrm{erg\,cm^{-3}}. \tag{20}$$

This is with respect to coordinate volume. To convert it to proper volume we need to introduce the redshift effect from $t = 0.5Q$ to $t = t_0$, which is a factor 0.1734. Thus the present energy density is

$$W_{\mathrm{present}} = W_{\min} \times 0.1734 \approx 3.96 \times 10^{-13}\,\mathrm{erg\,cm^{-3}} \tag{21}$$

which corresponds to a black body temperature of 2.68 K - very close to that observed!

Thus quantity-wise the starlight from several past generations of stars is sufficient to maintain a steady background of radiation, provided, some agency is available to thermalize it. The agency proposed is dust in the form of metallic needles, mostly of iron which absorb the ambient radiation and reradiate it in the microwaves. Provided this has gone on long enough, the radiation spectrum will approach the black body form. Calculation shows that indeed the thermalization has occurred through as many as 10^3 absorptions and remissions by iron whiskers - sufficient to ensure an extremely close approximation to the black body curve. The iron whiskers are typically $\sim$1 mm in length and 10^{-6} cm in radius of cross section. The iron itself is produced partly from stellar nucleosynthesis in supernovae. The required density in the form of such whiskers is only $\sim 10^{-35}$g cm^{-3}: well within the observed cosmic abundances of iron.

The background produced will be very smooth with a patchiness of density of the order of 10^{-5}. Fluctuations of density and temperature of this or larger order get smoothed out by redistribution of iron grains by the radiation pressure. On smaller scales the dynamical

This test has not, however, yielded any clearcut answer. There are several observational uncertainties. For example, there is no standard class of sources with a fixed yardstick for linear size. Recent work by Kapahi (1987) suggests that the median angular size falls off as $1/z$ rather than as required by the Friedmann cosmologies. Kellermann (1993) has applied this test to extremely compact radio sources and he reports an upturn in the angular size beyond $z > 1$ or so which he interpretes as being compatible with the standard cosmology with $k = 0$.

A detailed working out of Hoyle's formula for the QSSC shows it also to be compatible with Kellermann's findings. For the larger sources considered by Kapahi and others the linear size would be expected to be more and more compressed as we go more and more towards the oscillatory minimum. Calculations by Hoyle et al (1993: preprint) show that this leads to a fall off not very different from the $1/z$ law found by Kapahi.

6 The MCEs and Astrophysics

The minicreation events (MCEs) have several points of contact with astrophysics. I will briefly enumerate a few:

(i) Gravity wave sources: The explosive creation near compact massive objects makes them potential sources of gravity waves, provided the events are sufficiently anisotropic. Narlikar and Das Gupta (1993) have shown that such events in the mass range of 100-1000 $M_\odot$ can be detected by the laser interferometric detectors being planned worldwide. Further, the gravity wave background created by such MCEs can also significantly affect the timing mechanism of millisecond pulsars.

(ii) High energy sources: The explosive nature of energy generation in QSOs and AGN as well as in the gamma ray burst sources makes the MCSs ideal candidates for these energy sources. This is in keeping with Ambartsumian's conjecture (1988, 1965) that the AGN are likely sites for matter creation in explosive form.

(iii) The age of the universe: According to QSSC the universe is infinitely old but the average age of astronomical objects is $1/3P \sim 3 \times 10^{11}$ yrs. This makes many clusters much older than hitherto assumed. Even our Galaxy might have an age of this order with several generations of stars formed, evolved and burnt out. Thus the dark matter component in the Galaxy may be largely made of burnt out stars.

(iv) Hierarchy of structures: The largest structure to form in the MCEs is the so called supercluster of mass $\sim 10^{15} - 10^{16} M_\odot$. There are, however, MCEs on smaller scales going right down to galactic nuclei with masses $\sim 10^6 - 10^7 M_\odot$. It is, however, the former that keep the universe going steady state at all times. Further work is needed, however, in the actual mechanism of galaxy formation from explosively created matter.

7 Concluding Remarks

This approach is intended more in the spirit of opening up the field of cosmology to other ideas than those provided by the standard big bang cosmology. Thus the QSSC, like any scienfitic theory is to be judged vis-a-vis the big bang cosmology by how it performs

[15] Narlikar, J.V., *Introduction to Cosmology*, 2nd Edition, (Cambridge University Press, 1993).

[16] Narlikar, J.V. and Das Gupta, P., *M.N.R.A.S.* (1993) to be published.

[17] Smoot, G.F., *et al., Ap. J.* **396** (1992), L1.

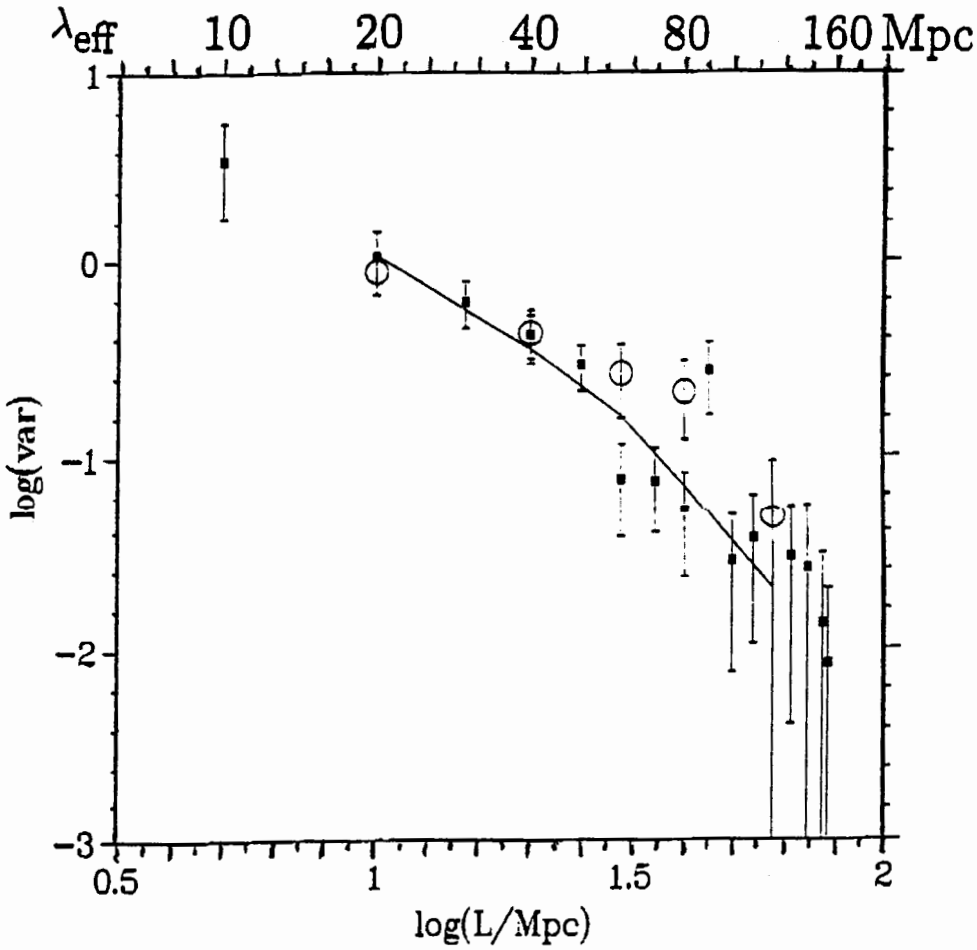

Figure 1: Galaxy number density fluctuation. Variances above Poisson are corrected for z-errors. Comparison with IRAS galaxies (circles) and CDM model (line).

Cunow 1993b,c) and low resolution redshifts for 0,9 million galaxies with $b_J \leq 20,5$ and $0 < z \leq 0,3$ (Schuecker 1993).

The MRSP sample is an efficient tool for the analysis of large-scale structures in the universe. Scales of up to $900\,h^{-1}$ Mpc (h=1 for $H_0 = 100\,\mathrm{km\,s^{-1}\,Mpc^{-1}}$) are covered by the data. Homogeneity and fluctuation analyses, such as count in cells, power spectrum analysis and related methods, indicate that no high amplitude fluctuations in density contrast are present on scales larger than $100\,h^{-1}$ Mpc. This is in agreement with the results obtained from IRAS galaxies, as indicated in Figure 1 (Schuecker et al. 1994).

Another part of the MRSP is concerned with the measurement of the Hubble constant H_0 and the deceleration parameter q_0. At the comparatively large redshifts of the MRSP galaxies, H_0 can be determined free from local effects. It is obtained by measuring the shift between the luminosity function (LF) of the Virgo cluster and an apparent luminosity function - apparent magnitudes and number densities are transformed to a reference redshift - from the MRSP data. The LF of the Virgo cluster was modified in order to represent a field sample. H_0 so determined is 39 or $54\,\mathrm{km\,s^{-1}\,Mpc^{-1}}$, respectively, for the lower and upper limit of the distance moduli of Virgo (Duemmler 1992,1994).

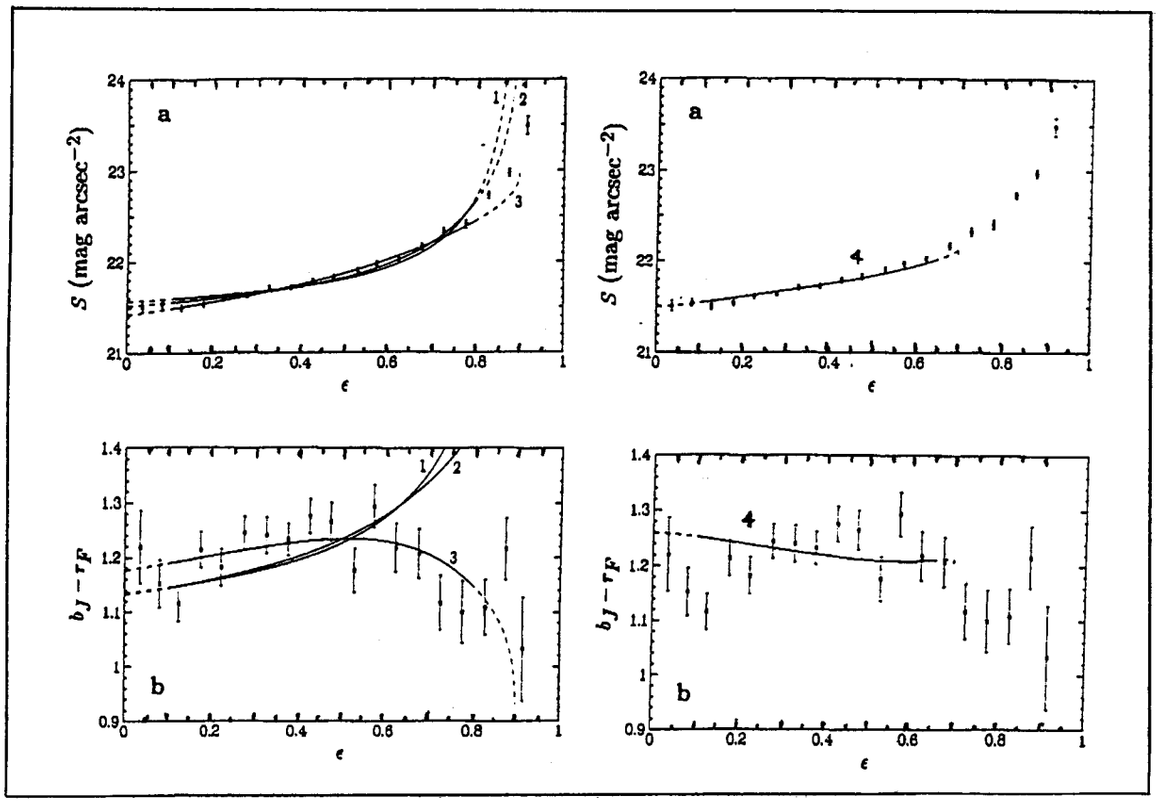

Figure 2: Variation of the projected surface brightness S for the J-band (insets a) and colour $b_J - r_F$ (insets b) with the apparent ellipticity ϵ for spiral galaxies with $b_J \leq 18$. The solid lines represent model-galaxy predictions for SCREEN-model (1), SLAB-model (2), SANDWICH-model (3) and 3-COMPONENT-model (4).

Models of inflationary universes predict the density parameter $\Omega_0 = 1$ or the deceleration parameter $q_0 = 0,5$ for the cosmological constant $\Lambda = 0$. The measurement of q_0 is therefore an important test for these models. In the MRSP, q_0 is determined by using a modified version of the classical redshift-volume test. Major problems for the determination of these parameters are effects caused by galaxy evolution. The MRSP galaxies do not show any significant variation of the mixture of galaxy types with magnitudes. This result, together with the properties of the differential galaxy number counts in the b_J passband, obtained for the MRSP sample, indicates, that no strong luminosity evolution is present for galaxies with $b_J \leq 20$ and $z \leq 0,3$. Based on these findings $q_0 = 0,5 \pm 0,3$ is determined. Further studies of colour and redshift distributions using several million galaxies are in preparation in order to confirm these preliminary results (Schuecker et al. 1994).

The MRSP catalogue is also used for statistical investigations of the internal absorption of spiral galaxies. A sample of 2300 galaxies with $b_J \leq 18$, for which b_J and r_F are available, are used for these measurements. Absorption values are obtained by investigating the variation of the projected surface brightness S (insets a in figure 2) and colour $b_J - r_F$ (insets b in figure 2) with apparent ellipticity ϵ, which is a measure of the inclination angle i of the galaxy. Figure 2 compares these data with model predictions. The results indicate that galaxy discs are not optically thin (Cunow 1992,1993c).

All measurements in the MRSP require accurately calibrated photographic magnitudes. Artificial variations of magnitude zero points within a field or from field to field would increase the measured fluctuation power, creating inhomogeneities in the observed galaxy distribution. The different zero points of the instrumental magnitudes on different plates are adjusted using the overlap regions of neighbouring fields. Large-scale zero-point gradients, however, may still be present after this procedure. The random error of the final plate zero points must not be larger than $\sigma \approx 0^m,05$, and any zero-point gradients must be removed. This can be achieved by measuring CCD sequences for approximately 30% of the ESO/SERC field distributed over the survey area.

For the magnitude calibration of the MRSP data, CCD sequences were obtained with the 0,9m-Dutch telescope at ESO/LaSilla and with the 1,0,-telescope at SAAO/Sutherland. For the calibration of b_J, B and V are needed. The r_F magnitudes are calibrated using filters V and R.

2 Magnitude Calibration with CCD Sequences

CCD sequences for 39 ESO/SERC fields were obtained with the 0,9m-Dutch telescope at ESO from 1991 to 1993 (Cunow 1993a,c). For 19 fields B, V and R exposures were taken; for the remainder only V and R.

With the 1,0m-telescope at SAAO, V and R images were taken in two observing sessions in 1992 and 1993. Johnson V and Cousins R filters were used. In the first run, 7 ESO/SERC fields were observed in 2 photometric nights. One ESO field, no. 412, was re-measured to allow for the comparison of the photometric systems at both sites. Exposure times range from 600s in V to 300s in R. The catalogue of these sequences is published in Cunow and Wargau (1993). It contains magnitudes for 86 galaxies and 59

stars with $14 < V < 21$. In the second run, data of another 7 ESO/SERC fields were observed in 3 photometric nights. The V images were exposed for 1200s and the R images for 600s. The catalogue containing these data is published in Cunow and Wargau (1994).

The CCD magnitudes are calibrated with the magnitudes of E-region stars given by Graham (1982). In each of the regions three stars with differing colours were observed. In order to obtain a large number of standard-star measurements with a minimum of observing time, photometric sequences in several globular clusters were also used.

Total magnitudes were determined for all objects by measuring aperture magnitudes, using several apertures of different sizes. The aperture chosen for a given object is the smallest one with a diameter which is at least twice as large as the object size. To avoid systematic errors due to the presence of neighbours, a clean subframe was created for each object.

Figure 3 gives the CCD versus the catalogue magnitudes for the calibration objects obtained at the SAAO 1,0m-telescope in 1992. Inset a gives the V measurements and inset b the R measurements. For the E-region stars - filled symbols - the scatter is $\sigma = 0^m,03$ in V and $\sigma = 0^m,02$ in R. For the cluster standards - open symbols - , the scatter is $\sigma = 0^m,05$ in V and in R. The random magnitude errors for the programme objects are $\sigma = 0^m,10$ for V and $\sigma = 0^m,11$ for R. These values are obtained from the scatter between multiple measurements of the same star on the CCD frames of the globular cluster sequences.

5 galaxies and 3 stars were observed both at ESO and SAAO. This allows a direct comparison between magnitudes for the programme objects obtained at different sites with different instruments, as indicated in Figure 4. The agreement resulting from the two setups is satisfactory in view of the intrinsic scatter and the small number of objects.

The MRSP catalogue of CCD sequences, available so far, contains 235 galaxies and 274 stars with $14 < V < 21$ on 27 ESO/SERC fields. The data, for which the reduction is not yet complete, cover further 25 ESO/SERC fields. Altogether, CCD data for 52 ESO/SERC fields are available. Figure 5 shows the distribution of the CCD fields over the chosen MRSP survey area. Up to now, the data cover 24% of the survey area.

The APM Galaxy Survey (Maddox et al. 1990) uses 185 fields of the ESO/SERC(J) survey. These data were calibrated using CCD sequences in B and V, available for 39 fields, which corresponds to 21% of their survey area. Hence, in the MRSP the mean density of the grid of CCD sequences over the survey area is about the same as in the APM Galaxy Survey. It is expected that the accuracy of the final r_F magnitudes in the MRSP is about the same as that for the b_J magnitudes of the APM survey.

For the calibration of the photographic magnitudes, the colour equations for B, V and b_J, and V, R, and r_F, must be determined. Figure 6 displays the two-colour diagrams $(B - b_J)$ versus $(B - V)$ for the MRSP sequences. The mean colour relations were obtained by straight-line fits, and are given in the figure caption. For the stars (top) the slope is $\alpha = 0,21 \pm 0,08$, which is in good agreement with results obtained by independent measurements, described in the literature. $\alpha = 0,65 \pm 0,04$ is found for the galaxies (bottom). The latter value is significantly larger than that obtained for the stars. B, V, and b_J magnitudes for galaxies of the APM Galaxy Survey are found in Maddox et al. (1990). Their data give an $\alpha = 0,49 \pm 0,07$. This is comparable to the MRSP result, insofar, as the difference between the mean colour relations for stars and galaxies is real.

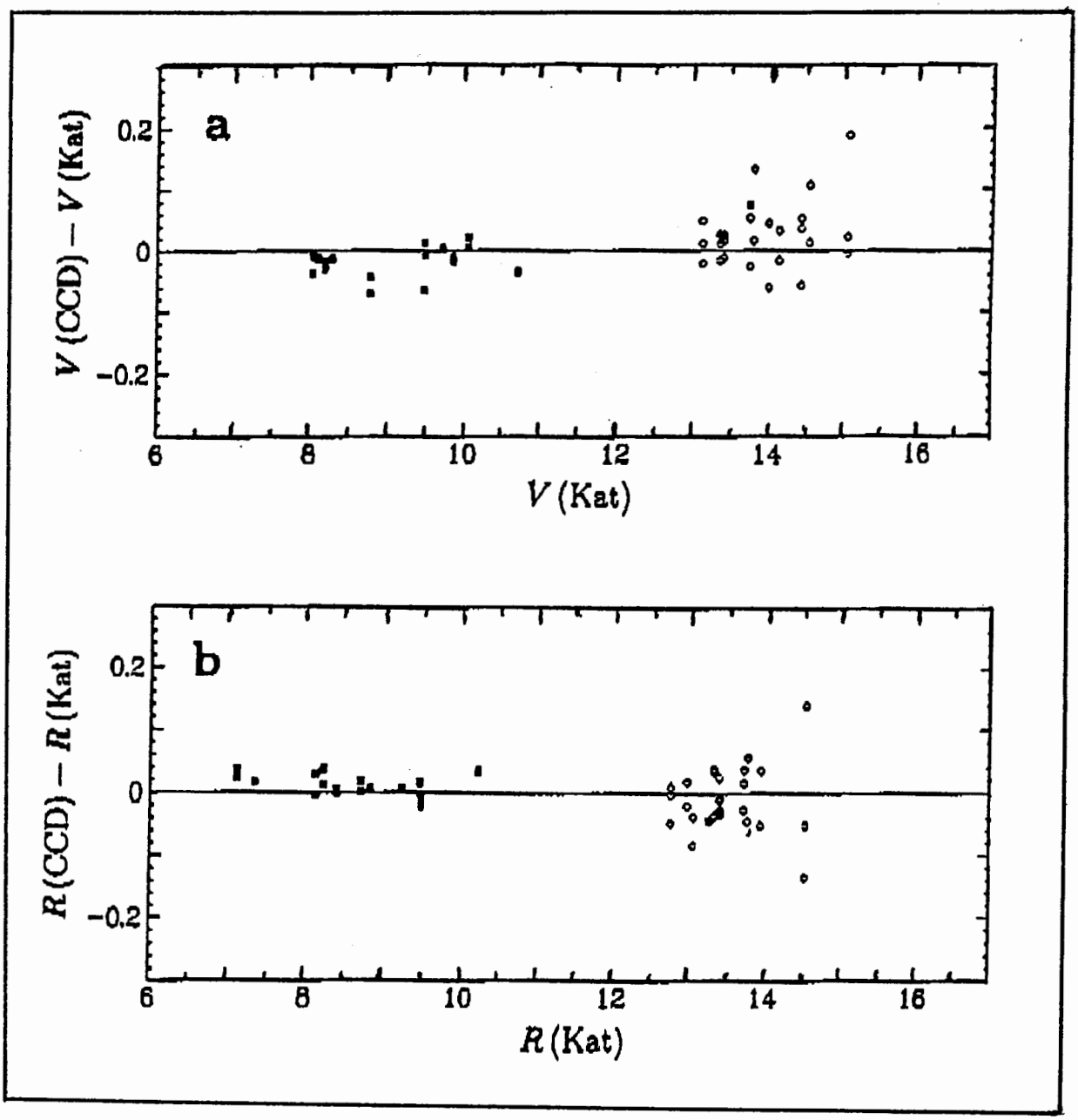

Figure 3: CCD magnitudes versus catalogue magnitudes for the calibration objects obtained at the SAAO 1,0m telescope in 1992. Inset a: V measurements; inset b: R measurements. Filled symbols indicate E-region stars and open symbols the globular cluster sequences.

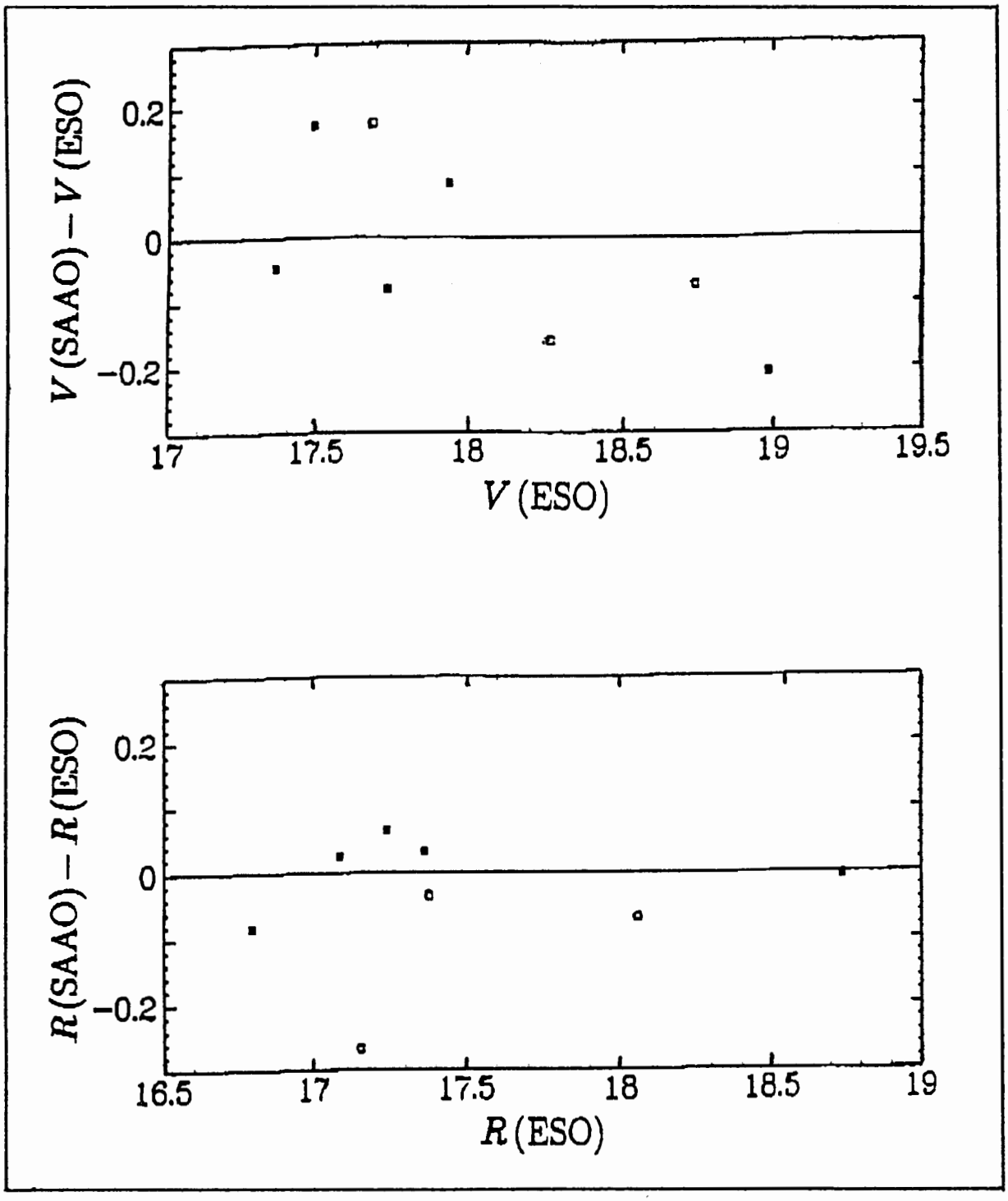

Figure 4: Comparison of magnitudes measured with the SAAO 1,0m telescope and magnitudes obtained with the ESO 0,9m Dutch telescope for 5 galaxies (filled symbols) and 3 stars (open symbols). Top: V measurements, bottom: R measurements.

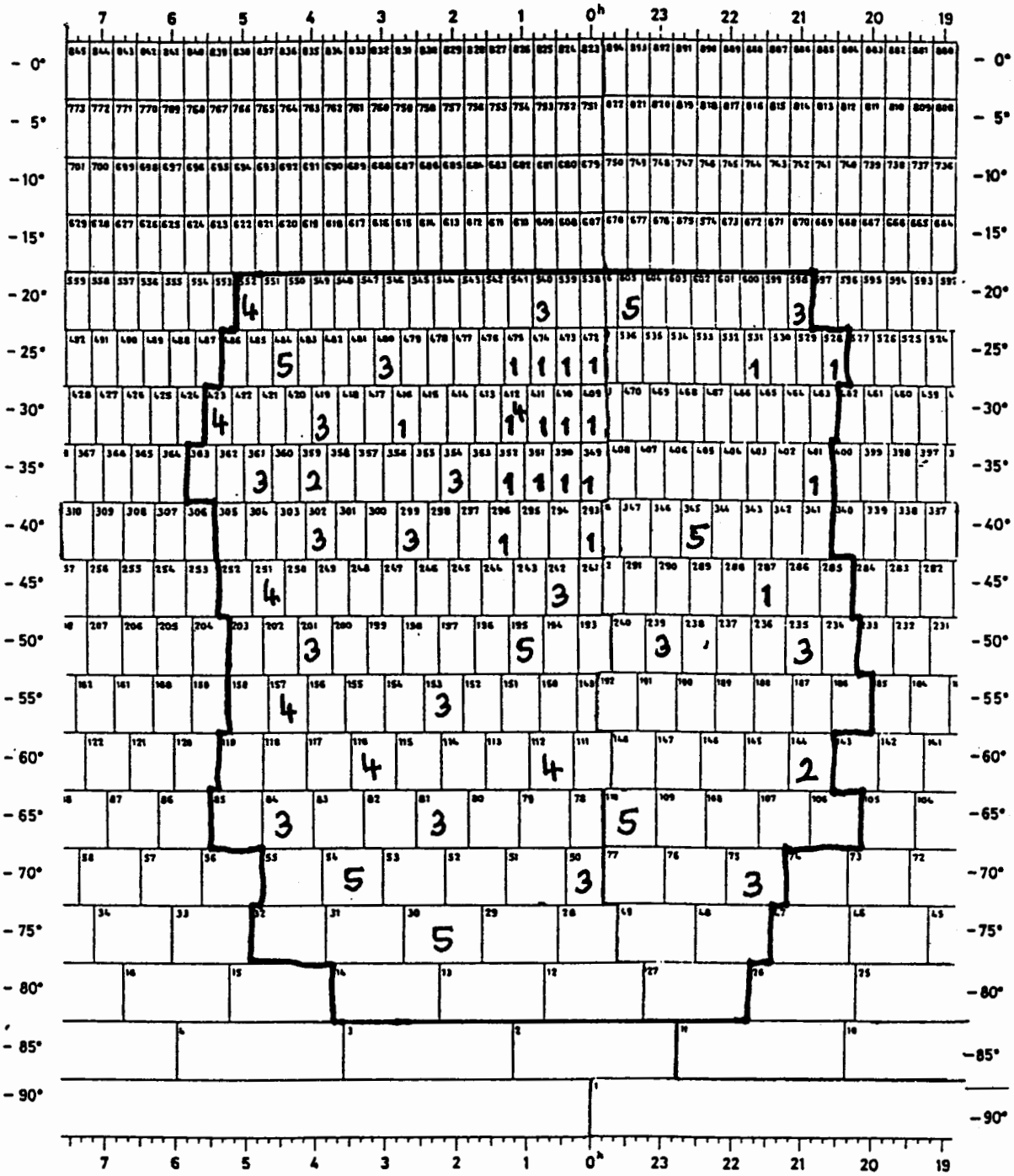

Figure 5: Distribution of CCD fields over the MRSP survey area. The number sets indicate: ESO data in BVR from 1991, 1992 (1); ESO data in VR from 1992 (2); ESO data in VR from 1993 (3); SAAO data in VR from 1992 (4); SAAO data in VR from 1993 (5).

If the relation between $(B-V)$ and $(B-b_J)$ is determined from galaxy colours, obtained from model spectra assuming redshifts $0 \leq z < 0,4$, a slope of $\alpha = 0,26 \pm 0,01$ is found. This is consistent with the derived value for the stars but not for the galaxies.

Figure 7 now gives the two-colour diagrams $(R-r_F)$ versus $(V-R)$ for the MRSP sequences. Again, the mean colour relations were obtained by straight-line fits, and are indicated in the figure caption. The slopes are $\beta = 0,07 \pm 0,06$ for the stars (top) and $\beta = -0,20 \pm 0,06$ for the galaxies (bottom). The difference is probably not significant. Unfortunately, these results cannot directly be compared with independent measurements, because no mean relation between $(R-r_F)$ and $(V-R)$ exists in the literature.

There are, however, two relations between B, R and r_F available in the literature.
Shanks et al. (1984) give: $r_F = R - 0,06\,(B-R)$,
and
Metcalfe et al. (1991) give: $r_F = R + 0,094\,(B-R)$.

For the MRSP data the corresponding relations are obtained by applying the mean relations between $(V-R)$ and $(B-R)$ to the measured equations relating r_F, V and R, which gives
for stars $r_F = R - 0,03\,(B-R)$
and
for galaxies $r_F = R + 0,03\,(B-R) + 0,06$.
The latter two relations fall between the relations given above.

3 Internal Absorption in Spiral Galaxies

Spectra of 5 galaxies with magnitudes $15 < B < 16$ were obtained by us with the SAAO 1,9m-telescope. In addition, for one of these galaxies, we obtained CCD-BVRI images and for another one CCD-VRI images at the SAAO 1m-telescope. The objects are Sb-galaxies having different inclination angle i between face-on and edge-on view. The analysis of the surface-brightness profiles of these galaxies, in comparison with profiles of model galaxies, provide information about the internal absorption in these objects. Together with the redshift information, absolute values for diameter, luminosity, luminous mass and dust mass can be derived.

These galaxies are representative for the MRSP sample, which is used for the statistical measurements of internal absorption. Comparison of the results obtained from the selected galaxies and from the statistical sample of galaxies is expected to yield information about the influence of possible selection effects and give an unbiased result for the mean internal absorption.

Follow-up observations of another 10 to 20 galaxies in order to obtain a sample, which provides information about the different opacities found in spiral galaxies, are planned.

Acknowledgements

The authors thank Dr R S Stobie for allocation of observing time at SAAO/ Sutherland. We also thank Drs J Menzies, J A C Caldwell and the SAAO staff for assistance during the observations and for pre-reducing the CCD images. WW thanks the University of South

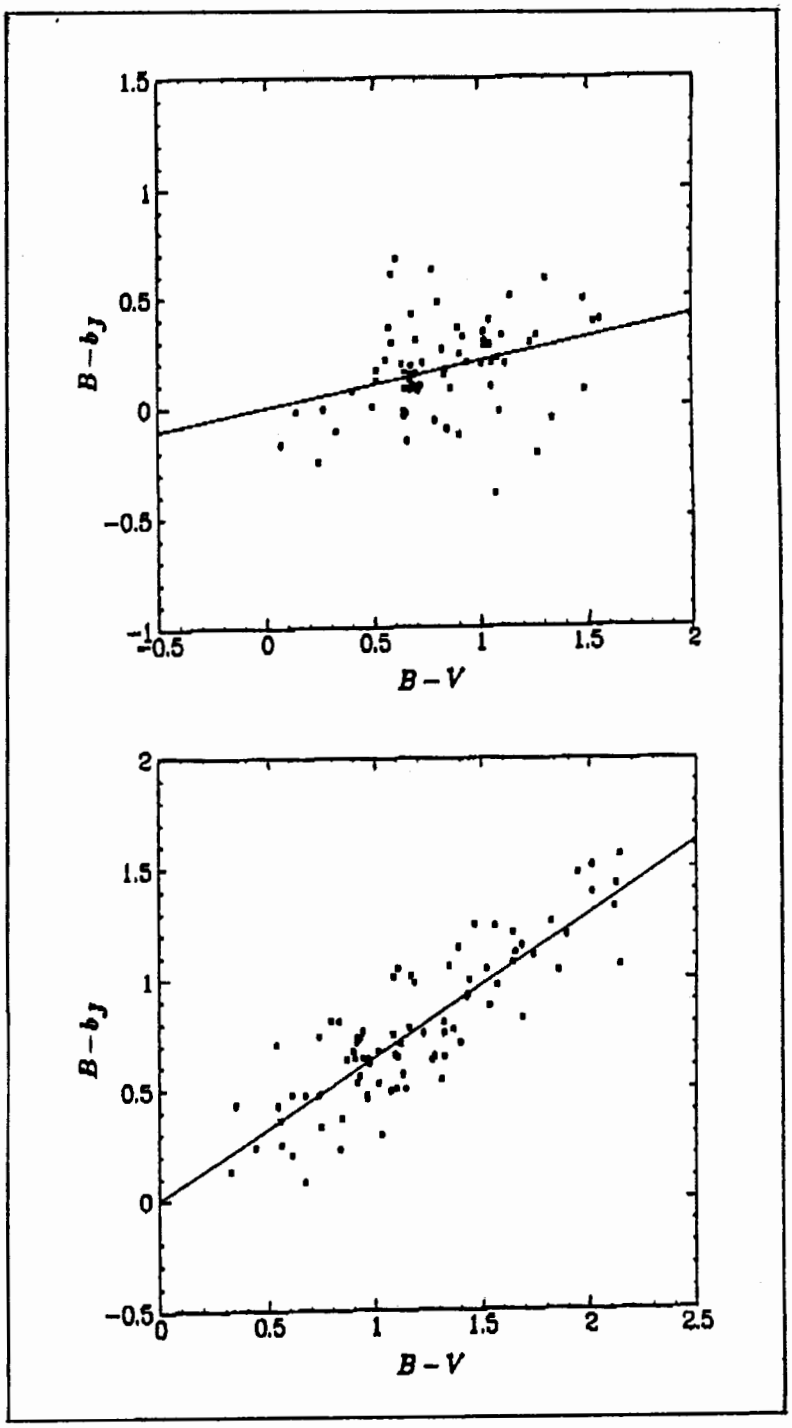

Figure 6: Two colour diagrams $(B - b_J)$ versus $(B - V)$ for the MRSP sequences.
Top: stars.
The solid line gives the colour relation : $B - b_J = 0,21(B - V)$.
Bottom: galaxies.
The solid line gives the colour relation $B - b_J = 0,65(B - V)$.

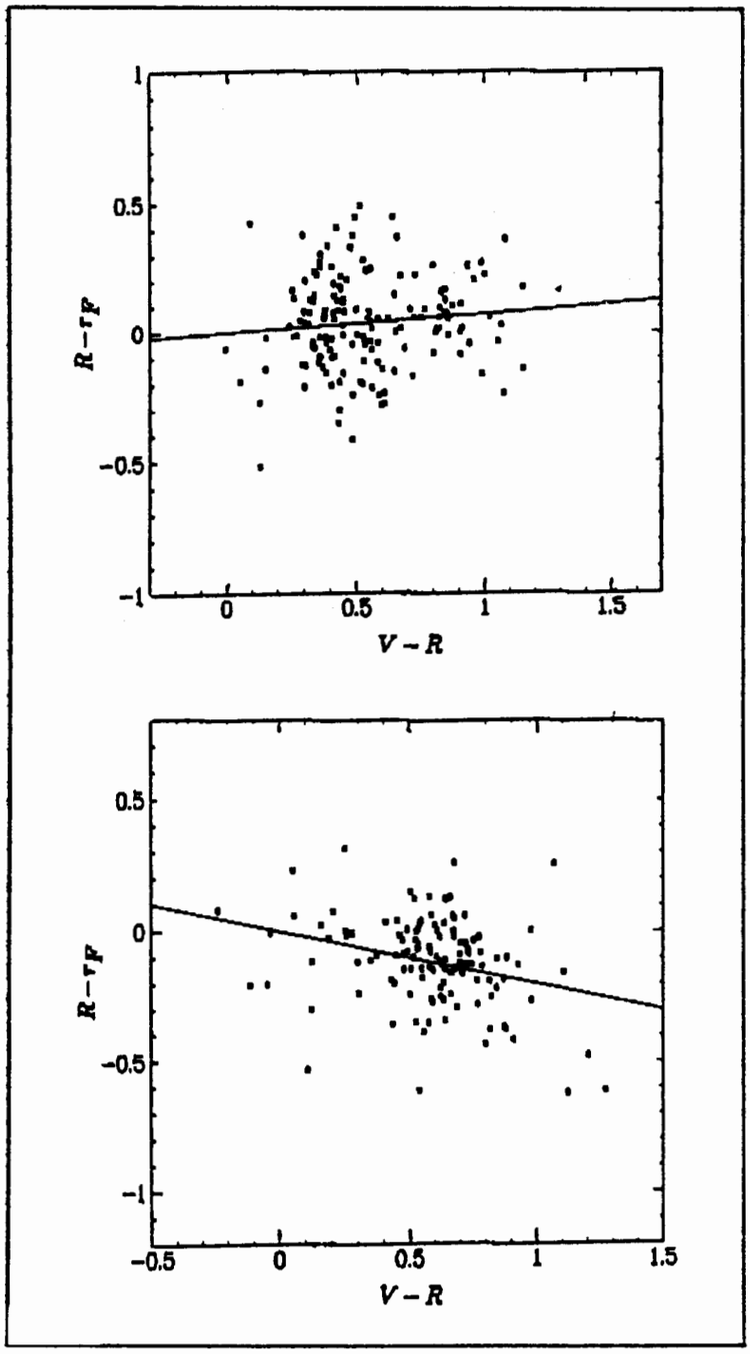

Figure 7: Two colour diagrams $(R - r_F)$ versus $(V - R)$ for the MRSP sequences.
Top: stars.
The solid line gives the colour relation : $R - r_F = 0,07(V - R)$.
Bottom: galaxies.
The solid line gives the colour relation $R - r_F = -0,20(V - R)$.

Africa for financial support. It is a pleasure for BC to thank the Department of Mathematics, Applied Mathematics and Astronomy of the University of South Africa for the invitation, the financial support and for the hospitality during her stays at the University where part of this research has been done. BC also thanks the Deutsche Forschungsgemeinschaft (DFG) for financial support under Se 345/20-1 for travel allowances to South Africa. Special thanks go to Prof W C Seitter and the members of the MRSP for many useful discussions. Financial support of the MRSP by the DFG under Se 345/14-1,2,3 is gratefully acknowledged.

References

[1] Cunow, B., 1992, MNRAS **258**, 251

[2] Cunow, B., 1993a, A&A Suppl. **97**, 541

[3] Cunow, B., 1993b, A&A **268**, 491

[4] Cunow, B., 1993c, PhD thesis, University of Muenster, FRG

[5] Cunow, B., Wargau, W., 1993, A&A Suppl. **102**, 331

[6] Cunow, B., Wargau, W., 1994, A&A Suppl. **107**, 277

[7] Duemmler, R., 1992, A&A **264**, 1

[8] Duemmler, R., 1994, PhD thesis, University of Muenster, FRG

[9] Graham, J.A., 1982, PASP **94**, 244

[10] Horstmann, H., 1992, PhD thesis, University of Muenster, FRG

[11] Horstmann, H., Schuecker, P., Seitter, W.C., Aniol, R., Budell, R., Cunow, B., Meijer, J., Teuber, D., Tucholke, H.-J., 1989, Digitised Optical Sky Surveys, eds. C. Jaschek, H.T. MacGillivray, Bull. Inf. Cent. Donnees Stellaires **37**, 43

[12] Maddox, S.J., Efstathiou, G., Sutherland, W.J., 1990, MNRAS **246**, 433

[13] Metcalfe, N., Shanks, T., Fong, R., Jones, L.R., 1991, MNRAS **249**, 498

[14] Naumann, M., Ungruhe, R., Seitter, W.C., 1993, ESO Messenger **71**, 46

[15] Schuecker, P., 1993, ApJ Suppl. **84**, 39

[16] Schuecker, P., Seitter, W.C., Boschan, P., Budell, R., Cunow, B., Duemmler, R., Naumann, M., Ott, H.-A., Spiekermann, G., Teuber, D., Ungruhe, R., 1994, Astronomy from Wide-Field Imaging, IAU-Symp. No. **161**, ed. H.T. MacGillivray, Kluwer Dordrecht, p. 699

[17] Seitter, W.C., 1992, Digitised Optical Sky Surveys, eds. H.T. MacGillivray, E.B. Thomson, Kluwer Dordrecht, p. 367

[18] Seitter, W.C., Ott, H.-A., Duemmler, R., Schuecker, P., Horstmann, H., 1989, Morphological Cosmology, eds. P. Flin, H.W. Duerbeck, Springer, Berlin, Lecture Notes in Physics Vol. **332**, p. 3

[19] Seitter, W.C., Boschan, B., Cunow, B., Duemmler, R., Feige, B., Naumann, M., Nolze, W., Ott, H.-A., Ritzmann, B.-M., Schuecker, P., Spiekermann, G., Teuber, D., Ungruhe, R., 1994, Cosmological Aspects of X-ray Clusters in Galaxies, ed. W.C. Seitter, NATO ASI Series, Kluwer, Dordrecht, p. 411

[20] Shanks, T., Stevenson, P.R.F., Fong, R., MacGillivray, H.T., 1984, MNRAS **206**, 767

[21] Spiekermann, G., Seitter, W.C., Boschan, P., Cunow, B., Duemmler, R., Naumann, M., Ott, H.-A., Schuecker, P., Teuber, D., Ungruhe, R., 1994 Reviews in Modern Astronomy Vol **7**, ed. G. Klare, Heidelberg, p. 207

Amateur Seismography

M D Overbeek
Box 212, Edenvale, 1610

Abstract

The links between Astronomy and Seismology are explored briefly: Mention is made of the fact that the Union Observatory operated a Wiechert seismograph for practically the whole of its existence. The SAAO operates two seismographs at its Sutherland station and the Royal Astronomical Observatory in Brussels has an active seismography section. Tribute is paid to Mohorovicic and Wegener, both of whom trained as astronomers, for their insight which led to the acceptance of the existence of the Earth's core and of continental drift. It is also pointed out that seismography of some Solar System bodies has already been performed.

Various methods of detecting seismic motion are described briefly, from the innovative Chinese seismoscope of the second century AD to sophisticated cryogenic superconducting microgravimeters in use today.

An amateur installation is described and stress is laid on the fact that only easily obtained materials need be used. Parallels between amateur made telescopes and seismographs are discussed.

Seismic traces obtained with professionally built, and amateur instruments are shown. A brief discussion of the possible benefit to the science of Seismology, of amateur work, is given.

various possibilities. For a closed universe, there is an interesting scenario for its quantum creation out of nothing, which, however, does not exist if it is not closed. Moreover, one cannot exclude the possibility of an ever-existing classical universe. The immediate task in that case will be to develop a scenario, by which our universe could evolve to its present form, possibly out of a tiny part of the parent universe. This will again tie up Planck scale physics with the large scale behaviour of the observable universe. The evolution in the post-Planckian era usually involves calculations in which particles are described by quantum field theories on a curved classical space-time. Inflationary models were intended to provide such a description of the early universe. The models had limited success, with the chaotic inflationary model looking superior to the other inflationary models. In the chaotic model, the universe is assumed to evolve out of a random distribution of initial data. However, in the actual formulation of the model[1], the initial values of the inflation field field ϕ are assumed to be very large ($\phi_0 \gg M_p$) so as to obtain a potential-driven inflation.

The fact that the space-time is classical then implies that the field ϕ and the space-time are ab initio isotropic and homogeneous. The model, therefore, uses only a part of the phase-space. It would indeed be interesting to consider also the case when $\phi_0 < M_p$. Since the space-time here need not be isotropic and homogeneous, the evolution will in general, be difficult to study. However, some progress can be made by considering a miniuniverse with lesser symmetry (say one with cylindrical symmetry). Recently, Senovilla [2] and Ruiz and Senovilla [3] have given a class of solutions, which describes such a universe. These solutions are smooth and regular everywhere, and also geodesically complete[4]. They satisfy the energy and causality conditions and all the physical and geometrical invariants are regular and finite. The solutions escape the singularity theorem by not satisfying one of the assumptions, i.e. the existence of compact trapped surfaces. This assumption cannot be indispensible for cosmological models. For example, even the open FRW model, which has the Big-Bang singularity, does not encounter a trapped surface. Of course, these solutions cannot describe the present universe, but these may be generalized to describe various stages of the early universe (miniuniverse). It is conceivable that there are many other inhomogeneous solutions which provide possible paths for a successful evolution, and it is not obvious that we must have a FRW universe right from the beginning.

We now show that it is possible to realize a chaotic model in an inhomogeneous space-time which permits two killing vector fields which are mutual and hyperspace orthogonal. We follow the notation of Ruiz and Senovilla[3] but consider only a sub-family,

$$ds^2 = T^{n+1}F^2\left(-dt^2 + H^2dr^2\right) + T^{1+n}GPd\theta^2 + T^{1-n}GP^{-1}dz^2, \tag{1}$$

where $T(t)$ satisfies the equation

$$\frac{\ddot{T}}{T} = \epsilon a^2, \epsilon = 0, \pm 1 \tag{2}$$

with a an integration constant. The functions F, H, G, P are functions of r only. These are related by

$$F^2 = (G/P)^n \tag{3}$$

$$\alpha' + \alpha\beta - \alpha\frac{H'}{H} = \epsilon n a^2 H^2 \tag{4}$$

$$(1-n)\beta' + n\beta^2 - 2n\beta\alpha + \alpha^2 - (1-n)\beta\frac{H'}{H} = n(1-n)\epsilon a^2 H^2 \tag{5}$$

where $\alpha = P'/P$ and $\beta = G'/G$ and dots and primes denote differentiation w.r.t. t and r respectively. Since there are only three relations, the functions can be written in terms of an arbitrary function $c(r)$.

The scalar field $\phi \equiv \phi(t,r)$ satisfies the equation

$$\ddot{\phi} + \dot{\phi}\frac{\dot{T}}{T} - \frac{\phi''}{H^2} - \frac{\phi'}{H^2}\frac{(GH^{-1})'}{GH^{-1}} + \frac{dv(\phi)}{d\phi}T^{n+1}F^2 = 0 \tag{6}$$

we will choose $G = H$ to simplify the equation. The evolution can now be described in stages:

1. *First inflationary stage*: Let us assume that at $t = 0$, $\dot{\phi}$ is much larger than ϕ and ϕ'' everywhere in a tiny part (greater than Planck size) of the universe, so that the relevant equation of state is that of stiff matter. In that case, the miniuniverse can be described by metric (1) with $-3 < n < -1$ and

$$c(r) = \left[-na^2 M(r+q)\right]^{-n} \tag{7}$$

$$P^2(r) = n^2 a^2 M^2 c^2(r), H(r) = G(r) = \frac{1}{a(r+q)} \tag{8}$$

$$T(t) = \cos h(at), \chi\rho = \chi\rho = \frac{1}{2}\dot{\phi}^2 \cdot \mathrm{T}^{-(n+1)}\mathrm{c}^{1-n} \tag{9}$$

where M, q and a are constants. If we write $n = -1-\delta, \delta > 0$, proper lengths along the three spatial directions will change with t as $T^{-\delta/2}, T^{-\delta/2}$ and $T^{(2+\delta)/2}$. If we consider a thin cylindrical shell of radius r and axis along the z-axis, its volume will change with proper time τ as

$$V_p(\tau) = V_p(0)\cos h^{(2-\delta)/2} at. \tag{10}$$

The space-time is highly anisotropic, there being a rapid expansion along the z-axis and a rather slow contraction along directions normal to it. However, the inflation ceases because the field ϕ increased rapidly. Neglecting ϕ'' and the potential term, we find from equation (6),

$$\phi(t,r) = \phi(0,r) + \frac{1}{F(r)}\left[\frac{2A}{a}\tan^{-1}\left(e^{at}\right) - \frac{\pi A}{2a}\right] \tag{11}$$

where A is chosen as a constant. If $\frac{\pi A}{2a} \gg \phi(0,r)\cdot F(r)$, everywhere, $\phi \cdot F(r)$ becomes almost a constant within a short time. As ϕ increases, the potential term becomes important, the stiff matter equation of state gets disturbed and the above solution no longer holds. The class of solutions (9) includes one relevant for a cosmological constant

($n = -1$), but the inhomogeneous universe cannot pass through it. Thus, a potential-driven inflation does not occur here. However, ϕ is supposed to be coupled to other fields, both scalars and fermions, which are produced. These particles thermalize, heating up the universe. The temperature attained depends on the model of particle production chosen. If we assume that the Baryogenesis is due to non-perturbative electroweak processes, a temperature $\sim 10^4 GeV$ is adequate. After thermalization, the universe is radiation dominated and another stage of rapid expansion follows.

2. *Radiation-dominated state*: This stage, beginning at a time t_1, can be described by the metric (2) with $n = 3$. This is the original Senovilla solution:

$$ds^2 = T^4 c^2 \left(-dt^2 + H^2 dr^2\right) + T^4 G P d\theta^2 + T^{-2} G P^{-1} dz^2 \tag{12}$$

where

$$T = \cosh b\,(t - t_1)\,, \rho = 3p = \frac{3}{5} k T^4 c^{-4}, k > 0. \tag{13}$$

There is now a contraction along the z-direction and expansions along directions normal to it. This peculiar two-stage inflation helps the universe to isotropize. Considering a thin cylindrical shell as before, the expansion can be written as

$$V(\tau_2) = V(\tau_1) \left(\frac{\cosh bt_2}{\cosh bt_1}\right)^3 \tag{14}$$

with

$$\tau = \frac{1}{2} F(r) \left[t + \frac{1}{2b} \sinh 2bt\right]. \tag{15}$$

It is obvious that for $t \ll \frac{1}{b}$, there is a rapid inflation, while for $t \gg \frac{1}{b}$, there is a power-law expansion, $v \sim \left(\frac{8b}{F(r)}\right) \cdot \tau^{3/2}$, which apart from the inhomogeneous factor, is similar to the FRW case. Since both the energy density and pressure fall, massive particles will eventually become non-relativistic and a matter-dominated era will begin.

3. *Matter-dominated era*: At the end of the second stage, the universe is in a position to become homogeneous and isotropic. Within the framework of the metric (2), there is only one window through which this may happen and this is during the matter-dominated era. The solution is, $n = 0, F(r) = H(r) = 1, G(r) = P(r) = r$. The metric is

$$ds^2 = T(t) \left[-dt^2 + dr^2 + r^2 d\theta^2 + dz^2\right] \tag{16}$$

where

$$T(t) = Bt^4, \rho = \frac{12}{Bt^6}, p = 0. \tag{17}$$

Rewriting (16) in terms of the proper time η, we have

$$ds^2 = -d\eta^2 + S^2(\eta) \left[dr^2 + r^2 d\theta^2 + dz^2\right], \tag{18}$$

which is the well-known Einstein-de Sitter universe. The model, therefore, leads naturally to a flat space, solving the flatness problem of the open universe. Note that, $\rho \sim S^{-3}, S \sim \eta^{2/3}$, as expected.

It is necessary to show that the universe does not tend to roll down to the symmetric state given by equation (16). A simple approach will be to study the stability of the solution (16). We put $H = 1$, without any loss of generality. We now consider linear perturbation of the functions $P(r)$ and $G(r)$ about the solution (16), making use of the field equations. We see that the solution remains invariant, modulo a trivial scaling. Thus, the symmetric state is very stable and given time, the universe will roll into it.

We have shown that a scenario in which a tiny part of an ever-existing universe becomes large, isotropy and homogeneity exist even if the inflaton field ϕ is not too large. Although we have considered a particular class of inhomogeneous solutions, it is quite possible that initial inhomogeneities of many different types permit a successful evolution. Our initial conditions are as much probable as those considered by Linde. Also, the concept of a singularity-free and ever-existing parent universe appears to be consistent with standard cosmological results.

S. Mukherjee would like to thank A. Beesham for discussions and the University of Zululand for hospitality.

References

[1] Linde, A.D., *Inflation and Quantum Cosmology* (Academic Press, NY 1990) and the references after chapter 1.

[2] Senovilla, J.M.M., *Phys. Rev. Lett.* **64**, 2219 (1990).

[3] Ruiz, E. and Senovilla, J.M.M., *Phys. Rev.* **D45**, 1995 (1992).

[4] Chinea, F.J., Fernandez-Jambrina, L. and Senovilla, J.M.M., *Phys. Rev. D45*, 481 (1992); N. Dadhich and L.K. Patel, IUCAA - 21/93 (Preprint).

Visual Observations and Evolution of Meteor Streams

T P Cooper
56 Tenth Avenue, Northmead, Benoni, 1501

Abstract

The purpose of my paper today is twofold. On the one hand I want to show how, using nothing more than the naked eye, we can make a significant contribution to meteor astronomy. On the other hand I want to appeal to more Southern African observers to become involved with our organised observing programs. While there is an effective net in the northern hemisphere and an enthusiastic group in Australia, a gap exists in the study of southern meteor showers because so few observers are active in this part of the world. Thus we can make a significant contribution, and hopefully today I can show you how simple this can be.

To do this I have structured my talk as follows:

the theoretical evolution of a meteor stream from a hypothetical comet
visual observations of the evolution
actual case study of the Geminid shower
the occurrence of meteor streams
some streams in need of observation

1 Evolution of Meteor Streams from Comets

While there is growing evidence that some meteor streams may have asteroidal origins [1,2], it is generally accepted that most are related to comets. Table 1 lists the current known or suggested cometary and asteroidal parents for meteor showers, and we see that the cometary parents considerably outweigh the asteroidal ones. It should be noted that some asteroids may be extinct comets, and that meteor showers associated with such asteroids may have had a cometary parent.

So, let us now consider the formation of a meteor stream from a hypothetical comet, travelling in an elliptical orbit around the sun, as shown in Figure 1. In the parts of its orbit far from the Sun, the comet remains in a state of semi dormancy. I say semi dormancy since some comets have been shown to be active while still far from the Sun. However, as the comet nears the Sun its frozen ices and gases start to vaporise, and stream away from the nucleus and coma, due to the orbital motion of the comet and the effects of the solar wind. In the parts of its orbit close to the Sun, hot spots form on the sunward side of the nucleus from which gases emanate in a process called "jetting". At the same time as the gases vaporise, they release dust grains from the nucleus which are left behind

in the comets wake. It is these dust grains which we may subsequently observe as meteors as they enter the Earth's atmosphere. During the 1986 apparition of comet Halley several important facts pertaining to its dust releases were found [3]:

- most dust appears to be released directly from the surface of the nucleus by the process of streaming. This process presumably leaves a fairly uniform trail of dust in the wake of the comet
- some dust is released from the interior of the nucleus, entrained in the gases emitted during jetting events. This process presumably results in more widespread and less uniform distribution of dust particles, particularly when the comet is in the vicinity of the Sun
- during periods of high activity the jets were emitting up to 30 tonnes of material per second, about 80% of which was water vapour
- the diameter of the dust stream just after perihelion passage was about 320000 km
- the comet was releasing significant amounts of dust while still over 1.3AU from the Sun

Thus the passage of a comet around the Sun leaves a considerable amount of dust in its wake which continues to move in an orbit very similar to the parent comet. The dust distribution is initially not uniform, but variable dependent on primarily the ejection velocity of meteoroids from the comet, the activity of the jets as they move in and out of sunlight, and on the degree of streaming, which increases as the comet approaches the Sun. Over a period of time, the newly laid dust stream is subjected to various forces which modify its characteristics. Particles are slowed down by the effects of solar radiation pressure and the solar wind, smaller particles being affected more than larger ones, resulting in separation of the different particle sizes. Gravitational forces experienced during their motion through space may affect their orbits. The initial non-uniformities in the stream may smooth out. The particles, initially concentrated close to the orbital path, gradually spread out and the stream becomes less dense. Finally, further passages of the comet around the Sun cause a further build-up of particles in the dust stream. All of these factors contribute to the evolution of the meteor stream, and the only way to monitor these changes is by visually observing the meteor shower each year over a long period.

2 Visual Observations of the Evolution

In Figure 2 we depict the path of the Earth through the hypothetical meteor stream. If we now assume that we are visual observers looking for the predicted appearance of the meteor stream each night, then what we will see depends on the nature of the stream. The most simple scenario is if the stream from our comet is perfectly symmetrical. The Earth first encounters the meteor stream at solar longitude $\lambda_\odot$s, and here we will start to visually detect meteors from the shower radiant at a Zenithal Hourly Rate (ZHR) perhaps slightly

higher than the background rate of sporadic meteors. As the Earth moves deeper into the stream the ZHR increases and peaks at solar longitude $\lambda\odot$m, the date of maximum of the shower. Thereafter the observed ZHR decreases until the Earth leaves the confines of the stream at solar longitude $\lambda\odot$e, and the ZHR becomes indistinguishable from the sporadic background.

This is just the most simple scenario. In Figure 3 we see some more likely stream profiles. Figure 3a shows the narrow profile of a compact new stream which has not yet had time to disperse. A typical example in reality is the Sigma Puppid stream of April, first observed in 1977, and formed by a recent passage of comet Grigg-Skjellerup [4]. In the discovery year ZHRs up to 75/hour were observed on the night of April 23, but activity on the nights before and after was undetected. The new stream will probably begin to disperse slowly, the maximum peak will become broader, the period of visibility of the shower will lengthen and the activity profile may become asymmetrical. The acitivity profile may then begin to look like that in Figure 3b, of which a typical example are the Quadrantids. Over much longer periods the stream eventually thins out, the shower becomes visible over maybe one or two months and the maximum peak becomes broader and flatter (Figure 3c and 3d). The Virginids in March are an extreme example of the latter; they are visible from February 3 to April 15, but the maximum on March 20 is barely distinguishable from the sporadic background. Only the occasional fireball remains in evidence of what was probably an active shower in ancient times.

Figure 3 shows two other scenarios. Figure 3e shows a shower with a sharp peak in activity in addition to a second, broader maximum. The first peak has been caused by the recent passage of the parent comet through the established stream formed by previous passages. This sharp peak has been a feature of the Perseid shower in the last two years caused by the return of comet Swift-Tuttle. In Figure 3f there are two distinct maxima, and two possible causes exist. Each peak may have been caused by two different passages of the same comet, or the stream is a hollow cylinder. The Eta Aquarids and Orionids show this type of profile.

What is certain about all these profiles is that they can be constructed by dedicated observers using no more than their naked eyes and a knowledge of how to record what they see. By observing the shower over its entire apparition we can generate an activity profile and by observing each year we can monitor changes in the evolution of the stream.

3 Results of Observations of the Geminids

The Geminids represent one of the best documented cases of a meteor shower where the activity profile has changed significantly. The shower has been well observed since 1901 and the stream profile has been generated by computer as shown in Figure 4. The expected activity profiles on the left may be explained by the theoretical stream profile shown on the right of Figure 5. The cross section across the stream is cigar shaped, but most of the particles lie in a concentrated bar at an angle of 25° to the rest of the stream. Due to a slow regression of the orbit of the stream, the Earth's orbit moves slowly across the section with time causing the observed profile to change. Before 1920 the Earth missed the concentrated bar altogether. Since 1920 the Earth has been slowly crossing the bar,

resulting in the superimposition of the bar activity on top of the normal activity profile. The model predicts that the Earth will begin to miss the bar again, perhaps towards the end of the century, and we need to observe the Geminids each year to see if this is the case. The model explains some observed properties of the Geminids:

- no records of the Geminids exist prior to 1862
- the observed activity profile at present times fits the predicted profile. The observed profile for the 1991 event is shown in Figure 5
- brighter meteors tend to occur earlier in the profile, indicating a sorting of the particle sizes by the effects of solar radiation. This also agrees with the observed data

The model also predicts that the Earth will start to miss the stream altogether some time in the next century, and the Geminids will cease to exist as an observable meteor stream. Only time and observation will tell.

4 Occurrence of Meteor Streams

We have already said that much can be done, but how many meteor showers can we observe? Most modern sources list about 20 major annual showers, and the IMO lists 29 major showers in its "Handbook for Visual Meteor Observations". But there are also many minor showers that are in need of study. Cook [6], in his well known list of 1973, names 58 showers in all, and Kronk [7], in his descriptive catalogue, names 109. My own working list summarizes 92 meteor showers, including all of those in the Cook and IMO lists, and is shown in Table 2. I use this list to draw up observing programs for the Comet and Meteor Section of ASSA.

5 Some Streams requiring Observation

Many of the streams in my working list are inactive in most years, but may suddenly show periods of heightened activity of a periodic nature. For example, the Monoceritids in November, normally inactive, showed brief but strong activity in 1985 [8,9]. Previous strong displays also occured in 1925 and 1935, and we should be on the alert for another strong display in the near future. Of course the periodic meteor storms of the Leonids, due to reoccur in 1998 or 1999, are well known.

Due to the periodic nature of many meteor showers it is important to observe as many of the known and suspected streams as possible each year, even if the shower is considered as minor, and even if the results appear to be negative each year. Many recurrences are probably missed simply because no-one was observing at the time.

In addition, many of the known showers require annual observation to help refine our knowledge of their behaviour and evolution. Here are a few showers that warrant observation:

Centaurids: The IMO (Alpha Centaurids) and Kronk (Theta Centaurids) list differing radiants and periods of visibility but the same maximum date for meteors emanating from Centaurus during February. Observation is required to clarify this activity.

Sigma Puppids: As mentioned previously, this is a newly discovered shower. Observations are required to monitor the evolution of the stream and to determine whether the stream has a period of 5,12 years like the parent comet.

Eta Aquarids and Orionids: Both showers have comet Halley as parent. It is important to monitor these showers to see the effects of the 1986 passage of comet Halley. The Eta Aquarids are poorly visible from the northern hemisphere and the monitoring of this shower is reliant on observers in Australasia and Southern Africa.

Ophiuchids: There is complex activity emanating from Ophiuchus during June, complicated by activity from the Scorpiids and Sagittarids. Observations are required to better understand the nature of this acitivity.

Alpha Capricornids: This shower is observed each year by the BAA, but is a southern shower, and we are better placed to cover the activity and complement their work.

Perseids: The 1993 display, due to the recent passage of the parent comet, was spectacular even from Southern Africa. Rates may increase up to 1997, and the shower warrants a special effort in future years.

Monoceritids (November): Needs observation to confirm the previously discussed periodicity.

Geminids: Though this shower is well observed from the northern hemisphere, our observations can help determine if the proposed model is correct.

6 Conclusions

My paper today has hopefully shown that we can contribute a wealth of information towards meteor astronomy. There exists a host of showers throughout the year suitable for observation. We need nothing more than our bare eyes to make these valuable observations. As was the case some decades ago, ASSA can re-establish itself as a renowned source of meteor observations. All we need is a few dedicated observers prepared to gaze at the heavens.

Acknowledgement

Figure 4 is reproduced with permission of Paul Roggemans of the International Meteor Organisation.

References

[1] Kresak, L., 1982, *Asteroids*, ed. T. Gehrels, University of Arizona Press, p. 300

[2] *Sky and Telescope*, March 1989, p. 245

[3] *Sky and Telescope*, various articles, but including March 1987, p. 243

[4] Roggemans, R. (ed.), 1989, *Handbook for Visual Meteor Observations*, Sky Publishing Corp., p. 114

[5] Roggemans, R., *ibid*, p. 180

[6] Cook, A.F., 1973, Evolutionary and Physical Properties of Meteriods, NASA SP-319, p. 183

[7] Kronk, G., 1988, in *Meteor Streams, a Descriptive Catalogue*, Enslow Publishers

[8] *Sky and Telescope*, May 1986, p. 436

[9] *Sky and Telescope*, February 1987, p. 124

Table 1. Parent bodies of meteor showers.

METEOR SHOWER	PARENT BODY
delta Leonids	MP 1987 SY
delta Pavonids	comet Grigg Mellish 1907 II
April Lyrids	comet Thatcher 1861 I
sigma Puppids	comet Grigg Skjellerup 1902 II
eta Aquarids	comet Halley 1910 II
Daytime Arietids	MP 1566 Icarus
June Bootids	comet Pons Winnecke 1915 III
Perseids	comet Swift Tuttle 1862 III
Cygnids	comet Iras Araki Alcock
alpha Aurigids	comet Kiess 1911 II
Draconids	comet Giacobini Zinner 1900 III
epsilon Geminids	comet Nishikawa Tagamizawa Tago 1987 e
Orionids	comet Halley 1910 II
Taurids	comet Encke 1977 XI and Minor Planets
Leonids	comet Tempel Tuttle 1866 I
Monoceritids (Nov)	comet 1944 I
Andromedids	comet Biela 1852 III
Puppid/Velids	MP 2102 Tantalus
Phoenicids	comet Blancplain 1819 IV
Monoceritids (Dec)	comet Mellish 1917 I
Geminids	MP 3200 Phaethon
Ursids	comet Tuttle 1790

Table 2. Working list of meteor streams. Meteor shower index by date.

SHOWER	MAXIMUM	START	END	SHOWER	MAXIMUM	START	END
Quadrantids	Jan 3	Jan 1	Jan 4	S iota Aquarids	Aug 5	Jul 15	Aug 25
eta Craterids	Jan 13	Jan 10	Jan 16	upsilon Pegasids	Aug 8	Jul 25	Aug 25
delta Cancrids	Jan 16	Jan 13	Jan 21	N delta Aquarids	Aug 12	Jul 14	Aug 25
alpha Crucids	Jan 19	Jan 6	Jan28	Perseids	Aug 12	Jul 23	Aug 23
alpha Centaurids	Feb 8	Jan 28	Feb 23	beta Cetids	Aug ?	?	?
theta Centaurids	Feb 8	Feb 6	Feb 15	kappa Cygnids	Aug 18	Aug 9	Oct 6
delta Leonids	Feb 26	Feb 5	Mar 19	N iota Aquarids	Aug 20	Jul 15	Sep 20
Pyxids	Mar 6	Mar 3	Mar 9	alpha Cygnids	?	Jul ?	Sep ?
gamma Normids	Mar 14	Feb 25	Mar 22	Aurigids	Sep 1	Sep 1	Sep 1
Virginids	Mar 20	Feb 3	Apr 15	beta Cygnids	Sep 17	Sep 16	Oct 6
Camelopardalids	?	Mar 14	Apr 7	Southern Piscids	Sep 20	Aug 31	Nov 2
Geminids	Mar 22	Mar 22	Mar 24	kappa Aquarids	Sep 21	Sep 11	Sep 28
delta Draconids	?	Mar 28	Apr 17	Daytime Sextantids	Sep 29	Sep 24	Oct 5
delta Pavonids	Apr 6	Mar 11	Apr 16	Annual Andromedids	Oct 3	Sep 25	Nov 12
sigma Leonids	Apr 17	Mar 21	May 13	sigma Orionids	Oct 3/4	Sep 14	Oct 29
kappa Serpentids	?	Apr 1	Apr 7	Gemini/Auriga	Oct 7	Oct 5	Oct 10
April Lyrids	Apr 22	Apr 16	Apr 24	October Draconids	Oct 9	Oct 6	Oct 10
sigma Puppids	Apr 23	Apr 16	Apr 25	Northern Piscids	Oct 12	Sep 25	Oct 19
mu Virginids	Apr 25	Apr 1	May 12	epsilon Geminids	Oct 19	Oct 14	Oct 27
alpha Bootids	Apr 28	Apr 14	May 12	Orionids	Oct 21	Oct 2	Nov 7
phi Bootids	May 1	Apr 16	May 12	Leo Minorids	Oct 24	Oct 22	Oct 24
alpha Scorpiids	May 3	Apr 11	May 12	Cetus	Oct 29	?	?
eta Aquarids	May 4	Apr 21	May 12	Southern Taurids	Nov 3	Sep 15	Dec 1
tau Herculids	Jun 3	May 19	Jun 14	Cepheids	Nov 9	Nov 7	Nov 11
chi Scorpiids	Jun 5	May 27	Jun 20	Pegasids	Nov 12	Oct 29	Nov 12
Daytime Arietids	Jun 7	May 29	Jun 29	Northern Taurids	Nov 13	Sep 19	Dec 1
Daytime zeta Perseids	Jun 7	Jun 1	Jun 17	Leonids	Nov 17	Nov 14	Nov 20
Librids	Jun 8	Jun 8	Jun 9	Monoceritids	Nov 21	?	?
Sagittariids	Jun 11	Jun 8	Jun 16	Tucanids	?	Nov 21	Nov 28
theta Ophiuchids	Jun 13	Jun 8	Jun 16	Eridanids	?	Nov 21	Nov 26
Sco/Sgr system	Jun 14	Apr 20	Jul 30	Puppids/Velids	Nov ?	Oct	Jan
Cepheids	Jun 15?	Jun 14	Jun 18	Hydrids	?	Nov 22	Nov 26
June Lyrids	Jun 16	Jun 11	Jun 21	Orionids	?	Nov 24	Nov 26
Ophiuchids	Jun 20	Jun 17	Jun 26	Andromedids	Nov 27	Nov 6	Dec 1
Piscis Australids	Jun 26	Jun 24	Jun 29	Phoenicids	Dec 5	Dec 3	Dec 5
Corvids	Jun 26	Jun 25	Jun 30	Monoceritids	Dec 10	Nov 27	Dec 17
Cetids	Jun 28	Jun 26	Jun 29	Northern chi Orionids	Dec 10	Dec 4	Dec 15
June Bootids	Jun 28	Jun 5	Jul 19	sigma Hydrids	Dec 11	Dec 3	Dec 15
Daytime beta Taurids	Jun 29	Jun 24	Jul 6	11 Canis Minorids	Dec 11	Dec 8	Dec 14
Sagittariids	Jul 8?	Jul 1	Jul 14	Southern chi Orionids	Dec 11	Dec 7	Dec 14
July Phoenicids	Jul 14	Jul 3	Jul 18	Geminids	Dec 14	Dec 4	Dec 16
omicron Draconids	Jul 16	Jul 7	Jul 24	delta Arietids	?	Dec 8	Dec 14
Capricornids	Jul 26	Jul 10	Aug 5	Piscids	Dec 16?	?	?
Piscis Australids	Jul 28	Jul 9	Aug 17	Ursids	Dec 22	Dec 17	Dec 24
S delta Aquarids	Jul 29	Jul 21	Aug 29	Coma Berenicids	?	Dec 12	Jan 23
alpha Capricornids	Jul 30	Jul 15	Aug 25	Velids	Dec 29	Dec 5	Jan 7

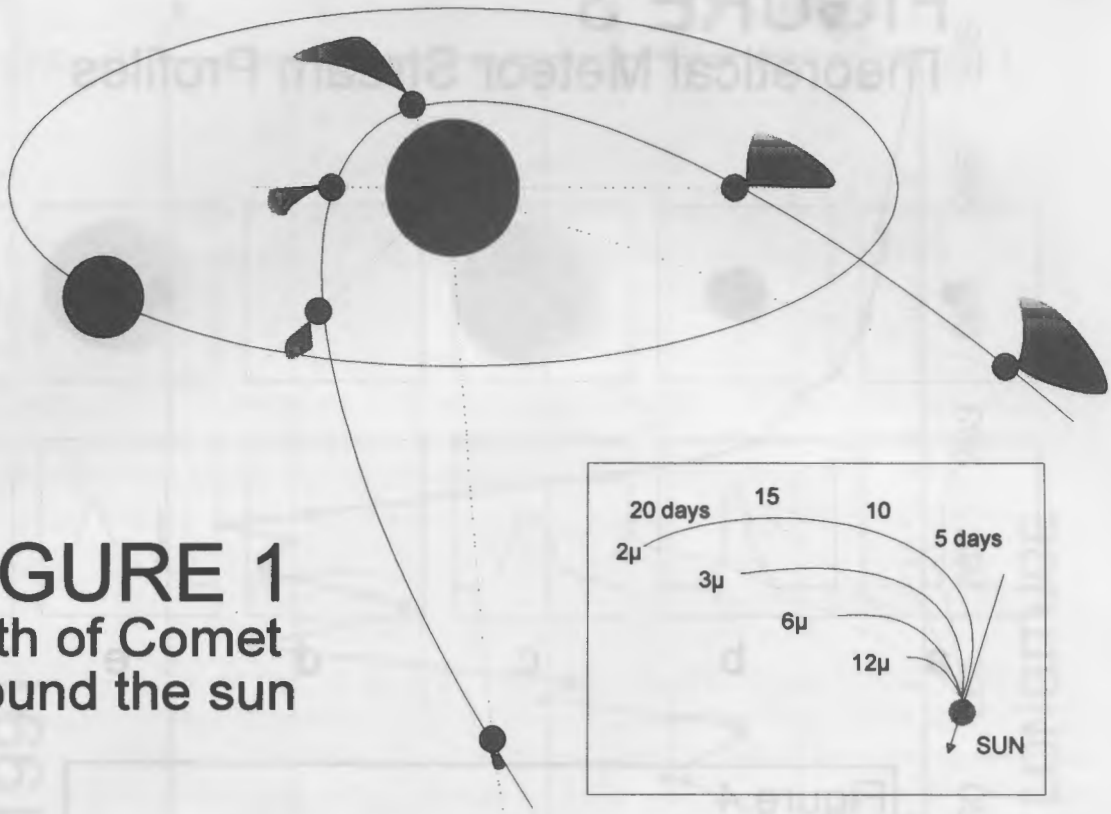

FIGURE 1
Path of Comet around the sun

FIGURE 2
Encounter of the earth with the Meteor Stream

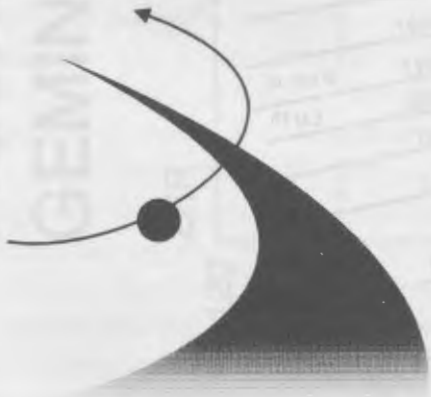

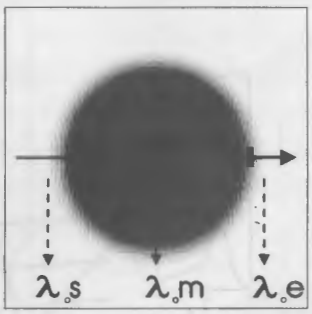

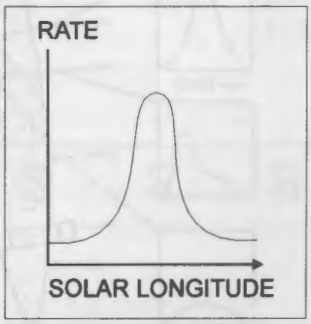

FIGURE 3
Theoretical Meteor Stream Profiles

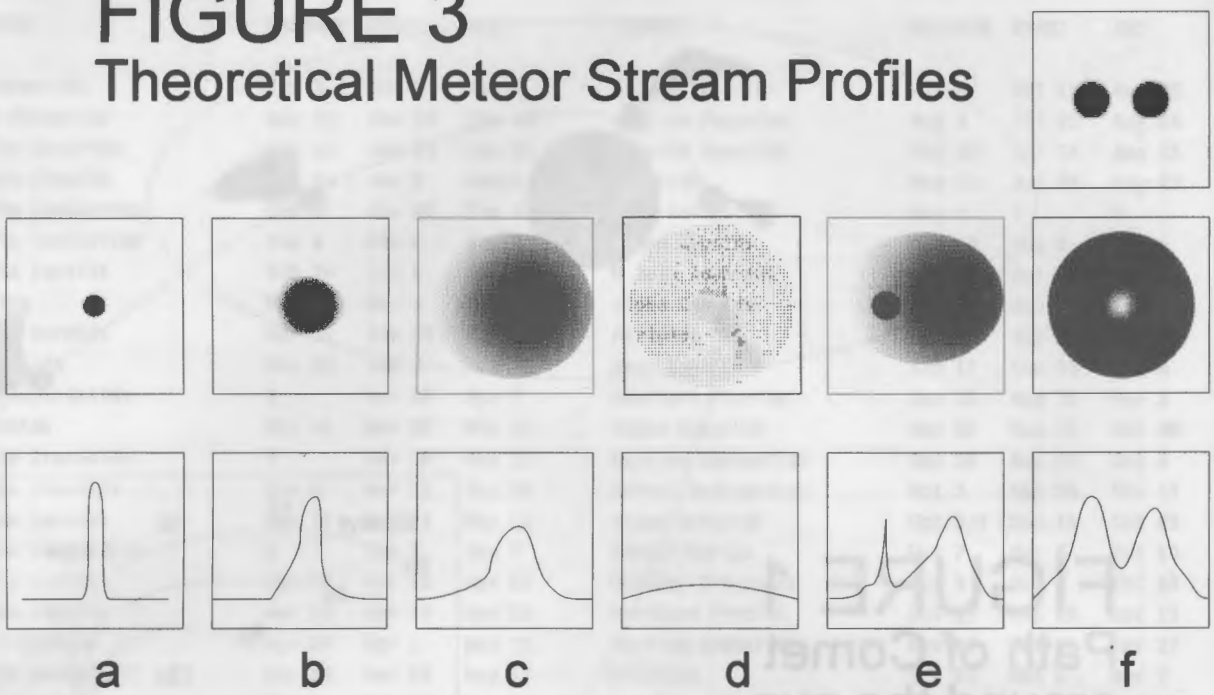

Figure 4
Modelled Activity Profiles
Geminid Meteor Shower

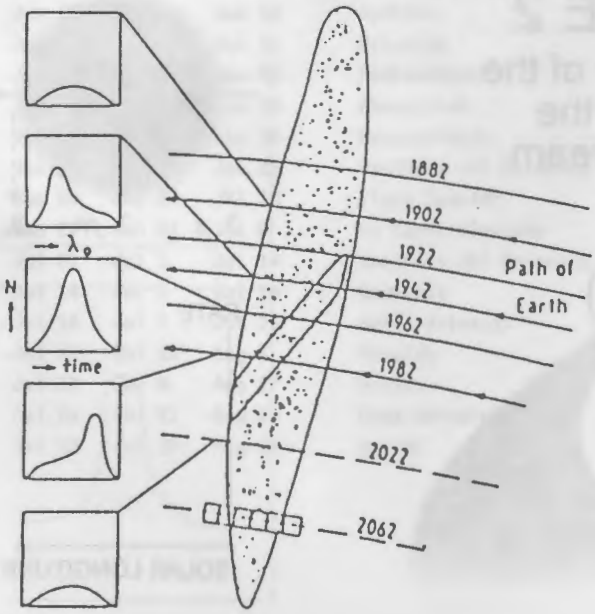

FIGURE 5
GEMINID RATES 1991

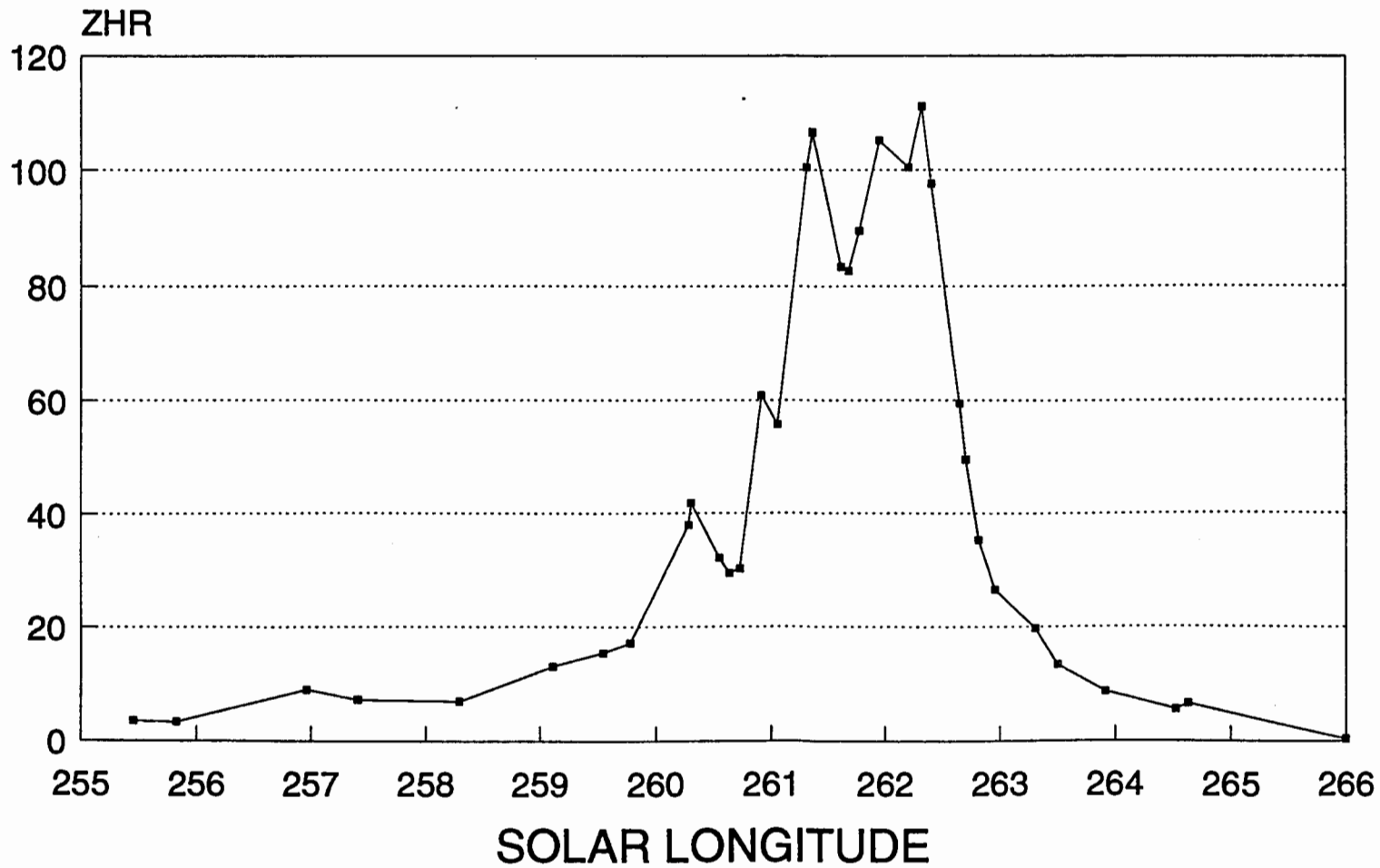

TeV Gamma-Ray Astronomy in South Africa

B Christo Raubenheimer
Space Research Unit, Department of Physics,
Potchefstroom University for CHE, Potchefstroom, 2520

Abstract

The Atmospheric Cerenkov Technique, as the basic principle of TeV gamma-ray astronomy is overviewed. The contribution of South Africa to this field is briefly discussed. A detailed overview of the new gamma-ray telescope of the Potchefstroom University is also given.

1 Introduction

Cerenkov (1937) discovered that relativistic particles (E≥20 MeV in air) could produce visible light when moving through a medium. The produced light is coherent, of short duration (a few nanoseconds) and is emitted in a cone with axis parallel to the incoming particle. In air the cone is very flat and can be easily detected against the Night Sky Background. It was soon realized that this effect could be used to study very high energy photons (with energies ≥100 GeV) coming from stellar objects. Such a photon enters the atmosphere and collides with an atmospheric nucleus producing a shower of relativistic electrons. The first collision usually takes place at an altitude of ~12 km and the resulting shower of electrons produces a light cone with a lateral diameter of a few hundred metres at sea level. Unfortunately, a similar signal can be produced by primary protons of cosmic ray origin and it is known that this effect was the main culprit for the slow development of this field. This so-called Atmospheric Cerenkov Technique (ACT) is the only possible way of studying gamma-rays at these energies.

The first detection of a Cerenkov signal of atmospheric origin was made by Galbraith & Jelley (1953). They used small detectors and could identify the signal as coming from extra-terrestrial cosmic rays. During 1973 and 1974 Grindlay et al. (1975) used the optical interferometer at Narrabri in Australia in the first TeV gamma-ray experiment in the Southern Hemisphere. He was able to detect the first southern source namely Cen A, the well known active radio galaxy. The first custom-made TeV gamma-ray telescope (a single 10 m tesselated reflector) started operation on Mt. Hopkins in the USA twenty-five years ago.

The initial results were disappointing and it was only during the 1980s that real progress was made with the concerted effort by a number of groups to use the periodic signature of known high energy objects to discriminate against the ever present background of Cerenkov events produced by high energy charged particles. Today there are 12 active TeV gamma-ray telescopes world wide (See Weekes 1992 for a review).

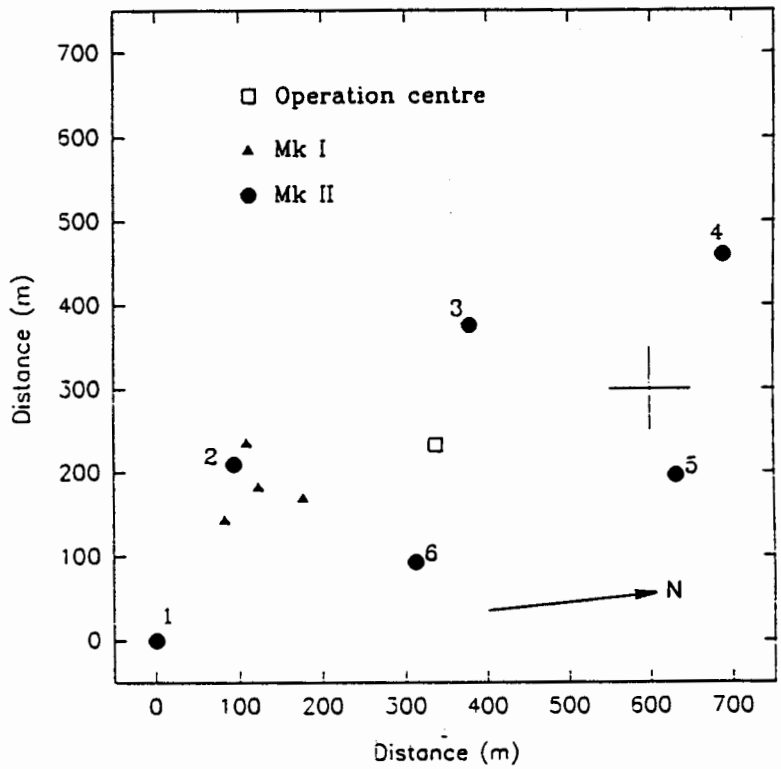

Figure 1: Ground plan of the Nooigedacht MkI and MkII gamma ray telescopes. The cross represents 26.9° S, 27.2° E.

2 The Mk I telescope

During April 1985 the Nooitgedacht Mk I gamma-ray telescope was commisioned to perform a viability study in the use of the Atmospheric Cerenkov Technique as a tool to glean additional information about the physical processes occuring in a range of stellar objects. The telescope is situated 35 km south of Potchefstroom in the Vredefort Dome (latitude 26,9°S, longitude 27,2°E, 1438 masl). The winter skies are clear and dry and are therefore ideal for such telescopes.

The telescope consists of four equatorially mounted mini-telescopes (MTs), 55 m apart (Figure 1). It uses a total of twelve f/0,43 rhodium coated searchlight mirrors (diameter 1,5 m) as reflectors (De Jager et al., 1986). Each MT contains three light detectors (LDs) consisting of a mirror focusing on a Philips XP2020Q photomultiplier tube (PMT).

The signals from the three LDs are fed to a 10ns coincidence channel which eliminates the flux of uncorrelated Night Sky Brightness. These ACT events are then latched to a rubidium oscillator where the arrival time is registered with an accuracy of 0,1μs. Through a telephone linkage to the CSIR time service, we are able to calibrate the local clock with UTC within an uncertainty of 0,1 ms. This timing system allowed the analysis of data from rapidly spinning objects like millisecond pulsars. The Mk I has a cosmic ray event rate of 1 Hz and an energy threshold ranging from 1 to 2 TeV. Most of these events are produced by the high energy proton background and the gamma-ray signal for detected sources usually consists of not more than a few percent of this isotropic background.

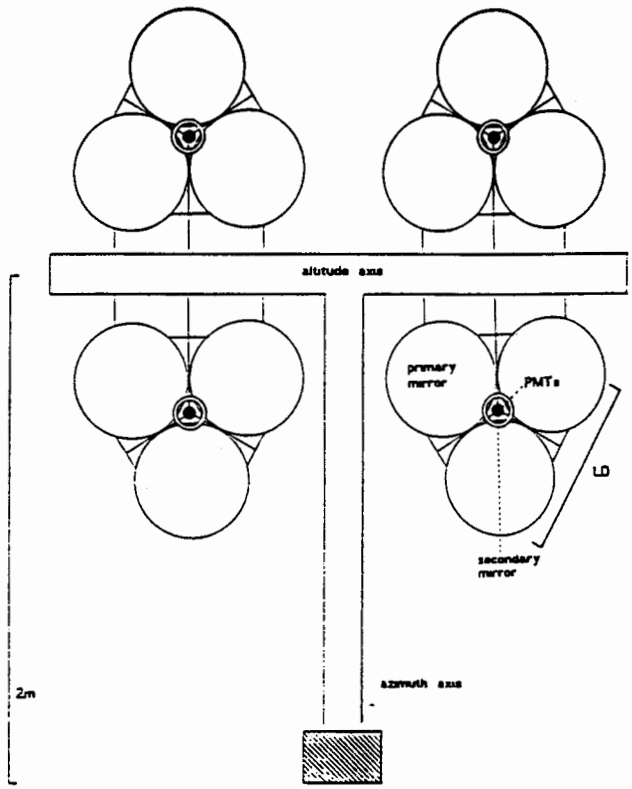

Figure 2: Schematic diagram of a MkII mini-telescope.

the optical characteristics of the mirrors and PMTs into consideration. It was assumed that the fluctuations in the number of photons and photo-electrons were Poissonian. We assumed an array of mini-telescopes and varied the following parameters: (i) the number of LDs per MT (Regardless of the number of LDs considered, an ACT event was defined when the number of photo-electrons in at least three LDs at any single MT exceeded a predetermined level), (ii) the mirror area per LD, (iii) the coincidence conditions between the LDs, (iv) the distance between the MTs (200 to 500 m), (v) the number of MTs and (vi) the configuration of the MTs. Throughout the study, the field of view was kept constant at $\sim 2^\circ$ in order to utilize the full Cerenkov light pulse.

The Mk II telescope resulting from these simulations is shown in Figures 1 and 2. It is deployed on the same terrain as the Mk I. It will consist of six MTs, with the distance between them ranging from 225 to 322 m (average 290 m). The MTs will be controlled from a central laboratory by means of six PCs linked through optical fibre to the MTs.

3.1 Light Detector (LD)

Each Cerenkov Light Detector (see Figure 2) consists of three adjustable spherical mirrors forming a f/1 primary collector with a focal distance of 1,94 m.

In the prime focus a photomultiplier with a 44 mm window defines a FWHM field of view of 1,5° for the on-source beam. The PMT is a Philips XP2242 with a silica window to partially suppress ultraviolet-rich proton showers (Zyskin et al, 1987). It is a 6-stage

system with a gain of $\sim 2\times10^5$ and a peak photon sensitivity at 320 nm. Simultaneous off-source measurements are made by using a Cassegrain ring mirror around the optical axis which focuses the light onto a second XP2242 PMT situated at the centre of the primary collector (Figure 2). This off-source annular field of view subtends an angle of 1,5° FWHM and is displaced from the on-source region by 4,0°. Since the ACT events are distinguished by a coincidence between at least three LDs we can operate the PMTs in the noise at a level of up to 20 kHz.

3.1.1 Mirrors

The primary collector consists of three, 6 mm thick locally produced glass mirrors, each with a diameter of 86 cm. They are slumped from flat soda glass in a mould with a 20 hour heating cycle resulting in a stress-free mirror. An aluminium layer is deposited under vacuum on the front surface. The aluminium layer is protected by a half wavelength (at 320 nm) amorphous aluminium oxide layer (Chemically deposited by the method of Hass, 1948). This layer is a selective interference reflector with a maximum reflection coefficient of 84% at 320 nm decreasing to 74% at 600 nm, suppressing some of the Night Sky Background which peaks in the red. This reflectivity is larger than the 55 to 65 % of the old rhodium reflectors. The higher reflectivity further enhances the effective reflector area which will be 42 m^2 compared to 21 m^2 of the MK I.

The secondary mirror is a 5 cm wide, machine polished, aluminium ring with an inner radius of 15 cm. It has a conical shape with a half top angle of 87°.

3.2 Mini Telescope (MT)

Each MT consists of four LDs (Figure 2) mounted paraxially. The LDs will operate in a three- or four-fold coincidence with a 10 ns gate, again slightly enhancing the gamma-ray signal, with its thinner Cerenkov light disk (Kenter, 1989). According to our simulations we expect a cosmic ray event rate of 0,6 Hz per MT with up to 5% of the events triggering more than one MT. The average expected energy threshold will be 0,7 TeV.

The four LDs are mounted on an alt-azimuth frame, with observations limited to zenith angles smaller than 60°. This will enable us to extend our sky coverage by 15° in declination (both north and south) and enable us to overlap our observations with the TeV telescopes in the Antarctic and Australia. Steering will be accomplished by absolute shaft encoders and stepper motors which are computer controlled and can maintain position to within 0,03°. Both tracking and drift scanning of objects will be possible.

4 Electronics

The PMT electronics were locally designed and consist of a Cockroft-Walton High Voltage supply on each PMT feeding the anode grounded dynode chain. Each PMT has a paddinglight servo loop keeping the current through the PMT constant during an observation. The PMT pulses are fed into an amplifier / discriminator and after a 10 ns AND-gate the 10 MHz clock (synchronized from a rubidium oscillator) is latched. All these circuits were designed locally and consist of hybrid surface mounted devices.

The time of arrival as well as other housekeeping information is then transferred through a RS232 optical fibre link to the laboratory, where the information is finally stored on 3.25 inch disks.

The registration of arrival times is with an accuracy of 0,1μs, controlled by a rubidium standard. UTC matchup is automatically achieved through a direct computer link via telephone cable to the national time calibration facility as well as a calibrated time signal on the commercial television broadcasts. This will ensure an accuracy of $\sim$1 ms in UTC matchup.

5 Conclusions

Although the total reflecting area of the Mk II (41 m^2) is only twice that of the Mk I, the improvement in counting rate proves to be a factor $\sim$5 - a result of the large distances between the MTs and the better quality and design of the optics. When the larger sky coverage and the simultaneous off-source measurements are taken into account we expect that the Mk II will be $\sim$10 times more sensitive than the Mk I. The first MT has started observations during October 1993 and the results so far corroborate the model predictions. Full operation of the telescope is expected to be winter 1994.

With the new telescope we hope to stay in the forefront of TeV gamma-ray astronomy, a new and exciting branch of astronomy to which South Africa can make a significant contribution without competition from space experiments.

Acknowledgements

All my colleagues in the Space Research Unit are thanked for their contributions towards the success of the Nooitgedacht telescopes. The financial support of FRD is gratefully acknowledged. We would like to acknowledge the essential contributions of the following persons and groups: PFG (Architectural) for the mirrors, the University's Geology and Instrumentation departments as well as Technical Services for the development of the infrastructure, Gerrit van Urk, Johan van der Merwe, Josef le Grange, Gerrit Lachmann, and Jim Gaidos.

References

[1] Brink, C., et al. 1990, *Ap. J.*, 346, L37.

[2] Brink, C., et al. 1993, *Ap. J.*, submitted.

[3] Cerenkov, P.A., 1937, *Phys. Rev.*, 52, 378.

[4] De Jager, H.I., et al. 1986, *S.A. Journ. Phys.*, 9, 107.

[5] De Jager, O.C., et al. 1988, *Ap. J.*, 329, 831.

[6] Galbraith, W. & Jelley, J.V. 1953, *Nature*, 171, 349.

[7] Grindlay, J.E., et al. 1975, *Ap. J.*, 197, L9.

[8] Gibson, A.I., et al. 1982, in *VHE Gamma-ray Astronomy* (Reidel), 97.

[9] Hass, G., 1948, *Journ. Optical Soc. Am.*, 39, 532.

[10] Kenter, A.T., 1989, *PhD-thesis, University of Madison, Wisconsin* (unpublished).

[11] Kerzman, M.P. & Sembrowski, G.H., 1993, *N.I.M.*, submitted.

[12] Meintjes, P.J., et al. 1992, *Ap. J.*, 401, 325.

[13] Nel, H.I., et al. 1992, *Ap. J.*, 398, 602.

[14] North, A.R., et al. 1986, *Nature*, 326, 567.

[15] North, A.R., et al. 1991, *Proc. 22nd Int. Conf. Cosmic Rays*, 1, 340.

[16] Raubenheimer, B.C., et al. 1986, *S.A. Journ. Sci.*, 84, 461.

[17] Hillas, A.M. & Patterson, J.R., 1990, *Journ. Phys. G.*, 16, 1271.

[18] Weekes, T.C., 1992, *Sp. Sci. Rev.*, 59, 315.

[19] Zyskin, Y.L., et al. 1987, *Proc. 20th Int. Conf. Cosmic Rays*, 2, 342.

GRAVITATIONAL WAVE CALCULATIONS ON NULL CONES

N T Bishop*
Department of Mathematics, Applied Mathematics and Astronomy, University of South Africa, P.O. Box 392, Pretoria, 0001

Abstract

It is likely that gravitational waves will be detected within the next decade. Gravitational wave theory is reviewed, and methods for calculating gravitational waves numerically, from astrophysical events, are discussed.

1 Introduction

Astronomical observations have been based almost entirely on the electromagnetic spectrum. Before the 1950's the only part of the spectrum that could be used was visible light, but now virtually the whole spectrum is open for observation, either through radio astronomy or through observations from satellites. This opening-up of the electromagnetic spectrum has played an important role in the development of our knowledge and understanding of the Universe.

It is likely that within the next decade gravitational waves will be detected [1], and this will permit a completely new class of observations that can "see" into the centre of energetic astrophysical processes. It is possible that gravitational wave astronomy will be as important in the next century as radio astronomy was in the second half of this century.

In section 2, the theory of gravitational waves, as well as prospects for their detection, are reviewed, and then, in section 3, methods for calculating gravitational waves numerically are discussed.

2 Gravitational waves

The basic idea is that the metric of general relativity g_{ij} is written as the Minkowski metric η_{ij} of that spacetime, plus a small correction h_{ij}. For the case of a plane wave moving in the x-direction:

*I thank the Foundation for Research Development for financial support.

$$g_{ij} = \eta_{ij} + h_{ij} = \begin{pmatrix} -1 & 0 & 0 & 0 \\ 0 & 1 & 0 & 0 \\ 0 & 0 & 1 & 0 \\ 0 & 0 & 0 & 1 \end{pmatrix} + \begin{pmatrix} 0 & 0 & 0 & 0 \\ 0 & 0 & 0 & 0 \\ 0 & 0 & a & b \\ 0 & 0 & b & -a \end{pmatrix} \tag{1}$$

with $a = a(t-x), b = b(t-x)$. For example, an harmonic wave at frequency ω would have

$$a = a_0 \sin[\omega(t-x)], b = b_0 \sin[\omega(t-x)] \tag{2}$$

where $a_0, b_0 (\ll 1)$ are the amplitudes of the two modes of polarisation. Suppose that two particles are distant l apart in the y plane. Then the effect of the gravitational wave (2) is to induce an acceleration in the proper distance between the two particles of

$$-\frac{1}{2} l\omega^2 (a_0 + b_0) \sin[\omega(t-x)] \tag{3}$$

It is this effect that various types of gravitational wave detector attempt to measure.

Gravitational waves are generated by changes in the relative motion of matter. For slow-moving, nearly Newtonian sources, the quadrupole moment of the source is defined as:

$$I_{ij} = \int_V \rho \left(x_i x_j - \frac{1}{3} \delta_{ij} x_k x_k \right) d^3x \tag{4}$$

Then the gravitational wave power output of the source is

$$\frac{dE}{dt} = \frac{1}{5} < \frac{d^3}{dt^3} I_{ij} \frac{d^3}{dt^3} I_{ij} > \tag{5}$$

where <> means time-averaged. To leading order, the metric perturbation is

$$h_{ij} = \frac{2}{r} \ddot{I}_{ij}^{TT}(t-r) \tag{6}$$

where r is the distance from the source, and $\ddot{I}_{ij}^{TT}$ is a technical variation of I_{ij} [2].

The above quadrupole formulas (4) to (6) are approximate, and the approximations would not be valid for strong gravitational fields such as black holes, or even neutron stars. In such cases, an accurate calculation of the gravitational wave field requires the full general theory of relativity, and has to be done numerically.

Over the years there have been many attempts made to detect gravitational waves, but to date the sensitivity of the experiments has not been sufficient. However, the decision by the United States to fund the LIGO (Laser Interferometry Gravitational Observatory) [1] project means that by the year 2000 gravitational waves will probably have been measured. One can calculate the probable magnitude of $\ddot{I}_{ij}^{TT}$ for various astrophysical events, and then use equation (6) to estimate the magnitude of the gravitational waves as a function of the distance r of the event from the Earth. The expected sensitivity of the first LIGO (expected in 1998) will be 10^{-21}, and the advanced system will have a sensitivity of 10^{-23}. This will be sufficient to detect several inspiralling events per year.

The important point is that a negative result would also be significant. It would mean that there was something seriously wrong with our understanding of astrophysical processes, or that equations (4) to (6) do not apply.

3 Numerical relativity

Most work on numerical relativity has been based on the $3+1$ Cauchy problem, where data are specified on a spacelike hypersurface and then evolved to the future [e.g. 3 – 5]. One problem with the Cauchy approach is that, for practical computer reasons, the outer boundary of the computational domain is in the strong-field region. An alternative approach based on the characteristic initial value problem (CIVP) on null cones will be described. In this case it is possible to compactify the radial coordinate so that the outer boundary of the computational domain is future null infinity.

The numerical formulation of the CIVP of general relativity has been studied by several authors [e.g. 6-10], particularly the case of axisymmetry without rotation in vacuum.

The coordinates are based on a family of outgoing null cones with vertices along a timelike geodesic G. The proper time along G is u, and u is constant everywhere on a given null cone. The radial coordinate r is the luminosity distance from the null cone's vertex. Angular coordinates θ, ϕ are defined in the usual way near $r = 0$ and propagate outwards in the null cone by means of radial null geodesics. We assume axial symmetry and so the metric is independent of ϕ. It is convenient to make the substitution

$$y = -\cos(\theta) \tag{7}$$

and the metric is then

$$ds^2 = -h_u du^2 - 2h_r du dr + 2h_y du dy + r^2 \left(\frac{e^{2q}}{F} dy^2 + F e^{-2q} d\phi^2 \right) \tag{8}$$

where h_u, h_r, h_y and q are functions of u, r and y, and $F = (1 - y^2)$. At the origin the coordinates must be a smooth Fermi system; this implies

$$h_u = +1 \;\; h_r = +1 \;\; h_y = 0 \;\; h_{y,r} = 0 \;\; q = 0 \tag{9}$$

Einstein's equations are

$$0 = E_{ab} = G_{ab} - kT_{ab} \tag{10}$$

where T_{ab} is the stress-energy tensor. The remarkable point about Einstein's equations is their simple form as a hierarchy of linear differential equations in r, with dependence on y as a parameter.

The required initial data are q everywhere on a null cone u=constant. Despite their structural simplicity, Einstein's equations are nevertheless very long and are not reproduced here. We will use $c_1, c_2 ... c_7$ to represent coefficients in the equations that depend on q and on metric variables that have been found earlier in the hierarchy. By 'depend' is meant functional dependence on the variable and on its derivatives within the null cone, specifically $_{,r,rr,y,yy,ry}$.

$$E_{11} = 0 \text{ is } 0 = c_1 h_r + h_{r,r} \text{ and leads to } h_r.$$

$$E_{12} = 0 \text{ is } 0 = c_2 + c_3 h_y + c_4 h_{y,r} + h_{y,rr} \text{ and leads to } h_y.$$

$$E_{10} = 0 \text{ is } 0 = c_5 + c_6 h_u + h_{u,r} \text{ and leads to } h_u.$$

$$EV = E_{22} - \frac{1}{2} g_{22} \left(g^{22} E_{22} + g^{33} E_{33} \right) = 0$$

$$\text{is } 0 = c_7 + (r q_{,u})_{,r} \text{ and leads to } q_{,u}. \tag{11}$$

In the CIVP we expect $q \propto f(u)$ for large r, so that in numerical computation δr can become large. Note that δr cannot be made large in the Cauchy formulation: the gravitational field variables $\propto f(t-r)$, so that both δt and δr must be much smaller than the wavelength of gravitational radiation.

We therefore investigate the compactification of the r coordinate within the context of the CIVP. An obvious and simple way to do this [11] is to make the coordinate transformation $r \to z$ where

$$r = z/(1-z), \; z = r/(1+r) \tag{12}$$

Making this transformation in the metric (6) leads to Einstein equations that are strongly singular at $z = 1$, in that they involve terms $(1-z)^{-n}$ with n as large as 4. It is therefore clear that for progress to be made the metric will have to be written in another form. Inspired by the form of the Bondi metric at future null infinity [8,12] and after some trial and error, we write the metric as

$$ds^2 = -\overline{h_u} r^2 e^{2\overline{q}} du^2 - 2\frac{e^{2\overline{b}} r^2}{z^2} du dz + 2\overline{h_y} r^2 e^{2\overline{q}} du dy + r^2 \left(\frac{e^{2\overline{q}}}{F} dy^2 + F e^{-2\overline{q}} d\phi^2 \right) \tag{13}$$

The coordinates are u, z, y and ϕ with $r = z/(1-z)$ and, as before, $F = (1-y^2)$. The metric variables $\overline{h_u}, \overline{b}, \overline{h_y}$ and $\overline{q}$ are functions of u, z, and y. The relationship between this metric and the metric (8) is

$$\overline{q} = q, \; \overline{b} = \ln\left(h_r^{\frac{1}{2}}\right), \; \overline{h_y} = \frac{h_y}{r^2 e^{2q}}, \; \overline{h_u} = \frac{h_u}{r^2 e^{2q}}. \tag{14}$$

The appropriate Einstein equations for the metric (13) were calculated using the computer algebra system REDUCE. The resulting equations appear to have some singularities at $z = 1$ in the form of terms with $(1-z)^{-1}$. However, we will show that all the solutions of the differential equations are, in fact, regular at $z = 1$. In order to do this we first note the behaviour, at $x = 0$, of the singular equation:

$$x \frac{dy}{dx} + (g_0 + x g_1(x)) y + (f_0 + x f_1(x)) = 0 \tag{15}$$

where f_0, g_0 are constant and $f_1(x), g_1(x)$ are regular at $x = 0$. The solution $y(x)$ is regular at $x = 0$ provided $g_0 < 0$; in this case the solution is

$$y = -(f_0/g_0) + Cx^{-g_0} + x \times \text{ (regular function of x)}. \tag{16}$$

In order to use the result (16) for the solution of Einstein's equations, we make the substitution $(1 - z) = x$ and note that $d/dz \to -d/dx$. $E_{11} = 0$ for the metric (13) is

$$\frac{d\bar{b}}{dz} = \frac{z(1-z)}{2}\left(\frac{d\bar{q}}{dz}\right)^2 \tag{17}$$

Numerical integration at $z = 1$ is straightforward; and further, a boundary condition on $d\bar{q}/dz$ at $z = 1$ is not required. $E_{12} = 0$ is of the form

$$\frac{dp}{dx} - \frac{2}{x}p\left[1 + xg_1(x)\right] - \frac{4e^{2(\bar{b}-\bar{q})}}{x}\frac{d\bar{b}}{dy}\left[1 + xf_1(x)\right] = 0 \tag{18}$$

where $p = d\overline{h_y}/dx$. The result (16) applies with $g_0 = -2$. Thus $d\overline{h_y}/dz$ is regular at $z = 1$ and is

$$\frac{d\overline{h_y}}{dz} = 2e^{2(\bar{b}-\bar{q})}\frac{d\bar{b}}{dy}. \tag{19}$$

The value of $\overline{h_y}$ at $z = 1$ can then be found by standard numerical methods. $E_{10} = 0$ is

$$\frac{d\overline{h_u}}{dx} - \frac{3\overline{h_u}}{x}\left[1 + xg_1(x)\right] - \frac{3\overline{h_y}^2}{x}F(y)\left[1 + xf_1(x)\right] = 0$$

The result (18) applies with $g_0 = -3$. Thus $\overline{h_u}$ is regular at $z = 1$ and is

$$\overline{h_u} = F(y)\overline{h_y}^2 \tag{20}$$

The expression $EV = 0$ (from equation (11)) can be written:

$$-x^2\frac{d}{dx}\left(\frac{1-x}{x}\bar{q}_{,u}\right) - \bar{q}_{,y}F(y)\overline{h_y} - \frac{1}{2}\overline{h_{y,y}}F(y) + xf_0 + x^2f_1(x) = 0 \tag{21}$$

Integrating

$$\bar{q}_{,u} = F(y)\left(\bar{q}_{,y}\overline{h_y} + \frac{1}{2}\overline{h_{y,y}}\right) + \frac{x}{1-x}f_0\ln x + xf_2(x) \tag{22}$$

Thus $\bar{q}_{,u}$ is continuous at $z = 1$ and is

$$\bar{q}_{,u} = F(y)\left(\bar{q}_{,y}\overline{h_y} + \frac{1}{2}\overline{h_{y,y}}\right) \tag{23}$$

4 Conclusion

It has been shown how to compactify CIVP coordinates so that a numerical calculation can be extended to future null infinity. These methods, perhaps combined with a Cauchy calculation in a central region, will be important in calculating gravitational waves at future null infinity, which in effect is where they will be measured.

References

[1] Abromovici A et al 1992 *Science* **256** 325-333

[2] Misner C W, Thorne K S and Wheeler J A 1973 *Gravitation* (Freeman, San Francisco) 989-992

[3] Centrella J M (ed) 1986 *Dynamical Spacetimes and Numerical Relativity* (Cambridge: Cambridge University Press)

[4] Evans C R, Finn L S and Hobill D W (eds) 1989 *Frontiers in Numerical Relativity* (Cambridge: Cambridge University Press)

[5] Bardeen J M and Piran T 1983 *Phys. Rep.* **96** 205-50

[6] Bishop N T, Clarke C J S and d'Inverno R A 1990 *Class. Quantum Grav.* **7** L23-L27

[7] Gomez R, Isaacson R A, Welling J S and Winicour J 1986 Numerical relativity on null cones *Dynamical Spacetimes and Numerical Relativity* ed J M Centrella (Cambridge: Cambridge University Press) pp 237-55

[8] Isaacson R A, Welling J S and Winicour J 1983 *J. Math. Phys.* **24** 1824-34

[9] Stewart J M and Friedrich H 1982 *Proc. R. Soc.* A **384** 427-54

[10] Bishop N T 1993 *Class. Quantum Grav.* **10** 333-341

[11] Gomez R, Winicour J and Isaacson R 1992 *J. Comput. Phys.* **98** 11-25

[12] Bondi H, van der Burg M G J and Metzner A W K 1962 *Proc. R. Soc.* A **269** 21-52

The Large Number Hypothesis Re-visited

A Beesham
Department of Applied Mathematics
University of Zululand, Private Bag X1001
Kwa-Dlangezwa

Abstract

A recent generalization of Dirac's large numbers hypothesis has been made which involves implications for the cosmological constant problem. This is analysed and compared with earlier work on the topic. Numerical coincidences have often led to important discoveries. Two of these concerning planetary dynamics and black hole thermodynamics are discussed.

1 Introduction

Numerical coincidences hav always attracted the attention of scientists. Most local dimensionless constants have values within an order of magnitude or so of unity. However there exist a number of notable exceptions which have been highlighted over the years. In this paper we describe some of these large numbers and their possible implications for the cosmological constant. Sometimes such numerological coincidences have led to important scientific discoveries, and we discuss two of these concerning planetary motion and black hole thermodynamics.

2 Large Numbers Hypothesis

Large numbers seem to have first found their way into scientific literature by Archimedes as early as around 216 BC. At the beginning of this century, Weyl, Eddington and Milne noticed coincidences between some very large numbers that occur in nature. For an excellent treatment about this history, we refer to the beautiful papers by Barrow [1,2] and the book by Barrow and Tipler [3]. The mystery surrounding this topic is usually associated with the name of Dirac [4], who initially considered two large dimensionless numbers that could be constructed from fundamental constants and cosmological quantities.

The first was the ration of the electric to the gravitational force between a proton and an electron

$$N_1 = \frac{e^2}{Gm_p m_e} \sim 10^{39} \tag{1}$$

The second was the age of the universe, expressed in atomic units (atomic light-crossing time)

$$N_2 = \frac{t_0}{e^2/(m_e c^3)} \sim 10^{39} \tag{2}$$

Several such large ratios can be constructed [2]. Based on such coincidences between such large numbers, Dirac [5], put forward his so-called *Large Numbers Hypothesis* (LNH) which states that

Any two of the very large dimensionless numbers occuring in Nature are connected by a simple mathematical relation in which the coefficients are of order unity.

Since the number N_2 contains the age of the universe, an immediate consequence of the LNH is that any large number of the order 10^{40} must be equated to N_2, and hence must be time dependent. Thus the LNH provides an explanation for the existence of large numbers of the order $(10^{39})^n, n = 1, 2, 3, ...$, as they are so large simply because the universe is as old as it is. To illustrate this idea further, consider the amount of matter in the visible universe, expressed in terms of the proton mass

$$N = \frac{4\pi (ct)^3 \rho}{3m_p} \sim \frac{c^3 t}{G m_p} \sim 10^{78} \tag{3}$$

According to the LNH, this number must vary as t^2.

Now, from the LNH, the number N_1 must vary as t. Since a variation of e, m_p or m_e would involve conflict with quantum physics, Dirac chose to consider instead a variation of G with time

$$G \sim 1/t \tag{4}$$

The implications of such a proposal have been investigated in great detail (see the list of references in Barrow [2] and Barrow and Tipler [3]).

3 Generalized Large Numbers Hypothesis

In 1935, Eddington [6] found another large number which involved the cosmological constant

$$N_3 = \frac{c}{H_0} \left(\frac{m_p m_e}{\Lambda} \right)^{1/2} \sim 10^{39} \tag{5}$$

where H_0 is the present value of the Hubble parameter. This expression (5) is the ratio of the radius of curvature of de-Sitter spacetime to the geometric mean of the electron and Compton wavelengths. Now according to Dirac's LNH, the number N_3 increase with time as

$$N_3 \sim t \tag{6}$$

Since there was no reason for Dirac to believe in a variable Λ, the obvious colclusion was that it must vanish.

Instead of considering $\Lambda = 0$, Berman [7], in a recent paper, has proposed a generalized large numbers hypothesis (GLNH)

$$N_1 \sim N_2 \sim N_3 \sim \sqrt{N} \sim t \tag{7}$$

From (5) and (7) it follows immediately that

$$\Lambda \sim 1/t^2 \tag{8}$$

The question that arises is whether it is really necessary to postulate a GLNH.

To answer this question, we note firstly that N_3 is a large dimensionless number which, according to the LNH, must vary as t. This means that either Λ must vanish, as pointed out by Dirac [5], or that Λ must vary as in (8) [2,3]. Hence it is not necessary to elevate the status of relation (5) to that of a GLNH, since relation (5) is but a consequence of the LNH.

Secondly the relationship (8) can also be derived from the LNH without recourse to the number (5) [8]. Consider Einstein's field equations (in suitable units) of general relativity with the cosmological term

$$R_{ab} - \frac{1}{2} R g_{ab} + \Lambda g_{ab} = G T_{ab} \tag{9}$$

where R_{ab} is the Ricci tensor, R the Ricci scalar, g_{ab} the metric tensor and T_{ab} the energy-momentum tensor. Let us try to make these equations compatible with the LNH with the minimum amount of modification possible. The LNH requires that G be a function of time as in relation (4). Now the Bianchi identities and the divergenceless of the energy-momentum tensor are, respectively,

$$\left(R_{ab} - \frac{1}{2} R g^{ab}\right)_{;b} = 0 \tag{10}$$

$$T^{ab}_{;b} = 0 \tag{11}$$

From equations (9), (10) and (11) we obtain

$$\Lambda_{;b} g^{ab} = G_{;b} T^{ab} \tag{12}$$

Since G is a function of time, it cannot have zero divergence, and thus equation (12) implies that Λ cannot be constant. Thus Dirac's LNH is not compatible with Einstein's general relativity. The simplest assumption that we can make about Λ is that it is a scalar function of time, and it only remains to determine its actual time dependence.

Let us consider the perfect fluid form for the energy-momentum tensor

$$T_{ab} = (\rho + p)\, u_a u_b + p g_{ab} \tag{13}$$

where ρ is the energy density, p the pressure and u_a the four-velocity of the fluid. In cosmology, it is always possible to choose $g_{00} = -1$. Then, taking the "00" component of equaiton (13), we obtain

$$T^{00} = \rho \tag{14}$$

Thus equation (12) yields

$$\dot{\Lambda} = -\rho\dot{G} \tag{15}$$

where the overdot denotes a derivative with respect to time.

We now only need the form of the energy density ρ to determine the time dependence of Λ. This may also be derived from the LNH as follows [5,8,9]. Assuming that mass is conserved (Dirac also considered the case when mass is not conserved [5], but later abandoned this idea [9]), we obtain

$$\rho R^3 = \text{ constant}$$

Dirac then considered the general expansion of the universe to be given by

$$R \propto t^n$$

Take a particular galaxy whose velocity of recession is 1/2. (We are using units in which the speed of light is unity.) This may be written as

$$\dot{R} = \frac{nR}{t} = \frac{1}{2}$$

Hence the distance of the galaxy from us is $t/(2n)$, so the total mass within this distance is proportional to ρt^3. By the LNH (3), this number must vary as t^2, and we then have

$$\rho t^3 \propto t^2$$

or the required result

$$\rho \propto \frac{1}{t} \tag{16}$$

From (4), (15) and (16), we then obtain our desired result

$$\Lambda \sim \frac{1}{t^2}$$

It is interesting to note that this time dependence of Λ provides a phenomenological solution to the cosmological constant problem [7]. Λ is so small now simply because the universe is as old as it is.

Hence, we may conclude that it is not necessary to postulate a GLNH as the so-called generalization follows directly from the LNH.

4 Planetary dynamics

In 1766, von Wittenberg [10] gave an algorithm for generating the radii of the planets

$$r_n = 0.4 + 0.3 \times 2^n; n = 0, 1, 2, ... \tag{17}$$

This formula agreed well with the radii of the six planets known at the time: Mercury, Venus, Earth, Mars, Jupiter and Saturn. Below are indicated the then measured values for these distances, as well as the predicted values according to (17)

Planet	Measured r_n (in AU)	n	"Predicted" r_n
Mercury	0.39	–	0.4
Venus	0.72	0	0.7
Earth	1.00	1	1.0
Mars	1.52	2	1.6
Jupiter	5.20	4	5.2
Saturn	9.55	5	10.0

It is interesting to note that the formula (17) is associated with the name of Bode [10], who inserted it into his astronomy book in 1772, but without reference to von Wittenberg.

The numerological relation (17) led to two great scientific discoveries. Firstly, it led to the discovery of Uranus by Hershel in 1781, which was found at exactly the predicted distance $r_6 = 19,2$ AU. Secondly, we see from the above table that there is a gap at $r_3 =$ 2.8 AU. An extensive search at this distance revealed the existence of the asteroid belt. This was regarded as a success for the formula since the asteroid belt could conceivably have been formed from the disintegration of a planet.

However, it also had two major failures. The next two predicted values are $r_7 = 38.8$ AU and $r_8 = 77.2$ AU. This was found to be in complete disagreement with the discoveries of Neptune and Pluto at 30.1 and 39.5 AU respectively. The question of whether the law (17) is physically relavant or whether it is possible to write the radii of the planets in such a numerological fashion continues to attract the attention of planetary astronomers to the present day.

5 Black Hole Thermodynamics

It was known before 1974 that the theoretical relations governing mechanical interactions between black holes were very similar to the laws of thermodynamics (see Barrow and Tipler [3] and references therein). If an entropy is associated with the area of a black hole, and a temperature with its surface gravity, then the zeroth, first and second laws of thermodynamics are equivalent to known properties of black holes. These similarities were not treated seriously since, from the classical viewpoint, no particle could emerge from a black hole. Hence, one could not associate a temperature with the black hole as it was not radiating.

However, spurred on by these coincidences, Hawking [11] discovered that black holes can radiate particles due to quantum effects, and thus they are black bodies. The surface area and gravity of the black hole determine the entropy and temperature of the radiated particles and the laws of equilibrium thermodynamics are obeyed. This discovery has led

to a tremendous flood of interest in exploring the inter-connections between general relativity, quantum mechanics an thermodynamics. This interest has arisen largely because of nemerological coincidence.

6 Conclusion

In this paper, we have explained the LNH and some of its implications for cosmology, in particular for the cosmological constant problem. Numerical coincidences have led to important discoveries, and we have discussed two of these, viz., in planetary dynamics and in black hole thermodynamics. No doubt, they will continue to lure scientists into studying them, and to lead to important discoveries in future. For further reading and for more references, we refer to Barrow [1,2] and to Barrow and Tipler [3].

7 Acknowledgements

I would like to express my sincere thanks to the organisers of the conference for their excellent organizations at the Second ASSA Symposium at the University of South Africa in Pretoria. The FRD provided financial support, for which I am grateful.

References

[1] Barrow, J.D., *Q. J. R. astr. Soc.* **22** (1981) 388.

[2] Barrow, J.D., in *Modern Cosmoloby in Retrospect*, ed. B. Bertotti, R. Balbinot, S. Bergia and A. Messina, Cambridge University Press, Cambridge, 1990.

[3] Barrow, J.D. and Tipler, F.J., *The Anthropic Cosmological Principle*, Oxford University Press, Oxford, 1986.

[4] Dirac, P.A.M., *Nature*, **139** (1937) 323.

[5] Dirac, P.A.M., *Proc. Roy. Soc.* **165** (1938) 199.

[6] Eddington, A.S., *New pathways in science*, Cambridge University Press, London, 1935.

[7] Berman, M.S., *Int. J. Theor. Phys.* **31** (1992) 1217.

[8] Lau, Y.K., *Aust. J. Phys.* **38** (1985) 547.

[9] Dirac, P.A.M., *Proc. Roy. Soc. Lond. A* **365** (1979) 19.

[10] Nieto, M.N., *The Titius-Bode las of planetary distances: its history and theory*, Pergamon, Oxford, 1972.

[11] Hawking, S.W., *Nature*, **248** (1974) 30.

Finding Density Fluctuations at Large Scales

Paul Haines
Department Mathematics, Applied Mathematics and
Astronomy, UNISA, PO Box 392,
PRETORIA, 0001

Abstract

I will describe two methods for looking at density on large scales. The first takes galaxies observed in infrared, by the IRAS satellite. The second method, called POTENT by its inventors (Dekel and Bertschinger), uses the observed peculiar motions of galaxies to find the large scale peculiar velocity field. These two methods can be combined to test various theories of structure formation.

1 Introduction

The standard cosmological model says that the universe is homogeneous and isotropic and expanding uniformly. Astronomers test these statements using a variety of methods. For example, the Hubble expansion shows that the expansion in radial directions is pretty much consistent with uniform expansion.

What does homogeneous really mean here? A homogeneous fluid is the same everywhere, and cosmologists often use the "perfect fluid approximation" although it's very clear that the universe is not homogeneous, since there are clumps (stars, galaxies, clusters, superclusters)[2]. This doesn't faze us though, because we can still say that it's homogeneous at *large scales*. This means, for example, that if I count all the galaxies in a huge sphere of radius 100 Mpc†, this count will be pretty much the same no matter where I place the center of this sphere.

The best evidence of isotropy (which means the universe looks the same in all directions) is the cosmic microwave background radiation (CMB), recently measured by the COBE satellite [3].

The standard theory says that the tiny perturbations observed in the CMB end up as LSS (large-scale structure). This is supposed to proceed via the gravitational instability picture, which I think is due to Jim Peebles of Princeton [1] and Yakov Zeldovich from Moscow. The idea is that initial perturbations (maybe due to some cosmic quantum field) will grow gravitationally. You can see that it's unstable by thinking about a big sphere of dust - left to itself, it will collapse, meaning the density grows. This is, after all, how stars form. For really large scales, though, the situation is complicated by the expansion

† $1 Mpc \approx 3 \times 10^{24}$ cm $\approx 3 \times 10^6\, l.y.$

of the universe. The dust tries to collapse but the universal expansion to some extent counteracts this. For a long time it seemed like there was no way out of this dilemma. There is still no universally recognized theory of galaxy formation!

So the program for people studying LSS is to inspect the deviations from the ideal homogeneous isotropic universe. This is clearly a scale-dependent endeavour. For example, consider a person consisting mostly of water. If the background "average" density of the universe is $10^{-29} g/cm^3$, then the fractional overdensity associated with this person is

$$\delta = \frac{\rho - \rho_{\text{background}}}{\rho_{\text{background}}} \approx \frac{1 - 10^{-29}}{10^{-29}} \approx 10^{29} \tag{1}$$

(This δ is dimensionless, and it's the main variable for LSS.) (If you believe the COBE results, then $\delta \approx 10^{-5}$ back when the universe was only about 100,000 years old.) Now, for the equations to be simple we want $\delta << 1$, that's the linear regime, so you might say that people are highly non-linear structures. But you'll only see these human density peaks if you average over scales with $r \approx 100$ cm. Furthermore, as far as cosmology is concerned, individual density peaks won't affect the cosmic Hubble expansion unless the gravitational potential is large compared to that potential associated with the expansion. In practice, even superclusters have only a very tiny affect on this expansion. So instead of looking at scales of 1 meter, I'm going to smooth using 1200 km/sec $= 12h^{-1}$ Mpc. (It's convenient to smooth in "velocity space" because this way one can avoid the controversy about the value of the Hubble parameter!) If we count the galaxies inside a sphere with radius 12 Mpc, we might expect to find about 1000.[‡]

I will describe two methods for finding the fractional overdensity δ. One method actually counts galaxies. Sometimes people try to make complete surveys, i.e. find every single galaxy in a certain region, and then get a redshift for each galaxy. For example, completeness is the goal of the CfA survey [4]. The IRAS survey looks only for galaxies that are found in the infrared. Tony Fairall has another approach: he includes every single galaxy redshift he can find, and his pictures reveal plenty of large scale structure [5]. Some people complain that his redshift catalogue doesn't have well defined selection criteria etc etc but for the purpose of identifying large scale structures such as voids and superclusters, it is very good. Now there are two problems with getting density from any redshift survey: one is the problem of peculiar velocities and the other is the problem of galaxy "bias".

Peculiar velocities of galaxies are the motions that don't follow the general Hubble flow [9]. That means the redshift of a galaxy doesn't give the distance. (There's more on this in the POTENT section below.) "Bias" in this case means that the galaxies are not necessarily good tracers of the underlying background matter distribution[12]. It's possible that galaxies are more likely to form in dense regions. It's also possible that there's some physical "antibias" – i.e., galaxies are maybe discouraged from forming in really dense regions. The point is that since cosmologists believe galaxies make up only around 1% of the matter in the universe, it's not clear if the distribution of galaxies is the same as the distribution of the underlying matter.

[‡]The little "h" is defined by $H = 100h$ km/sec/Mpc; it is between 1/2 and 1.

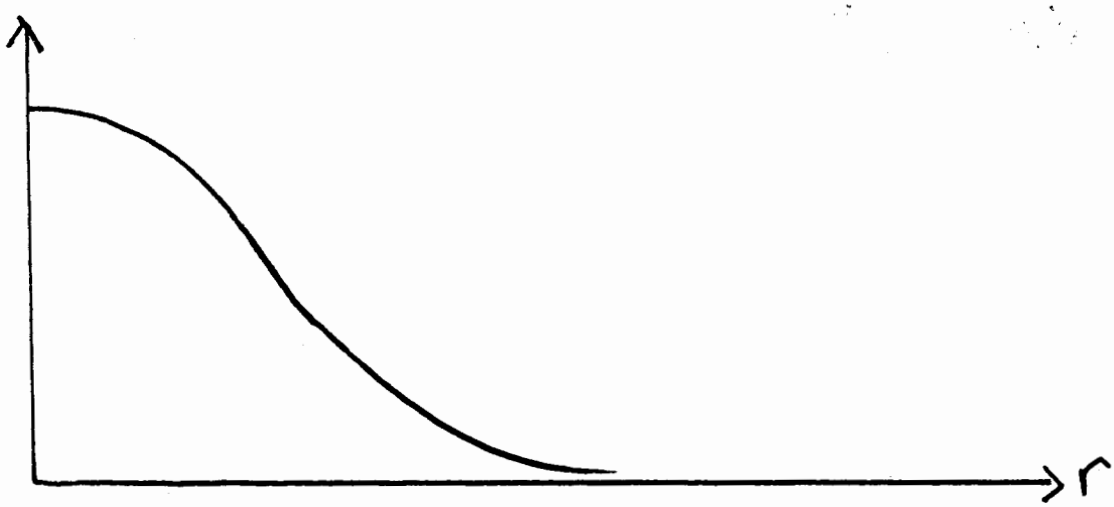

Figure 1: A sample selection function.

The second method I will describe is called POTENT [6]. If you treat galaxies as test particles (this means pretend they have no mass) and then look to see if there are large scale flow patterns in the velocity flow patterns of galaxies. These patterns could in principle be used to determine the distribution of matter, including the dark matter. The great advantage here is that the "bias" doesn't affect the outcome. The main problem, described below, is that the method depends on distance estimators for galaxies, and these estimators are still controversial.

2 IRAS

One source of information comes from the IRAS sample of galaxies. The IRAS (Infrared Astronomical Satellite) satellite mapped the sky in the infrared wavelengths [15]. Now most of this radiation did not come from galaxies; for example the dust of the Milky Way is studied using data from this same survey. Anyway, the data is run through a series of hoops, and the ones that get through are probably galaxies. In this case, 2684 galaxies were found and almost all of them have optical counterparts.

The "hoops": (1) point-like source at 60μm, (2) $f_{60} > 1.933$ Jy, (3) $f_{60}^2 > f_{12} \times f_{25}$, (4) $|b| > 5$. The notation: "f_{60}" means the flux at 60 microns, etc. Condition (2) reflects the limits of the satellite. Condition (3) distinguishes between stars and galaxies. Condition (4) cuts out the galactic disk region, which is full of dust which emits lots of infrared. (Actually, there are other small regions of the sky that are cut out due to a problem with the satellite. All-in-all, about 87% of the sky is covered.)

Because the survey is magnitude limited, we don't see many of the distant galaxies. Only the brightest distant galaxies are seen. So we use a **selection function** to correct for these effects. A simple selection function looks like this:

This means that the number of galaxies one sees decreases with distance. Note: We have to assume that the actual number density is roughly constant! So, assuming that there are just as many distant galaxies as nearby ones, one could try to correct for the

selection effects. Another note: it is hard to include actual evolution of galaxies into the selection effect. It is still unknown if young galaxies (meaning distant galaxies) are intrisically brighter or dimmer that present-day galaxies. The controversy boils down to this: new galaxies might have brighter, younger stars, but also more obscuring gas and dust. If distant galaxies are brighter just because they are younger (or dimmer because they are younger – take your pick!) this will affect the density derived from some selection function. For example, a distant cluster of galaxies might have 1000 galaxies, but we might only see 100 of them, because the others are too faint at that great distance. Here's the selection function from Strauss et al [11]:

$$\Phi(r) = Ar^{-2\alpha}\left(1 + (\frac{r}{r_*})^2\right)^{-\beta} \tag{2}$$

with $\alpha = 0.527$, $\beta = 1.78$, and $hr_* = 4400$ km/sec. These constants are found via a fitting procedure.

Then using this function, the "weight" of each observed galaxy is $1/\Phi$ (which means distant galaxies have more weight) and the density is formally

$$D(\mathbf{r}) = \sum_i w(r_i)\delta^3(r - r_i) \tag{3}$$

where $w(r) = \frac{1}{n_1\Phi(r)}$ is the normalised weight, $n_1 = \frac{1}{V}\sum_i \frac{1}{\Phi(r_i)}$ is the average number density inside the volume V, and δ^3 is the three dimensional Dirac delta function. In practice, this is where the smoothing takes place; instead of the Dirac delta, I use a three-dimensional Gaussian window function [13,14].

Figure 2 is a picture of the IRAS galaxies. Figure 3 is the density that one derives from it, in one slice, using a Gaussian window with half-width 1200 km/sec to smooth. Unfortunately this is only the *number* density of galaxies. Worse, it's only the number density of galaxies detected by IRAS – this is a problem because the IRAS galaxies are much more likely to be spiral galaxies than ellipticals, because they have more dust, but it is well known that elliptical galaxies are more clustered than spiral galaxies. So, how is the IRAS number density related to the actual density? Again, there is no correction for the peculiar velocity here. Incidentally, these pictures all use Supergalactic Coordinates (SGX,SGY,SGZ). These were introduced by G. de Vaucouleurs. The north pole of these coords is at l = 47.37 degrees, b = 6.32 degrees (galactic coords) with the origin at l = 137.37 degrees and b = 0. This means the Supergalactic plane is roughly perpendicular to the plane of the galaxy. It's more or less chosen to be the most interesting plane in the sky – which of course is also a controversial thing. It is possible that we see more structure in a plane perpendicular to our galaxy simply because we don't see well through the dust in the disk of the Milky Way. In any case, many interesting objects are near this plane, including the Perseus-Pisces supercluster, Virgo, Coma, the Local Void, and the Hydra-Centaurus clusters, sometimes known as The Great Attractor.

3 POTENT

One of the most exciting things in LSS studies is the development of new and better distance estimates for galaxies. From these we can get some idea about the radial peculiar

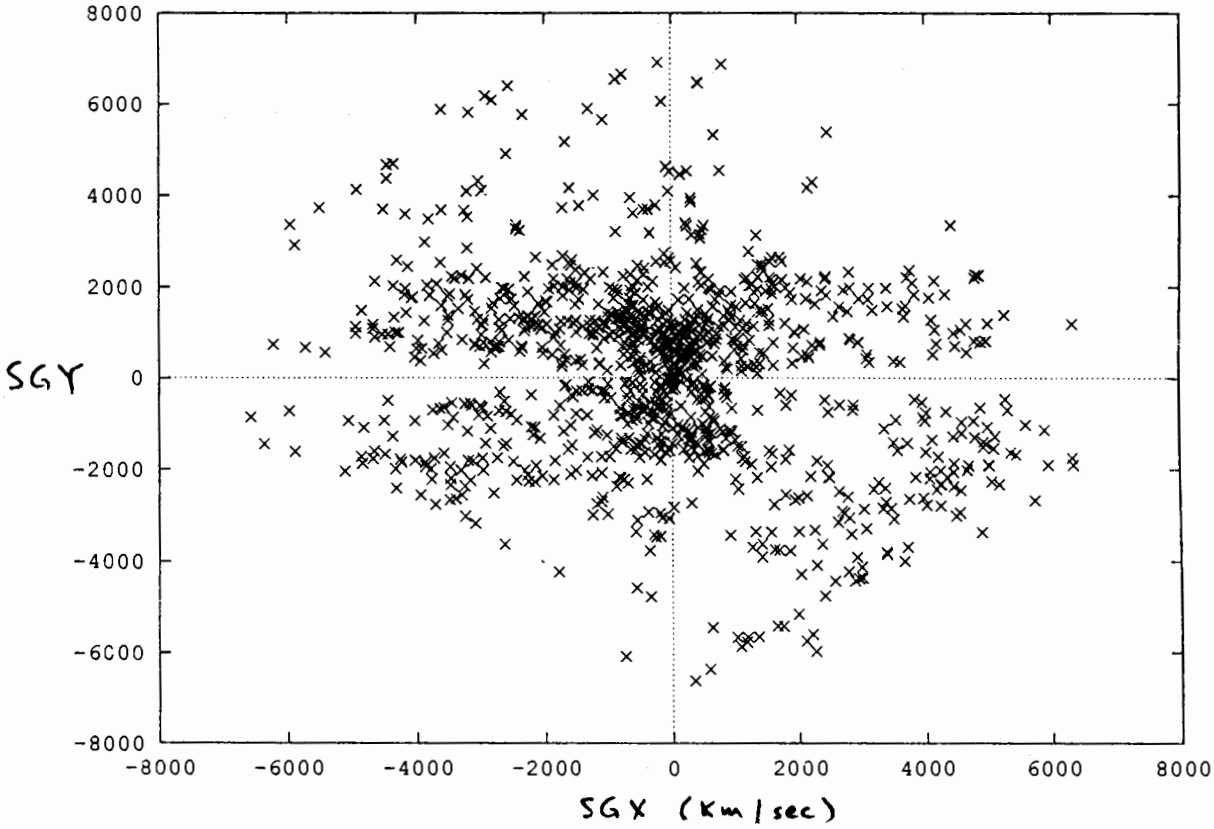

Figure 2: IRAS galaxies with $|SGZ| < 1500$ km/sec, projected onto the plane $SGZ = 0$.

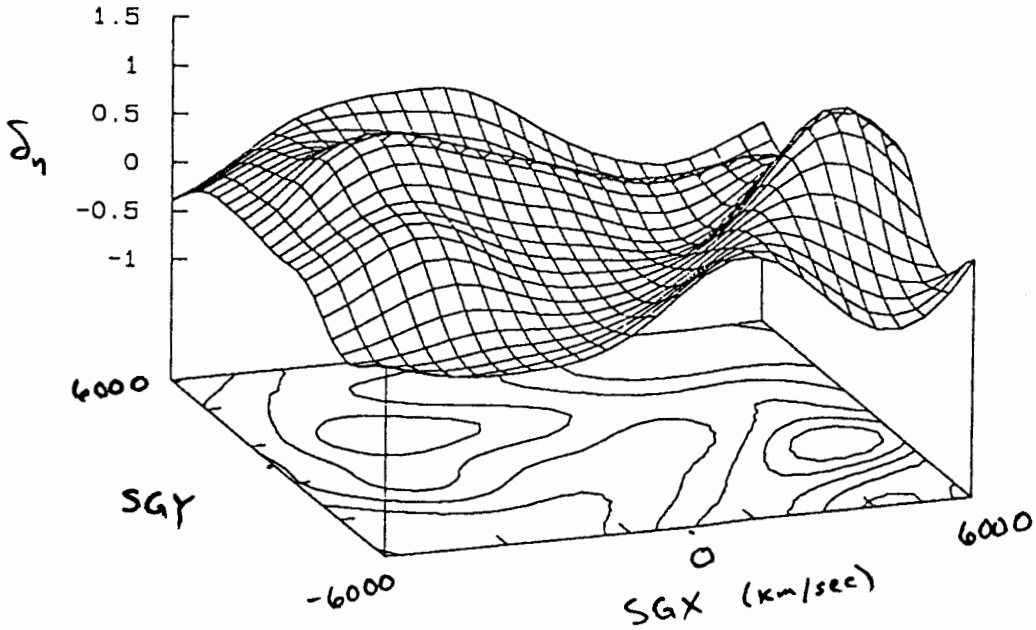

Figure 3: Density from the IRAS sample, in the slice SGZ = 0

velocities of galaxies.

To see how one calculates the peculiar velocity, here's one example: if a galaxy has redshift $cz = 3000$ km/sec, this is the total redshift, and it has two parts. One part is due to the Hubble expansion, Hr. The other part is due to the peculiar velocity along the line of sight. The radial peculiar velocity is then $v_r = cz - Hr$.

This only gives the radial component of this peculiar velocity; to get the velocity in all three dimensions, POTENT assumes that the vorticity of the "cosmic fluid" is zero. The mathematical formula for vorticity is $\vec{\omega} = \nabla \times \vec{v}$. In a regular fluid, you can think of vorticity this way: if you stick a very small paddlewheel into a stream etc etc. It's probably true that there is no (or very little) vorticity at the large scales considered here. The velocity comes from the acceleration, which comes from the newtonian gravitational potential, and gravity is a "conservative field" so you don't expect vorticity. In a real fluid, you get vorticity if there's viscosity etc and, although it is possible that the background really does have non Newtonian properties, we will assume there are no such problems.

In the linear regime (which means that the fluctuations in the density are much smaller than the average density), there is a simple relation between the overdensity and the peculiar velocity field:

$$\delta = -\nabla \cdot \vec{v}$$

This is the divergence of v. What it means is that if there is a region where the velocity points away from some point, then that point is underdense. Contrariwise, if the velocity is converging towards some region (convergence is like negative divergence), one might suspect a large concentration of matter there.

The Great Attractor could be such a region. In the POTENT analysis, it appears to be the greatest concentration of mass in the region within 6000 km/sec of the Milky Way. It's existence is still controversial, mostly because it depends on the distance estimators.

Figure 4 shows some of the radial peculiar velocities of galaxies near the supergalactic plane. The dot is the real position of the galaxy, and the line shows the radial peculiar velocity. Even from this picture, it is possible to see the Great Attractor, or at least a flow of galaxies towards $SGX = -3000$, $SGY = 3000$. Figure 5 shows the density derived using these peculiar velocities and POTENT, in the supergalactic plane. The data was obtained from Dave Burstein [10] and Stephane Courteau [7].

4 Further development

Recently, the original POTENT team has joined forces with an IRAS group, and they have compared the two density fields [8]. There are all sorts of problems with statistics and questions about smoothing scales but the main result is that the density fields are consistent with each other and also consistent with a universe with $\Omega = 1$ and $b = 1$. Actually they found that for $\Omega = 1$, it was more likely that $b = 0.7$ (antibias) but there is a large error bar. So it is not inconceivable that the light (from galaxies) traces the underlying (mostly dark) matter.

As you can see, there are still plenty of questions. I'd like to point out that most people were very surprised by the large value of galaxy peculiar velocities. Lately they

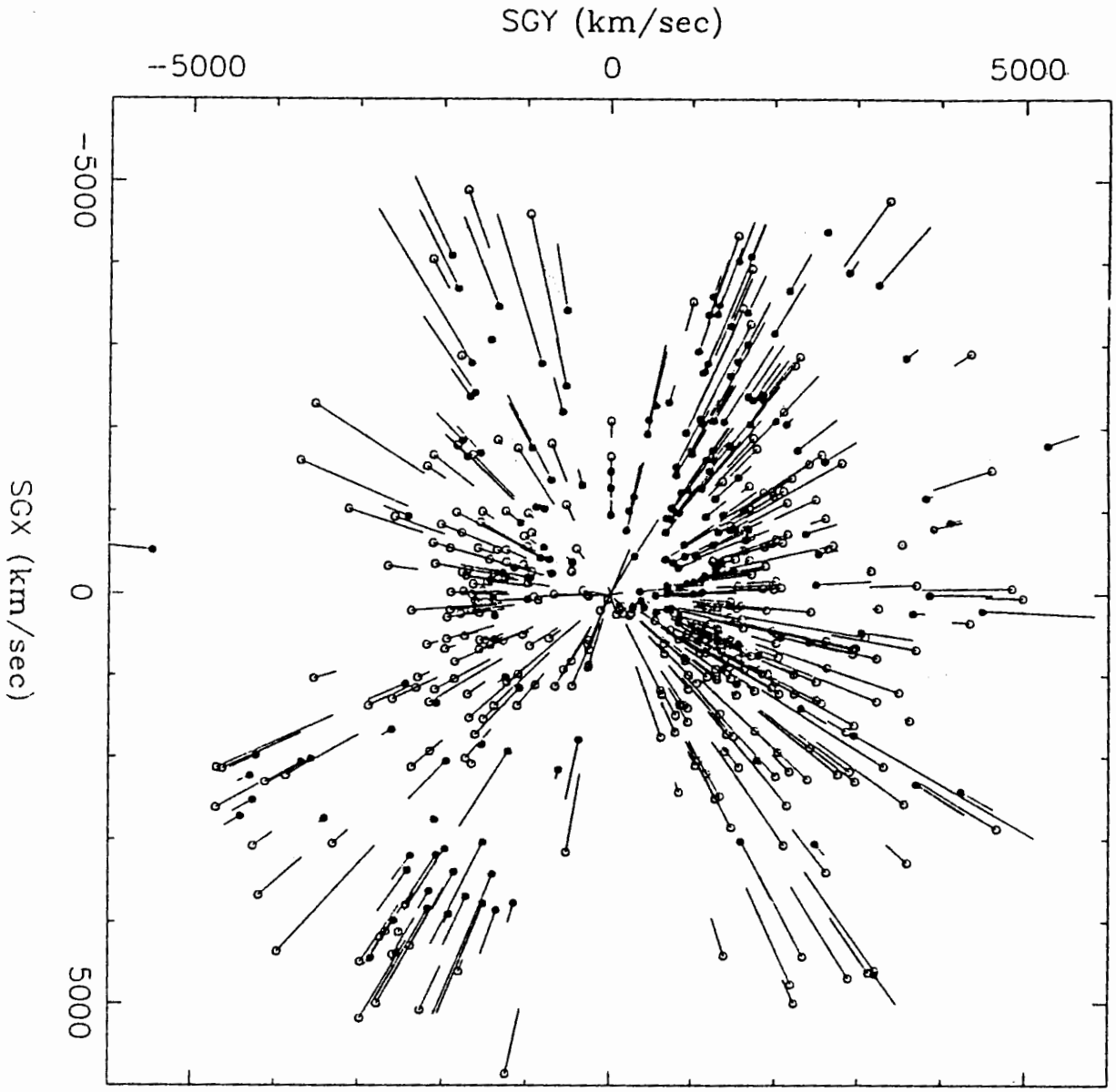

Figure 4: Radial peculiar velocities in the sample, with $|cz| < 1500$ km/sec. This is the supergalactic plane. Circles mark the positions of galaxies projected onto the SG plane after correcting for Malmquist bias.

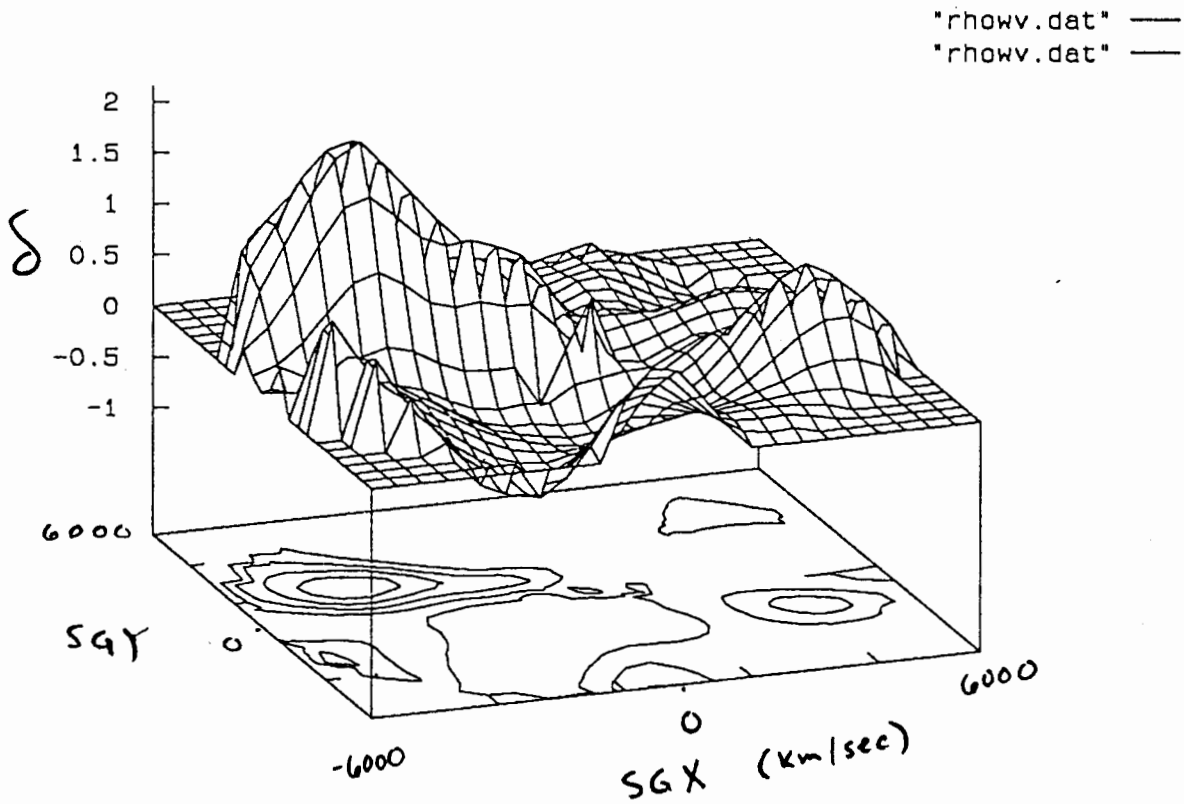

Figure 5: Fractional overdensity from POTENT. This is the supergalactic plane. Note the "Great Attractor" near (-4000,2000) and part of Perseus-Pisces near (3000,-3000).

have been surprised by super large scale structure, such as the "Great Attractor" and the "Great Wall". The size of large voids, such as the void in Boötes, was another surprise. Perhaps we shouldn't be surprised if there are more surprises.

5 Conclusions

It seems possible that by studying the distribution of galaxies and the peculiar velocities of galaxies, the actual density of the universe might be found. It is even possible that the resulting density field might agree with current theories of galaxy formation after a Hot Big Bang.

Acknowledgements

It is a pleasure to thank G.F.R. Ellis and N. Bishop for discussions.

I got the IRAS data thanks to Michael Strauss, and I got the peculiar velocity data from Dave Burstein and Stephane Courteau.

References

[1] Peebles. P.J.E., 1980. *The Large-Scale Structure of the Universe*, Princeton University Press, Princeton, NJ.

[2] Weinberg, S., 1972. *Gravitation and cosmology*, John Wiley and Sons, New York.

[3] Smoot, G.F. et al., 1992. *Astrophys. J. Lett.*, **396**, L1. (COBE)

[4] de Lapparent, V., Geller, M.J., and Huchra, J.P., 1986. *Astrophys.J.Lett*, **302**, L1. (CfA slice)

[5] Fairall A.P. & Jones A., 1991. "Southern Redshift Catalogue" Publ. Dept. Astr. Univ Cape Town, No. 11.

[6] Bertschinger, E., Dekel, A., Faber, S.M., Dressler, A. & Burstein, D., 1990. *Astrophys.J.*, **364**, 370.

[7] Courteau, S., Faber, S.M., Dressler, A., and Willick, J.A., 1993.*Astrophys.J.*, submitted.

[8] Dekel, A., Bertschinger, E., Yahil, A., Strauss, M.A., Davis, M. & Huchra, J.P., 1993. *Astrophys.J.*, **412**, 1. (Comparing IRAS and POTENT)

[9] Faber, S.M. & Burstein, D., 1988. In: *Large-scale Motions in the Universe*, eds Rubin, V.C. & Coyne, G., Princeton University Press, Princeton, NJ, p.115.

[10] Lynden-Bell, D., Faber, S.M., Burstein, D., Davies, R.L., Dressler, A., Terlevich, R.J., & Wegner, G., 1988. (7 Samurai)

[11] Strauss, M.A., Davis, M.,, Yahil, A., & Huchra, J.P., 1993. *Astrophys.J.*, **385**, 421.

[12] Kaiser, N., 1987., *Mon. Not. R. Astr. Soc.*, **227**, 1. (bias)

[13] Kaiser, N., Efstathiou, G., Ellis, R., Frenk, C., Lawrence, A., Rowan-Robinson, M., & Saunders, W., 1991. *Mon. Not. R. Astr. Soc.*, **252**, 1.

[14] Saunders et al., 1991. *Nature*, **349**, 32. Strauss, M.A., Davis, M., Yahil, A. & Huchra, J.P., 1992. *Astrophys.J.*, **385**, 444.

[15] Yahil, A., 1988. In: *Large-scale Motions in the Universe*, eds Rubin, V.C. & Coyne, G., Princeton University Press, Princeton, NJ, p.219.

Nearby Large-scale Structures in the Universe

A P Fairall
Department of Astronomy, University of Cape Town
Private Bag 698531, Rondebosch, 7700

Abstract

A review of the recognition of nearby (cz < 15 000 km s^{-1}) large-scale structures is presented. A selection of recent plots of nearby structures, mainly those from the author's "Southern Redshift Catalogue" is presented. They show a labyrinth of intersecting wall-like structures. There is a tendency for parallel walls to occur, similarly a tendency for walls to intersect at right angles.

Soon after Hubble [1] opened the "Realm of the Nebulae", he made the first investigation as to how the nebulae - or rather galaxies - were distributed across the sky. He did this by simply aiming the 100-inch telescope in many different directions in the sky, and then counting how many galaxies were recorded in each photograph. His conclusion was that "Except for the influence of obscuring clouds, there is no evidence of conspicuous systematic variation in the distribution of nebulae over the sky". The "obscuring clouds" referred to the zone of avoidance - the Milky Way. Hubble supposed that galaxies were distributed much like nearby stars. While some clustering occurred, most were scattered randomly over the field.

Hubble's conclusion was not exactly correct. The narrow field of view of his telescope meant that he was looking straight through nearby conglomerations. His scientific "rival", Shapley, had more success using wide-angle photographs from smaller aperture instruments. A good example [2] is his "remote cloud of galaxies in Centaurus" that is today known as the "Shapley Region" and is a contender for a "Great Attractor".

Another great pioneer whose work concerned the distribution of galaxies was Fritz Zwicky, under whom the author worked as a student. Of Swiss nationality, Zwicky spent most of his scientific life at the California Institute of Technology. By his being the first to explore the dynamics of clusters, Zwicky [3] made the remarkable discovery that the mass of the Coma cluster (as found from the application of the Virial theorem) was much greater than the sum of the apparent masses of the member galaxies. This was the beginning of the recognition of "dark matter", a topic in vogue today, yet few investigators took note of Zwicky,s work at the time. Zwicky's words are as appropriate today: "We must know how much dark matter is incorporated in nebulae (i.e. galaxies) in the form of cool and cold stars, macroscopic and microscopic solid bodies, and gases".

It is worth making the point that research in fields that form the cutting edge of science often attract the most energetic - and most competetive - investigators. Very often the rivalry [4] has brought about personality conflicts and animosity. Clearly, both Hubble

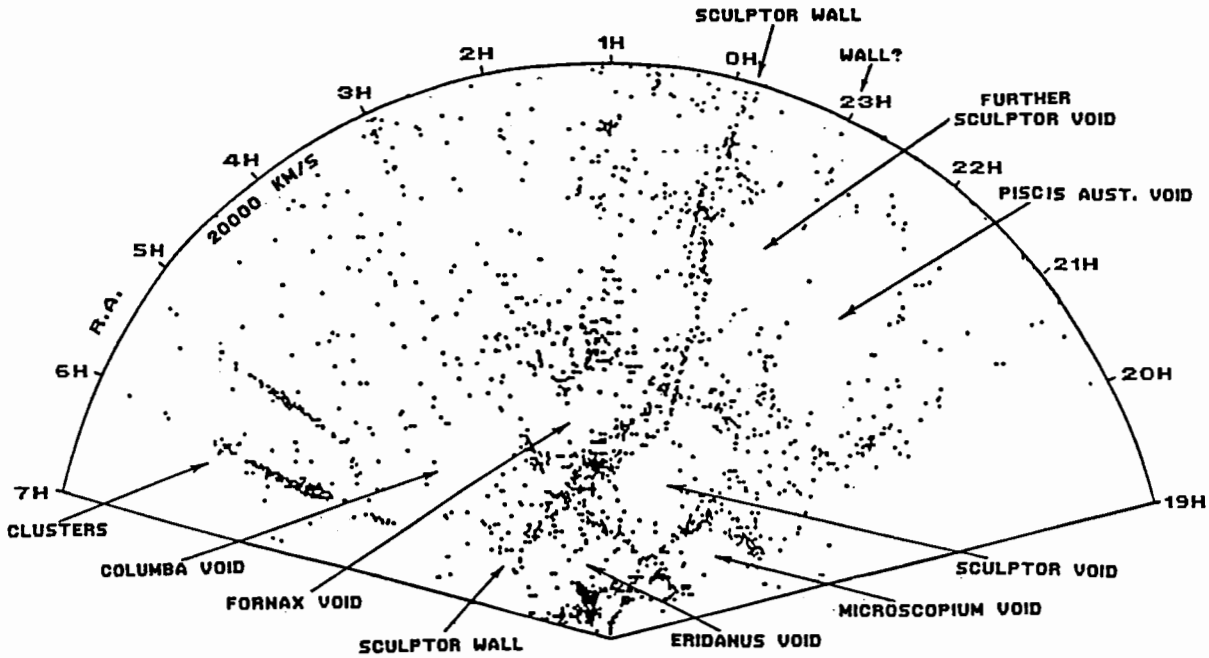

Figure 1: Redshift plot[17] to cz = 20000km s^{-1} for galaxies with R.A. between 19^h and 7^h and Declination $-22°$ to $-42.5°$.

and Shapley were very competetive, yet Zwicky's case is very sad. His bluntness led him to isolation from many of those who would have been his colleagues. For similar reasons, much of his work was initially passed over. Only nowadays, some years after his death, is the value of his contribution being appreciated.

One major contribution, made by Zwicky, was the push to employ Schmidt telescopes - which have a fast f-ratio and a wide-angle field of view - for extragalactic research. Following success with a small prototype, Zwicky had a much larger version (18/30 inch) built. A suitable dark site had to be found, and the telescope became the first on Mount Palomar in southern California - later the site for the famous 200-inch telescope. So successful was this Schmidt telescope, that it led to building of the 48-inch Palomar Schmidt that was to carry out the now-celebrated National Geographic-Palomar Observatory sky survey.

This survey recorded thousands of galaxies in each of its 6×6 degree photographs. It also enabled the first move towards examining the large-scale three-dimensional distribution of galaxies. Since a small galaxy nearby may mimic the appearance of a large galaxy far away, distances are not readily apparent for individual galaxies. However, the relative distance of a cluster of galaxies - with its variety of members - can more easily be gauged. Two investigators moved to use the Palomar Sky Survey for the purpose of using clusters to map the large-scale distribution of galaxies. The first was
the survey of clusters by George Abell - his database has proved the foundation for numerous ongoing studies. The other was done by Zwicky.

Zwicky's [5] "Catalogue of Galaxies and of Clusters of Galaxies" catalogued thousands

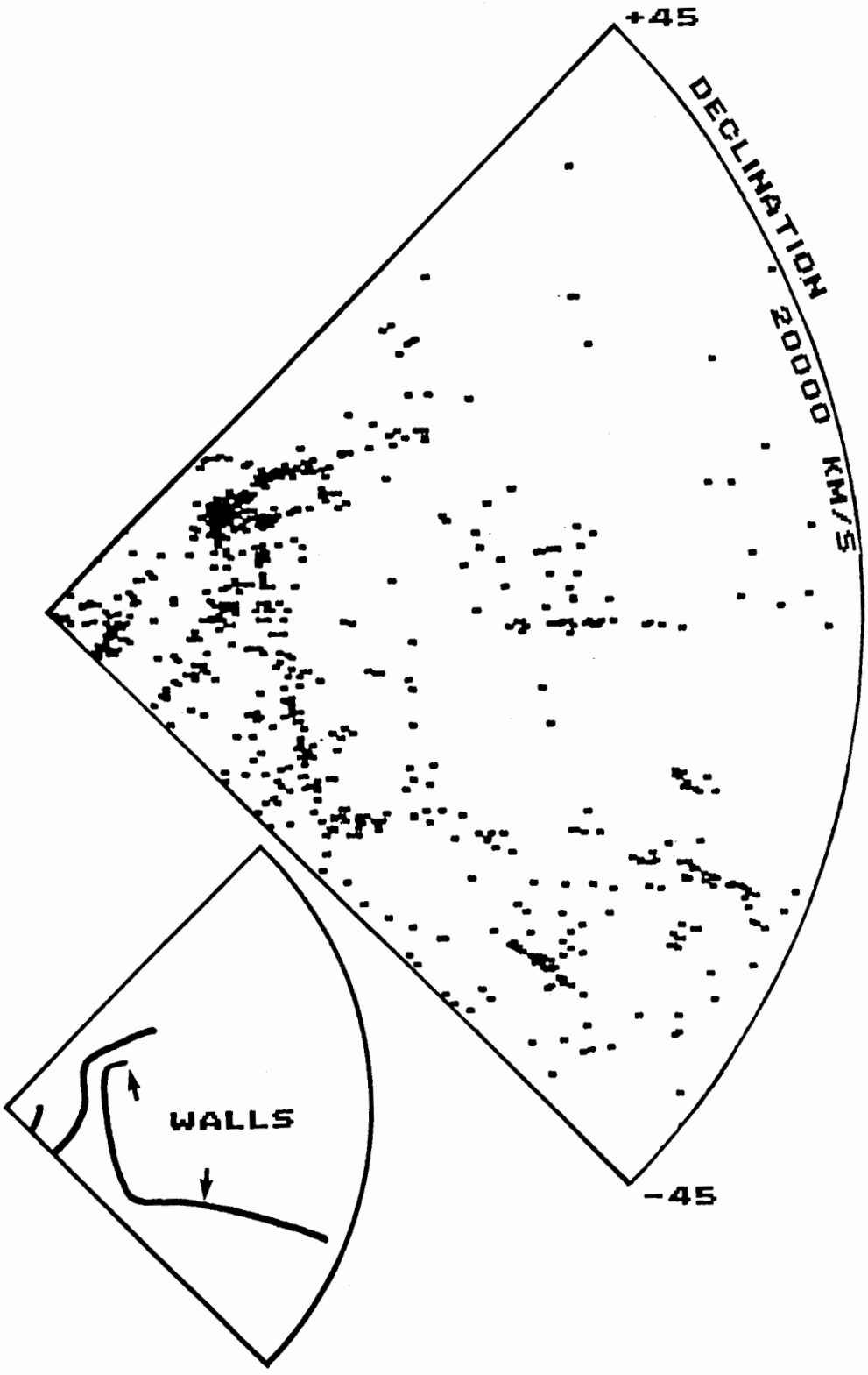

Figure 2: Redshift plot[16] to cz = 20000km s^{-1} for galaxies with R.A. between 0^h0^m and 0^h59^m and Declinations +45° and −45°.

of individual galaxies (those brighter than magnitude 15,7) and showed the outer contours of clusters, within which he counted hundreds, sometimes thousands, of galaxies. At the time, the contours were criticised, since they appeared to show the clusters to be vastly more extended than others thought to be the case. Time was to prove Zwicky correct.

In part, the acceptance of observational data in cosmology has been governed by the degree to which it fits the theoretical expectations. The estimates of mass densities, up to perhaps the 1970s, implied that clusters of galaxies were the largest structures in the universe (that gravity could assemble). Ideas that structures larger than clusters could exist were not really welcome. This is particularly true in regard to the work of Gerard de Vaucouleurs, whose work on the distances and distributions of nearby galaxies led him to suggest the existence of a "supergalaxy", as portrayed by his plots [6]. As with Zwicky, de Vaucouleurs had the correct insight.

An alternative way of probing the large-scale distribution of galaxies was to come about. Distances to individual galaxies can be inferred from their cosmological velocities of recession (the Hubble law), but relatively few redshifts were available at this time. However, from the late 1960s, spectrographs could be fitted with electronic image intensifiers, which greatly increased their speed. Today, the 1,9 m telescope at the South African Astronomical Observatory can register in a few minutes as good a spectrum of a galaxy as the Palomar 200-inch telescope could achieve in a few hours in the early 1960s. Consequently, the production of galaxy redshifts (and their infrared cosmological distances) has escalated dramatically. Thus we have been able to plot the three-dimensional distributions of ever increasing numbers of galaxies.

In general, there are two types of "redshift surveys". The first would be to establish a "controlled" sample of galaxies (usually magnitude-limited or diameter-limited); the second would simply be to use "all-available" redshifts. The later approach was first tried in 1976 by the Estonian cosmologist Jaan Einasto, using the then new version of the de Vaucouleurs Reference Catalogue.

Einasto [4] made a remarkable discovery - the three-dimensional distribution showed a cellular structure. There seemed to be apparently empty voids - surrounded by walls of galaxies - not unlike the frothy texture sometimes
exhibited by liquid media. Such a cellular structure was completely unexpected in terms of the physics thought to be involved. Further, the size of the cells was way beyond what was considered to be size of the largest possible conglomeration. Einasto announced his results at the 1976 IAU General Assembly, but the result seemed so far fetched that few people took notice. However, the following year, he hosted an international conference, and again pushed the idea of the cellular structure. News of the claim travelled widely, but the converts were few - the idea seemed to overthrow all that was understood about clustering. Criticism was also levelled because the data was seen as uncontrolled, and conservative thinking did not accept it. It was also seen to support the Russian theoretical cosmological view - of "pancaking" over American views of galaxy formation.

However, the plots of redshifts obtained in the late 1970s, particular by Chincarini, Rood, Gregory and Thompson not only confirmed the tendency for galaxies to conglomerate in "superclusters" - much more extended than clusters, but also confirmed the existence of empty spaces between such structures. A classic plot produced by Gregory and Thompson [7] showed an extended structure running from the Coma cluster, behind

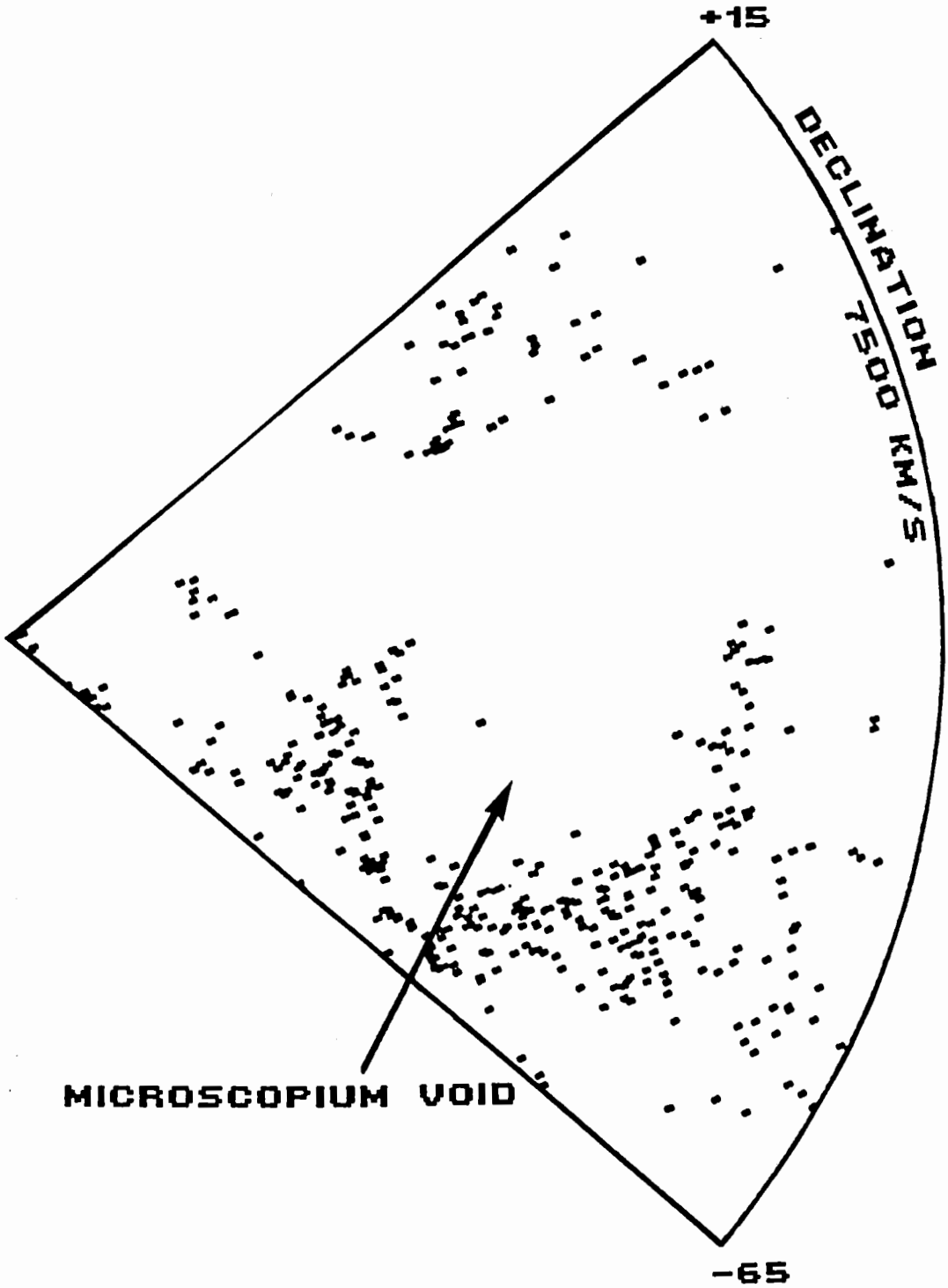

Figure 3: Redshift plot[16] to cz = 7500km s^{-1} for galaxies with R.A. between 19^h00 and 20^h59 and Declinations +15° and −65°. The obscuration by the Milky Way affects the central portion of the diagram.

foreground voids. In 1980, the existence of a very much larger void in Bootes was claimed by Kirschner et al. [8]

The first proper redshift survey of "controlled data" - the "CfA1" survey (to limiting magnitude 14,5 from the Zwicky catalogue) was carried out by Marc Davis, John Huchra, David Latham and John Tonry [9] and colleagues at the Harvard-Smithsonian Center for Astrophysics. The data reveal voids and something of a frothy structure, but was not quite dense enough to show the distinct cellular structure claimed by Einasto. However, on the basis that the luminosity function of galaxies is universal, a magnitude-limited survey allows for the extraction of numerous quantitative parameters and measures.

From a personal standpoint, the Gregory and Thompson plot and the CfA1 survey inspired the author to plot data from his list of compact galaxies and redshift catalogue [10,11] - the start on an ongoing series. In 1985, plots of Huchra's ZCAT, by the author and students [12], confirmed Einasto's cellular structure and identified numerous voids.

The first portion of a deeper CfA2 survey (to Magnitude 15,5) was released as "A Slice of the Universe" [13] in early 1986. This confirmed the cellular structure, and suggested what was described as a soapsud texture. This work and its accompanying plot was widely publicized (e.g. Time Magazine). The slice includes the Coma Cluster which contributes the central axis of a pattern resembling a "stick man".

Haynes and Giovanelli [14] also obtained many 21 cm velocities in Pisces-Perseus that, when plotted, showed similar structure.

The southern equivalent to the CfA1 survey - the SSRS [15] (Southern Sky Redshift Survey) was completed by a collaboration that included John Menzies and Ian Coulson at the South Africa Astronomical Observatory (SAAO). Luiz da Costa, now based at CfA, is leading a similar collaboration for SSRS2 - the southern equivalent of the CfA2 survey. The author is one of the collaborators and extensive use has been made of SAAO.

In parallel to this "controlled" survey, the author has continued to produce plots from catalogued data. A selection of the most recent plots [16,17] accompany this article.

The plots clearly confirm the cellular structure, but at the same time reveal that many of the "surfaces" that surround the voids are segments of larger wall-like structures. Some of these are massive structures, best termed "great walls" - the prototype being identified in the CfA2 data in the northern skies. The walls are usually larger than the voids, so it seems more likely that the voids are the spaces left between the walls, rather than the whole texture being created by the growth of voids. There are tendencies for walls to run parallel to each other, or to intersect at right angles. The northern "Great Wall" and the great "Sculptor Wall" in the south are also approximately at right angles. The lengths of some of these walls seem considerable, and their presence appears to be providing a strong challenge to cosmological theories based on cold dark matter. Cosmological theories, however, are still to address the formation of parallel and orthogonal structures.

The picture of large-scale structures is somewhat incomplete, due to the obscuration of the Milky Way. Some special surveys are now being made to map structures at very low galactic latitudes. Amongst these is a survey by Renee Kraan-Korteweg, Chantal Balkowski and the author, that has also made use of SAAO.

It is a remarkable time to be working in this field. We are seeing features that were unknown only ten years ago. The complete mapping of nearby large-scale structures will reveal the fabric of the cosmos, and should provide the deciding test for cosmological

theory.

References

[1] Hubble, E., 1936, *The realm of the Nebulae*, Yale Univ. Press.

[2] Shapley, H., 1930, *Harvard Observatory Bulletin No. 874*, p 9.

[3] Zwicky, F., 1937, *Ap. J.*, **86**, 217.

[4] Overbye, D., 1991. *"Lonely Hearts of the Cosmos"*, Harper Collins.

[5] Zwicky, F., Herzog, E., Wild, P., Karpowitz, M., Kowal, C.T. 1960-68, *Catalogue of Galaxies and of Clusters of Galaxies*, Caltech.

[6] de Vaucouleurs, G., de Vaucouleurs, A., 1964, *Reference Catalogue*, Texas.

[7] Gregory, S.A. and Thompson, L.A., 1978, *Ap. J.*, **222**, 784.

[8] Kirshner, R.P., Oemler, A., Schechter, P.L. and Shectman, S.A., 1981, *Ap. J.*, **248**, L57.

[9] Davis, M., Huchra, J., Latham, D.W. and Tonry, J., 1982, *Ap. J.*, **253**, 423.

[10] Fairall, A.P., 1983, *MNRAS*, **203**, 47.

[11] Fairall, A.P. and Winkler, H., 1984, *In "Clusters and Groups of Galaxies"*, ed. F. Mardirossian et al., Reidel.

[12] Fairall, A.P. and students, 1985, *Publ. Dept. Astr. Univ. Cape Town*, No. 8.

[13] de Lapparent, V., Geller, M. and Huchra, J.P., 1986, *Ap. J.*, **302**, L1.

[14] Haynes, M.P. and Giovanelli, R., 1986, *Ap. J.*, **306**, L55.

[15] da Costa, L.N., Pelligrini, P.S., Sargent, W.L.W., Toury, J., Davis, M., Meiksin, A., Latham, D.W., Menzies, J. and Coulson, I., 1988, *Ap. J.*, 327, 544.

[16] Fairall, A.P., Palumbo, G.G.C., Bettolani, G., Kauffmann, G., Jones, A. and Baiesi-Pillastrini, G., 1990. *MNRAS*, **247**, 21P.

[17] Fairall, A.P. and Jones, A., 1991, *"Southern Redshifts - Catalogue and Plots"*, Publ. Dept, Astr. Univ. Cape Town, No 11.

Dynamical Symmetries in Relativistic Kinetic Theory

R Maartens and D R Taylor

Department Computational and Applied Math and

Centre for Nonlinear Studies,

University of the Witwatersrand, PO Wits 2050, South Africa

Abstract

This paper is part of a programme investigating symmetries that are defined at a physical or observational level, rather than purely geometrically. Here we generalise previous work on dynamical "matter" symmetries of relativistic gases. If the matter symmetry vector is surface-forming with the dynamical Liouville vector, then Einstein's equations reduce it to a Killing symmetry of the metric. We show that this conclusion is unaltered if the gas particles are subject to a non-gravitational force (including the electromagnetic force on charged particles), or if the gravitational field obeys the higher order field equations. In the Brans-Dicke theory, the matter symmetry reduces to a homothetic symmetry of the metric. This is also the case for a generalised conformal symmetry in Einstein's theory. We consider the problem of relaxing the surface-forming assumption in an attempt to determine whether there are dynamical symmetries that do not necessarily reduce to geometrical symmetries of the metric.

1 Introduction

Much work has been done on symmetries in fluid spacetimes (see [1,2] and references therein). The approach in most cases has been to assume, sometimes without clear phys-

ical or observational reasons, a geometrical symmetry of spacetime, and then to consider the consequences for the fluid properties. Similarly, most work on symmetries in relativistic kinetic theory starts from a geometrical symmetry of spacetime and investigates the consequences for the distribution function $f(x,p)$ (see [3] and references therein). This paper is motivated by a desire to define a fundamental symmetry at a *physically observational or dynamical* level, rather than purely geometrically. Previous attempts include the Postulate of Uniform Thermal Histories of Bonnor and Ellis [4], which aimed to give an observational definition of homogeneity in fluid spacetimes; dynamical path symmetries of particle motion (see [5] and references therein); and the dynamical matter symmetries defined in relativistic kinetic theory by Berezdivin and Sachs [6]. In this paper, we take the view that any fundamental concept of dynamical symmetry should have a foundation in the microsopic model of relativistic kinetic theory. Therefore, we aim to generalise the work of [6] on dynamical matter symmetries. A previous paper [5] dealt with generalising work on dynamical path symmetries.

There is an important distinction between the dynamical matter symmetries of Berezdivin and Sachs and dynamical path symmetries of particle motion [5]. The latter symmetries are defined by an invariance of phase space orbits. It is not clear whether they have any observable consequence since they map orbits in phase space into each other. Dynamical matter symmetries on the other hand may be defined directly in terms of measurements of the particle distribution function [6]. It is shown in [5] that matter and path symmetries are equivalent only if they both arise from an underlying homothetic symmetry of the spacetime metric.

Our investigation of matter symmetries aims to clarify the relation between these dynamical symmetries and geometrical symmetries. Although matter symmetries in relativistic kinetic theory are an important concept in a dynamical approach to symmetries, they have received little attention. We have recently situated matter symmetries within a broader class of vector fields on the tangent bundle [5]. Oliver and Davis [7] considered some mathematical properties of matter symmetries in the context of classifying geometrical symmetries. However, as far as we are aware, no work has been done to extend the original kinetic theory results of Berezdivin and Sachs. We aim to do so in this paper.

Berezdivin and Sachs were unable to find a solution to the general case and had to assume that the matter symmetry vector field and the Liouville vector field (geodesic spray) were 2-surface forming in phase space. With this assumption, they showed that Einstein's field equations imply that the dynamical matter symmetry necessarily arises from an isometry of the spacetime. In other words, the field equations transmit the dynamical symmetry directly to the geometry. We try to generalise their result in various directions: (a) considering the effect of non-gravitational forces; (b) considering alternative field equations ; (c) generalising the definition of matter symmetry to a conformal matter symmetry ; (d) considering matter symmetry vector fields that form 3-dimensional integral surfaces with the Liouville vector field.

Section 2 contains a brief summary of relativistic kinetic theory for a collision-free gas. Section 3 is a brief review of lifted vector fields and transformations on the tangent bundle, which includes the Berezdivin and Sachs matter symmetry as a particular case. Section 4 outlines the results of Berezdivin and Sachs and provides an alternative derivation of their main result . We believe that our derivation is more direct and clear. Also, it may be extended to the more general cases, unlike the Berezdivin and Sachs methods. Section 5 details the extensions and generalisations made to the results of Section 4. We find that the presence of a non-gravitational 4-force (including electromagnetism) does not qualitatively alter the Berezdivin and Sachs result, but merely leads to an additional symmetry constraint on the force field. The restrictive Berezdivin and Sachs result also holds for higher order field equations. However, the Brans-Dicke theory allows for a less restrictive behaviour: the matter symmetry arises from a homothetic symmetry of the metric. The long range scalar field of the theory inherits this homothetic symmetry. The generalisation of the matter symmetry by introducing a conformal matter symmetry is shown to force the spacetime to admit a homothetic metric symmetry. Finally, the attempt to generalise the 2-surface forming condition to a 3-surface forming condition is unsuccessful. We are unable to solve the equations that arise from this condition, although we can show that in a special case the spacetime admits a Killing tensor.

In all cases the results and indications point to a surprising "resilience" of geometrical symmetries, in the sense that they are the source for dynamical matter symmetries (a

similar point holds for path symmetries [5]). In the concluding Section 6 we discuss why this may be the case and point to possible generalisations.

2 Collision–free Gas

We first give a brief review of the relativistic kinetic theory of a collision-free gas (see [3] and references therein for further details). The distribution function $f(x,p)$ determines the number of particles near each event x in spacetime M, with 4-momenta near p. The momentum space P_x is the region in the tangent space T_xM consisting of future-directed, non-spacelike tangent vectors. Phase space P is then the union of all P_x. The mass-shell $P_x(m)$ consists of all 4-momenta p^a such that $p_a p^a = -m^2$. The mass-shells are the fibres of the phase space $P(m)$ for particles of rest mass m. Then $P(m)$ is a hypersurface in P, which is in turn a region of TM, the tangent bundle. Local coordinates $\{x^a\}$ on M induce local coordinates $\{x^a, p^b\}$ on TM, and $P(m)$ is given locally by

$$g_{ab}(x^c)p^a p^b = -m^2 \tag{1}$$

By choosing p^α ($\alpha = 1,2,3$) as coordinates on each mass-shell, we induce local coordinates $\{x^a, p^\alpha\}$ on $P(m)$ with p^0 determined by (1) at each point of $P(m)$. Since free uncharged particles not subject to collisions follow geodesics, all possible uncharged particle motions are given by (1) and

$$\frac{dx^a}{dv} = p^a \,, \qquad \frac{dp^a}{dv} = -\Gamma^a_{bc}\, p^b p^c \tag{2}$$

where v is an affine parameter ; for $m > 0$, $v =$ (proper time)$/m$. The family of intersecting geodesics on M represented by (2) is naturally lifted $[x^a(v) \to (x^a(v), dx^a/dv)]$ into a non-intersecting congruence of phase orbits in P. The tangent vector field to these phase orbits is the Liouville vector field (or geodesic spray)

$$\mathbf{L} = p^a \left(\frac{\partial}{\partial x^a} - \Gamma^b_{ca}\, p^c \frac{\partial}{\partial p^b} \right) \tag{3}$$

From (1) and (3), $\mathbf{L}(m) = 0$, so that $\mathbf{L}$ is tangent to $P(m)$. Furthermore, f is constant along the phase flow since the gas is collision-free. This yields the Liouville (or Vlasov)

equation:

$$\mathbf{L}(f) = 0 \tag{4}$$

In the case of charged particles (charge e), the Liouville vector field (3) generalises to:

$$\mathbf{L}_* = \mathbf{L} + eF^a{}_b\, p^b \frac{\partial}{\partial p^a} \tag{5}$$

where F_{ab} is the electromagnetic field tensor. Equation (5) follows since the integral curves of $\mathbf{L}_*$ are the lifts of charged particle trajectories: $Dp^a/dv = eF^a{}_b p^b$. Then the Liouville equation (4) generalises to the charged particle case: $\mathbf{L}_*(f) = 0$.

The presence of a velocity-independent, non-gravitational 4-force $mh^a(x)$, implies that the particle trajectories are given by: $Dp^a/dv = h^a$. Then the natural lifts of these trajectories are the integral curves of the generalised Liouville vector field for motion under a velocity-independent 4-force :

$$\mathbf{L}_* = \mathbf{L} + h^a \frac{\partial}{\partial p^a} \tag{6}$$

In the absence of collisions, the Liouville equation (4) again generalises to $\mathbf{L}_*(f) = 0$. The second moment of f defines the kinetic energy-momentum tensor

$$T^{ab} = \int p^a p^b f dP \tag{7}$$

where $dP = (-g)^{\frac{1}{2}} dp^{0123}$ and the integration is over P_x. For a gas of identical particles (mass m), $dP = (-g)^{\frac{1}{2}} dp^{123}/(-p_0)$ and the integration is over $P_x(m)$. In the case of a self-gravitating gas, the source of the gravitational field is (7). The Einstein field equations

$$G_{ab} \equiv R_{ab} - \tfrac{1}{2} R g_{ab} = T_{ab} \tag{8}$$

and equation (4) form the self-consistent Einstein-Liouville system of equations, since the integrability conditions

$$T^{ab}{}_{;b} = 0 \tag{9}$$

follow identically from (4) and (7).

The Einstein-Liouville system of equations can be generalised to alternative gravitational field equations. Fourth-order gravitational field equations are derived from a

quadratic gravitational Lagrangian [8]:

$$\begin{aligned} G^*_{ab} \equiv \; & R_{ab} - \tfrac{1}{2}Rg_{ab} + 2q\left[R(R_{ab} - \tfrac{1}{4}Rg_{ab}) - R_{;ab} + g_{ab}\Box R\right] \\ & + r\left[2(R_{acbd} - \tfrac{1}{4}g_{ab}R_{cd})R^{cd} - R_{;ab} + \tfrac{1}{2}g_{ab}\Box R + \Box R_{ab}\right] = T_{ab} \end{aligned} \tag{10}$$

where q and r are constants, $\Box = g^{ab}\nabla_a\nabla_b$, and (9) follows identically from (10), consistently with (4) and (7). The scalar-tensor Brans-Dicke gravitational field equations are [9]:

$$G^*_{ab} \equiv \phi(R_{ab} - \tfrac{1}{2}Rg_{ab}) - \omega(\phi_{;a}\phi_{;b} - \tfrac{1}{2}g_{ab}\phi_{;c}\phi^{;c})/\phi - (\phi_{;ab} - g_{ab}\Box\phi) = T_{ab} \tag{11}$$

where ω is a coupling constant, and (9) implies $\Box\phi = (3+2\omega)^{-1}T^a{}_a$.

3 Lifted Transformations on the Tangent Bundle and Matter Symmetries

In this section we situate the matter symmetries of Berezdivin and Sachs [6] within a general class of vector fields on TM (see [5] and the references therein for further details).

The coordinate basis vectors $\left\{\partial/\partial x^a, \partial/\partial p^b\right\}$ on TM do not transform covariantly. In order to provide a covariant splitting of vector field components on TM, it is necessary to use the anholonomic connection basis of horizontal and vertical vector fields

$$\mathbf{H}_a = \frac{\partial}{\partial x^a} - \Gamma^b{}_{ac}\, p^c \frac{\partial}{\partial p^b} \quad , \quad \mathbf{V}_a = \frac{\partial}{\partial p^a} \tag{12}$$

where

$$[\mathbf{H}_a, \mathbf{H}_b] = -R^d{}_{cab}\, p^c \mathbf{V}_d \quad , \quad [\mathbf{H}_a, \mathbf{V}_b] = \Gamma^c{}_{ab}\mathbf{V}_c \quad , \quad [\mathbf{V}_a, \mathbf{V}_b] = 0 \tag{13}$$

Then any vector field on TM can be split covariantly into components with respect to $\{\mathbf{H}_a, \mathbf{V}_b\}$ where the components and the basis vectors transform covariantly (i.e. like rank 1 tensors on M). The Liouville vector field (3) can be written is this basis as $\mathbf{L} = p^a\mathbf{H}_a$.

Any vector field Y^a on M generates point transformations along its integral curves. In addition we can define a smooth local rule governing the transport of tangent vectors along the integral curves of Y^a. For a linear transport rule, any tangent vector u^a at x is

transported to u'^a at x', where $u'^a = \Omega^a_b(x;\epsilon)u^b$. The linear *transport lifts* are the vector fields on TM which define these transformations [5]:

$$\mathbf{Y^A} = Y^a(x)\mathbf{H}_a + A^a_b\,(x)p^b\mathbf{V}_a \tag{14a}$$

where

$$A^a_b(x) = \partial\Omega^a_b(x;0)/\partial\epsilon + \Gamma^a_{bc}(x)Y^c(x) \tag{14b}$$

is the rank 2 tensor field on M which covariantly defines the transport of tangent vectors along Y^a. Suitable choices of A^a_b allow us to regain all of the standard lifted vector fields as special cases of (14) [5]. In particular, the matter symmetries of Berezdivin and Sachs are members of the subclass of (14) in which the transport rule Ω is *Lorentz transport* along Y^a. This implies

$$A_{(ab)} = 0 \tag{15a}$$

The matter symmetry vector fields in addition leave the distribution function invariant:

$$\mathbf{Y^A}(f) = 0 \tag{15b}$$

Note that (15a) implies $\mathbf{Y^A}(m) = 0$. Thus by (1), (3), (4) and (15) the vector fields $\mathbf{L}$ and $\mathbf{Y^A}$ are everywhere tangent to the 6-dimensional hypersurface $\{m =$ constant, $f =$ constant $\}$ of P. Our definition is equivalent to the original definition of Berezdivin and Sachs – that *a matter symmetry arises when observers at different points along Y^a–curves, using Lorentz frames, measure the distribution to be the same.*

Matter symmetries in fact arise in a well-known class of distributions – those which are isotropic in momentum space relative to some 4-velocity field u^a:

$$f(x,p) = F(x, u_a p^a) \tag{16}$$

Clearly f is invariant under the isotropy group of u^a in momentum space, i.e. under the rotation subgroup of the Lorentz group, with Lie algebra generators of the form $A^a_b p^b \partial/\partial p^a$ where $A_{ab}u^b = 0 = A_{(ab)}$. Thus the generators are matter symmetry vector fields that are vertical ($Y^a = 0$) [6]. Ehlers, Geren and Sachs [10] showed that for a dynamically isotropic distribution of the form (16) the spacetime is either stationary or

Robertson-Walker. In this case, matter symmetries give rise to very restrictive geometrical symmetries.

An important special case of linear transport lifts arises when the transport rule is Lie transport along Y^a, so that $A_{ab} = Y_{a;b}$ and we write the *complete (or Lie) lift* as

$$\widetilde{\mathbf{Y}} = Y^a \mathbf{H}_a + Y^a_{\ ;b}\, p^b \mathbf{V}_a \tag{17}$$

The rate-of-change of the distribution function under a spacetime symmetry Y^a is then $\widetilde{\mathbf{Y}}(f)$ [3,11]. By (15a), for a complete lift (17) to be a matter symmetry, Y^a must be a Killing vector field.

An alternative approach to dynamical symmetries is via invariance of the phase orbits, rather than invariance of the distribution function as in (15b). A vector field $\mathbf{Z}$ on phase space is a *dynamical path symmetry* of $\mathbf{L}$ if it maps curves of $\mathbf{L}$ (phase orbits) into each other, i.e. [5]

$$[\mathbf{Z}, \mathbf{L}] = \ell\, \mathbf{L} \tag{18}$$

for some scalar $\ell(x,p)$. If $\ell = 0$, then $\mathbf{Z}$ is known as a dynamical Lie symmetry (in this case, the parameter is invariant under the mapping of the phase orbit). *A matter symmetry that is also a path symmetry is the complete lift of a homothetic Killing vector field* (independently of any field equations) [5].

The identity [11]

$$\nabla_c \int p^a \cdots p^b \Psi(f) dP = \int p^a \cdots p^b \Psi'(f)\, \mathbf{H}_c(f) dP$$

leads, for $\Psi(f) = f$, to

$$T^{ab}_{\ ;c} = \int p^a p^b \mathbf{H}_c(f) dP$$

which gives, using integration by parts

$$\int p^a p^b \mathbf{Y}^{\mathbf{A}}(f) dP = T^{ab}_{\ ;c} Y^c - A^a_{\ c} T^{cb} - T^{ac} A^b_{\ c} - A^c_{\ c} T^{ab} \tag{19}$$

Equation (19) holds for any linear transport lift of the form (14a). If $\mathbf{Y}^{\mathbf{A}}$ is a matter symmetry then (15) and (19) imply

$$\mathcal{L}_Y T^{ab} = (A^a_{\ c} - Y^a_{\ ;c}) T^{cb} + T^{ac}(A^b_{\ c} - Y^b_{\ ;c}) \tag{20}$$

which was given by Berezdivin and Sachs [6]. Using the field equations for T^{ab}, (20) determines the fundamental link between dynamical matter symmetries and the geometrical properties of spacetime. In fact, Berezdivin and Sachs did not use equation (20). In this paper (20) is the crucial equation, and we are able to simplify considerably the derivation of their result by using it.

It is not surprising, but non-trivial to show, that matter symmetries form a Lie algebra. Using (13), (14) and (15) we find that for constants s and t

$$s\mathbf{Y}^{\mathbf{A}} + t\mathbf{Z}^{\mathbf{B}} = \mathbf{W}^{\mathbf{C}}$$

where $W = sY + tZ$ and $C = sA + tB$, which clearly implies $C_{(ab)} = 0$. Also [5]

$$[\mathbf{Y}^{\mathbf{A}}, \mathbf{Z}^{\mathbf{B}}] = [\mathbf{Y}, \mathbf{Z}]^{\mathbf{C}}$$

where

$$C = \nabla_Y B - \nabla_Z A - [A, B] - R(Y, Z)$$

is a rank 2 tensor field on M and $R(Y, Z)_{ab} = R_{abcd}Y^c Z^d$. By the symmetries of R_{abcd} and the skewness of A and B, it follows that C is skew and consequently that $[\mathbf{Y}, \mathbf{Z}]^{\mathbf{C}}$ is a matter symmetry.

Berezdivin and Sachs [6] pointed out that if $\mathbf{Y}^{\mathbf{A}}$ is a matter symmetry, then any scaling that is constant on momentum space

$$\mathbf{Y}^{\mathbf{A}} \to \overline{\mathbf{Y}}^{\overline{\mathbf{A}}} = e^{\lambda(x)}\mathbf{Y}^{\mathbf{A}} \tag{21a}$$

preserves its properties (15) as a matter symmetry, so that only the directions of Y^a and A_{ab} on M are important and not their magnitudes. We note also that scaling preserves the Lie algebra since it is linear and since

$$[e^{\lambda(x)}\mathbf{Y}^{\mathbf{A}}, e^{\phi(x)}\mathbf{Z}^{\mathbf{B}}] = e^{\lambda(x)+\phi(x)}\left\{[\mathbf{Y}, \mathbf{Z}]^{\mathbf{C}} + (\mathcal{L}_Y\phi)\mathbf{Z}^{\mathbf{B}} - (\mathcal{L}_Z\lambda)\mathbf{Y}^{\mathbf{A}}\right\}$$

(Thus the Lie algebra of matter symmetries is infinite-dimensional over the phase space, but not on each momentum space.) We will refer to (21a) as a gauge transformation, so that the basic properties of matter symmetries are gauge invariant. As expected,

the key equation (20) is gauge invariant. Equation (21a) gives rise to an important gauge freedom:

$$\overline{Y}_{a;b} = e^{\lambda}[Y_{a;b} + Y_a \lambda_{;b}] \tag{21b}$$

In particular, if $Y_{a;b} = Y_a \sigma_b$ where $\sigma_{[a;b]} = 0$, then by (21b), Y_a may be rescaled to a Killing vector field.

4 The Berezdivin and Sachs Result

In deriving their main result Berezdivin and Sachs do not motivate the 2-surface forming condition. It is difficult to see any alternative approach in searching for conditions implied by the matter symmetry properties. However, it is not clear what physical meaning may be attached to this assumption. Geometrically, the assumption is a natural generalisation of a dynamical path symmetry: the phase orbits are mapped by $\mathbf{Y^A}$ into paths within the $\mathbf{Y^A}$, $\mathbf{L}$ 2-surfaces, rather than into each other (i.e. into the $\mathbf{L}$ 1-surfaces).

At each point in phase space, $\mathbf{Y^A}$ and $\mathbf{L}$ span a 2-plane in the tangent space. However, in general the tangent 2-planes may not mesh together to form 2-surfaces. By Frobenius' theorem the condition for $\mathbf{Y^A}$ and $\mathbf{L}$ to be 2-surface forming is that $[\mathbf{Y^A}, \mathbf{L}]$ be in the tangent 2-plane at each point. If this condition does not hold, $[\mathbf{Y^A}, \mathbf{L}]$ together with $\mathbf{Y^A}$ and $\mathbf{L}$ generates 3-planes which, in turn, may or may not mesh together to form 3-surfaces. The most general case is that the matter symmetry $\mathbf{Y^A}$ and dynamical vector field $\mathbf{L}$ generate 6-dimensional integral surfaces. (Berezdivin and Sachs [6] claim that the most general case is 8-dimensional; however, the constraint equations $\mathbf{L}(m) = 0 = \mathbf{L}(f)$, $\mathbf{Y^A}(m) = 0 = \mathbf{Y^A}(f)$ restrict the integral curves of $\mathbf{L}$ and $\mathbf{Y^A}$ (and all their Lie brackets) to lie in the intersection of the hypersurfaces $\{m = \text{constant}\}$ and $\{f = \text{constant}\}$, which is of dimension 6.) Berezdivin and Sachs were unable to make progress with the general case, and assumed that $\mathbf{Y^A}$ is 2-surface forming with $\mathbf{L}$. Using this assumption they proved the following result [6]:

For a gas obeying the Einstein–Liouville equations, a correctly scaled matter symmetry that is 2-surface forming with the Liouville vector field is the complete lift of a Killing vector field on spacetime.

In this section we will outline an improved derivation of their result, which, unlike their derivation, may be applied to the case when $\mathbf{Y^A}$ is not 2-surface forming with $\mathbf{L}$ (see Section 5). The 2-surface forming condition is

$$[\mathbf{Y^A}, \mathbf{L}] = k(x,p)\mathbf{Y^A} + \ell(x,p)\mathbf{L} \tag{22}$$

for some scalars k and ℓ on P. By (18), Y^A is a dynamical path symmetry if $k = 0$. By (3), (12), (13), (14) and (15)

$$[\mathbf{Y^A}, \mathbf{L}] = (A^a{}_b - Y^a{}_{;b})p^b\mathbf{H}_a + (R^a{}_{bcd}\, Y^d - A^a{}_{b;c})p^b p^c \mathbf{V}_a \tag{23}$$

By (21) and (22), the 2-surface property is gauge invariant, with gauge freedom

$$\overline{k} = k - \lambda_{;a}p^a \quad , \quad \overline{\ell} = e^\lambda \ell \tag{24}$$

Thus there is a gauge freedom to scale away k provided it is of the form $k(x,p) = \alpha_a(x)p^a$ where $\alpha_{[a;b]} = 0$. (This will be shown to be the case below.) Then in this case $\overline{\mathbf{Y}}^{\overline{\mathbf{A}}}$ is a dynamical path symmetry. (Clearly the dynamical path symmetry property is not invariant under the matter symmetry gauge transformations.)

Expanding k and ℓ on each momentum space:

$$k(x,p) = \alpha(x) + \alpha_a(x)p^a + \alpha_{ab}(x)p^a p^b + \cdots \tag{25a}$$

$$\ell(x,p) = \beta(x) + \beta_a(x)p^a + \beta_{ab}(x)p^a p^b + \cdots \tag{25b}$$

we note that the gauge freedom (24) implies $\alpha \to \alpha - \lambda_{;a}\, p^a \quad , \quad \beta_{a_1 \ldots a_r} \to e^\lambda \beta_{a_1 \ldots a_r}$ $(r = 0, 1, \ldots)$. Substituting (25) into (22) and comparing with (23), yields a system of equations in powers of p^a. To fourth order these give

$$\alpha Y_a = 0 = \alpha A_{ab} \tag{26a}$$

$$A_{ab} - Y_{a;b} = Y_a \alpha_b + \beta g_{ab} \tag{26b}$$

$$R_{a(bc)d}\, Y^d - A_{a(b;c)} = A_{a(b}\alpha_{c)} \tag{26c}$$

$$Y_a \alpha_{(bc)} + g_{a(b}\beta_{c)} = 0 = Y_a \alpha_{(bcd)} + g_{a(b}\beta_{cd)} \tag{26d}$$

$$A_{a(b}\alpha_{cd)} = 0 = A_{a(b}\alpha_{cde)} \tag{26e}$$

The higher order equations have the same form as (26a,d,e). Then it is easily shown that the only possible non-zero coefficients are α_a and β, so that $k(x,p) = \alpha_a(x)p^a$ and

$\ell(x,p) = \beta(x)$. Covariantly differentiating (26b) and then symmetrising on ab and anti-symmetrising on bc yields [6]

$$g_{ab}\beta_{;c} - \beta_{;(a}g_{b)c} - \beta[\alpha_{(a}g_{b)c} - g_{ab}\alpha_c] + (Y_a\alpha_{[b;c]} + Y_b\alpha_{[a;c]}) = 0 \tag{27}$$

Assuming $\beta \neq 0$ we can choose the gauge potential in (21) and (24) to be $\lambda = -\log\beta$ so that (27) reduces to

$$g_{ab}\overline{\alpha}_c - \overline{\alpha}_{(a}g_{b)c} + (\overline{Y}_a\overline{\alpha}_{[b;c]} + \overline{Y}_b\overline{\alpha}_{[a;c]}) = 0 \tag{28}$$

Following [6] we contract (28) with $\xi^a\xi^b$ where ξ^a is arbitrary subject to $\xi^a\xi_a \neq 0$, $\xi^a\overline{Y}_a = 0 = \xi^a\overline{\alpha}_a$. Then (28) yields $\overline{\alpha}_a = 0$, so that $\overline{\mathbf{Y}}^{\overline{\mathbf{A}}}$ is a dynamical path symmetry by (18). Thus if $\beta \neq 0$, the 2-surface forming assumption reduces to the assumption that the matter symmetry is a dynamical path symmetry – and therefore it is the complete lift of a homothetic Killing vector [5]. Indeed by (26b) ($\beta \neq 0$):

$$\overline{Y}_{a;b} = \overline{A}_{ab} - g_{ab} \quad \Rightarrow \quad \mathcal{L}_{\overline{Y}}g_{ab} = -2g_{ab} \tag{29a}$$

At this point Berezdivin and Sachs employed an involved and ingenious argument to show that (29a) produces a contradiction when the field equations (8) are invoked. However, using (20) we can bypass their argument to immediately arrive at the result. Equation (20) with (29a) gives

$$\mathcal{L}_{\overline{Y}}T^{ab} = 2T^{ab} \tag{29b}$$

However, Einstein's field equations (8) with (29a) imply

$$\mathcal{L}_{\overline{Y}}T^{ab} = 4T^{ab} \tag{30}$$

using the identities for homothetic Lie derivatives [12]. This contradiction means that $\beta = 0$, and (29a) is not true. (Note that a non-zero cosmological constant does not affect this result). The importance of (20) is evident when comparing the complicated arguments of Berezdivin and Sachs with the straightforward derivation above. With $\beta = 0$, (27) implies $\alpha_{[a;b]} = 0$ so that (locally) $\alpha_a = \lambda_{;a}$ for some λ. Choosing λ as gauge potential, (21) and (26b) show that $\overline{Y}_{a;b} = \overline{A}_{ab}$, so that $\overline{Y}_a$ is Killing and $\overline{\mathbf{Y}}^{\overline{\mathbf{A}}}$ is its complete lift. We note that since $\overline{k} = 0 = \overline{\ell}$, $\overline{\mathbf{Y}}^{\overline{\mathbf{A}}}$ is not only a dynamical path symmetry

of $\mathbf{L}$ but furthermore a Lie symmetry [5]. Thus it turns out that the 2-surface assumption reduces to the condition that the matter symmetry is also a Lie symmetry of $\mathbf{L}$.

Berezdivin and Sachs have then shown that, at least in the 2-surface forming case, the Einstein field equations reduce the dynamical symmetry to a geometrical symmetry. In Section 5 we will investigate whether we can avoid this restrictive result by considering non-gravitational forces, by looking at alternative field equations or by relaxing the 2-surface forming condition.

5 Extensions of the Berezdivin and Sachs Result

5.1 Gas particles subject to non-gravitational forces

We follow [6] in assuming that $\mathbf{Y^A}$ is 2-surface forming with $\mathbf{L}$, but we consider whether non-gravitational forces may alter the result that the dynamical matter symmetry reduces to a Killing symmetry. We thus investigate the possibility that the dynamical symmetry degenerates to a geometrical symmetry mainly because the particles are in free fall. In fact this is not the case; an external force does not qualitatively alter the conclusion of Section 4.

First consider the case of charged particles, where the 4-force is the Lorentz force on each particle due to the collectively generated electromagnetic field. Using the 2-surface forming condition (22), with the generalised Liouville vector field (5) and the definition (14) of the matter symmetry, we get the charged particle generalisation of (23)

$$\begin{aligned}[\mathbf{Y^A}, \mathbf{L}_*] &= k(x,p)\mathbf{Y^A} + \ell(x,p)\mathbf{L}_* \\ &= (A^a{}_b - Y^a_{;b})p^b\mathbf{H}_a + \\ &\quad \{e(F^a{}_{b;c}Y^c + [F,A]^a{}_b)p^b + (R^a{}_{bcd}Y^d - A^a{}_{b;c})p^bp^c\}\mathbf{V}_a \end{aligned} \tag{31}$$

which yields two conditions:

$$(A^a{}_b - Y^a_{;b})p^b = kY^a + \ell p^a \tag{32a}$$

$$e(F^a{}_{b;c}\,Y^c + [F,A]^a{}_b)p^b + (R^a{}_{bcd}\,Y^d - A^a{}_{b;c})p^bp^c = kA^a{}_bp^b + \ell F^a{}_bp^b \tag{32b}$$

Equation (32a) is identical to the equation for the neutral ($e = 0$) case in Section 4, and using the expansions (25) again leads to $k(x,p) = \alpha_a(x)p^a$, $\ell(x,p) = \beta(x)$. An

argument identical to that of Section 4 shows that $\beta = 0$, $\alpha_a = \lambda_{;a}$ and $\overline{\mathbf{Y}}^{\overline{\mathbf{A}}}$ is the complete lift of the Killing vector field $\overline{Y}^a$. Then (32b) gives the additional symmetry condition that the electromagnetic field be invariant under the Killing symmetry:

$$\mathcal{L}_{\overline{Y}} F_{ab} = 0.$$

Thus the electromagnetic force fails to prevent the dynamical matter symmetry from reducing to a Killing symmetry. On the contrary, the dynamical matter symmetry forces the electromagnetic field to obey the same geometrical symmetry as the spacetime metric.

The same conclusion emerges when we look at a velocity-independent non-gravitational 4-force mh^a. The 2-surface forming condition with the generalised Liouville vector field (6) is

$$\begin{aligned} [\mathbf{Y}^{\mathbf{A}}, \mathbf{L}_*] &= k(x,p)\mathbf{Y}^{\mathbf{A}} + \ell(x,p)\mathbf{L}_* \\ &= (A^a{}_b - Y^a_{;b})p^b \mathbf{H}_a + \{(h^a_{;b} Y^b - A^a{}_b h^b) + (R^a_{bcd} Y^d - A^a_{b;c})p^b p^c\}\mathbf{V}_a \end{aligned} \quad (33)$$

Equation (33) yields (32a) and the additional condition

$$(h^a_{;b}\, Y^b - A^a_b\, h^b) + (R^a_{bcd}\, Y^d - A^a_{b;c})p^b p^c = kA^a_b p^b + \ell h^a \quad (34)$$

As before, (32a) leads to a Killing symmetry. Then (34) implies the same geometrical symmetry for the 4-force as for the spacetime metric:

$$\mathcal{L}_{\overline{Y}} h^a = 0\,.$$

In summary:

For a gas subject to a Lorentz or velocity-independent 4-force and obeying the Einstein-Liouville equations, a matter symmetry that is 2-surface forming with the Liouville vector field reduces to a Killing symmetry.

5.2 Alternative gravitational field equations

The derivation of the results of Section 4 is dependent on the form of the field equations. We investigate the effect that alternative gravitational field equations have on this result.

(37) holds. Consequently the result of Section 4 is relaxed to:

For a gas obeying the Liouville and Brans-Dicke field equations, a matter symmetry that is 2-surface forming with the Liouville vector field reduces to a homothetic Killing symmetry provided the long-range scalar field transforms homothetically.

5.3 Conformal Matter Symmetries

It may be that the Berezdivin and Sachs invariance (15*b*) is too restrictive, and that a more genuinely dynamical symmetry will result from generalising (15*b*). We try a conformal generalisation:

$$\mathbf{Y}^{\mathbf{A}}(f) = -2\psi(x)f \tag{38}$$

where $A_{(ab)} = 0$. (Note that (38) was also suggested by Oliver and Davis [7] in another context.) We retain the 2-surface forming assumption (22) and derive (29) as before. Substituting (38) into the identity (19) gives

$$\mathcal{L}_Y T^{ab} - (A^a{}_c - Y^a{}_{;c})T^{cb} - T^{ac}(A^b{}_c - Y^b{}_{;c}) = -2\psi T^{ab} \tag{39}$$

By (29) $\overline{Y}^a$ is a homothetic Killing vector field. The gauge invariant (39) gives, with (29*a*)

$$\mathcal{L}_{\overline{Y}} T^{ab} = (2 - 2\overline{\psi})T^{ab} \tag{40}$$

where $\overline{\psi} = \psi/\beta$. Comparing (30) and (40), we see that $\psi = -\beta$. Thus we are not forced to conclude that $\beta = 0$ as was the case for a non-conformal matter symmetry. In summary:

For a gas obeying the Einstein-Liouville equations, a conformal matter symmetry that is 2-surface forming with the Liouville vector field arises from a homothetic symmetry on spacetime.

It may be possible to generalise (15*b*) in other, more dynamical, directions. Our conformal generalisation allows only a slight modification of the restrictive Berezdivin and Sachs result from a Killing to a homothetic symmetry.

5.4 Matter symmetries that are not 2-surface forming with L

Our final attempted generalisation is the most difficult and the least conclusive. In the case when $\mathbf{Y^A}$ and $\mathbf{L}$ generate 3-surfaces, we are unable to determine whether in general the matter symmetry collapses to a geometrical symmetry. However, under special conditions we find that $Y_{(a;b)}$ is a Killing tensor.

By (29)

$$\mathbf{W} \equiv [\mathbf{Y^A}, \mathbf{L}] = (A^a{}_b - Y^a{}_{;b})p^b\mathbf{H}_a + (R^a{}_{bcd}Y^d - A^a{}_{b;c})p^bp^c\mathbf{V}_a \tag{41}$$

and the conditions that $\mathbf{Y^A}$ and $\mathbf{L}$ generate 3-dimensional integral surfaces are

$$[\mathbf{L}, \mathbf{W}] = k(x,p)\mathbf{Y^A} + \ell(x,p)\mathbf{L} + n(x,p)\mathbf{W} \tag{42a}$$

$$[\mathbf{Y^A}, \mathbf{W}] = k'(x,p)\mathbf{Y^A} + \ell'(x,p)\mathbf{L} + n'(x,p)\mathbf{W} \tag{42b}$$

for some scalars $k, k', \ell, \ell', n, n'$ on P. Note that the 3-surface property is gauge invariant: the gauge freedom (21) gives

$$\overline{\mathbf{W}} = e^\lambda[\mathbf{W} - (\lambda_{;a}p^a)\mathbf{Y^A}] \tag{43a}$$

$$\overline{k} = k - \lambda_{;ab}p^ap^b + (\lambda_{;a}p^a)^2 + n(\lambda_{;a}p^a) \ , \ \overline{\ell} = e^\lambda\ell \ , \ \overline{n} = n + 2\lambda_{;a}p^a \tag{43b}$$

and more complicated gauge transformations for k', ℓ' and n', which we will not use.

Now by (3), (14a) and (41)

$$[\mathbf{L}, \mathbf{W}] = (2A^a{}_{b;c} - Y^a{}_{;bc} - R^a{}_{bcd}Y^d)p^bp^c\mathbf{H}_a + (R^a{}_{bce;d}Y^e + 2R^a{}_{bce}Y^e{}_{;d} - R^a{}_{bce}A^e{}_d - A^a{}_{b;cd})p^bp^cp^d\mathbf{V}_a \tag{44}$$

$$\begin{aligned}[\mathbf{Y^A}, \mathbf{W}] \ = \ & (A^a{}_{b;c}Y^c - Y^a{}_{;bc}Y^c + Y^a{}_{;c}Y^c{}_{;b} - 2Y^a{}_{;c}A^c{}_b + A^a{}_cA^c{}_b)p^b\mathbf{H}_a \\ & + \{[R^a{}_{bce;d}Y^e + R^a{}_{bce}Y^e{}_{;d} - A^a{}_{b;cd}]Y^d + 2R^a{}_{bde}Y^eA^d{}_c - R^a{}_{bde}Y^eY^d{}_{;c} - A^a{}_{b;d}A^d{}_c \\ & + A^a{}_{b;d}Y^d{}_{;c} + R^a{}_{dce}Y^eA^d{}_b - R^d{}_{bce}Y^eA^a{}_d\}p^bp^c\mathbf{V}_a \end{aligned} \tag{45}$$

Owing to the complexity of the right-hand sides of (44) and (45) the method of Berezdivin and Sachs [6] is not applicable. Our method of Section 4 carries over to this case; we expand k, ℓ, and n in each momentum space to get (25) and

$$n(x,p) = \gamma(x) + \gamma_a(x)p^a + \gamma_{ab}(x)p^ap^b + \dots \tag{46}$$

The functions k', ℓ' and n' in (42b) can be expanded in a similar way. Substituting (25), (46) and their primed counterparts into (42), and using (44) and (45), we obtain, after lengthy calculations, a system of equations in powers of p^a. To third order, these give:

$$\alpha Y_a = 0 = \alpha A_{ab} \tag{47a}$$

$$Y_a \alpha_b + \beta g_{ab} + \gamma(A_{ab} - Y_{a;b}) = 0 \tag{47b}$$

$$Y_a \alpha_{(bc)} + g_{a(b}\beta) + A_{a(b}\gamma_{c)} - Y_{a;(b}\gamma_{c)} = 2A_{a(b;c)} - Y_{a;(bc)} - R_{a(bc)d}Y^d \tag{47c}$$

$$A_{a(b}\alpha_{c)} + \gamma[R_{a(bc)d}Y^d - A_{a(b;c)}] = 0 \tag{47d}$$

$$A_{a(b}\alpha_{cd)} + R_{a(bc|e|}Y^e\gamma_{d)} - A_{a(b;c}\gamma_{d)} = R_{a(bc|e|;d)}Y^e + 2R_{a(bc|e|}Y^e{}_{;d)} - A_{a(b;cd)} - R_{a(bc|e|}A^e{}_{d)} \tag{47e}$$

$$\alpha' Y_a = 0 = \alpha' A_{ab} \tag{48a}$$

$$Y_a \alpha'_b + \beta' g_{ab} + \gamma'(A_{ab} - Y_{a;b}) = A_{ac}A^c_b + A_{ab;c}Y^c - Y_{a;bc}Y^c + Y_{a;c}Y^c_{;b} - 2Y_{a;c}A^c \tag{48b}$$

$$Y_a \alpha'_{(bc)} + g_{a(b}\beta'_{c)} + A_{a(b}\gamma'_{c)} - Y_{a;(b}\gamma'_{c)} = 0 \tag{48c}$$

$$A_{a(b}\alpha'_{c)} + \gamma'\left[R_{a(bc)d}Y^d - A_{a(b;c)}\right] = \left[R_{a(bc)e;d}Y^e + R_+\right]$$
$$R_{a(b|de|}Y^e A^d_{c)} - R_{a(b|de|}Y^e Y^d_{;c)} - A_{a(b;|d|}Y^d_{;c)} + R_{a(b|de|}Y^d A^e_{c)} +$$
$$\mathrm{R}_{ad(b|e|}Y^e A^d_{c)} - A_{ad}R^d_{(bc)e}Y^e \tag{48d}$$

$$Y_a \alpha'_{(bcd)} + g_{a(b\beta'_{cd})} + A_{a(b\gamma'_{cd})} - Y_{a;(b\gamma'_{cd})} = 0 \tag{48e}$$

$$A_{a(b\alpha'_{cd})} + R_{a(bc|e|}Y^e\gamma'_{d)} - A_{a(b;c\gamma'_{d})} = 0 \tag{48f}$$

We see that equations (47b) and (47d) are related to the 2-surface forming conditions (26a) and (26b) according to the nature of the coefficient γ. If $\gamma \neq 0$, we may use a rescaling with $\lambda = \log\gamma$ to transform (47b) and (47d) into (26a) and (26b). In this instance, the 3-surface case degenerates to the 2-surface case. In order to have a non-degenerate 3-surface case we require that $\gamma = 0$, which implies $\beta = 0 = \alpha_a$ by (47b, d). (Note that $\gamma = 0 = \beta = \alpha_a$ is gauge invariant.) Furthermore, either (26a) or (26b) does not hold. If we define

$$U_{ab} = Y_{a;b} - A_{ab} \tag{49a}$$

$$V^a_{bc} = \mathcal{L}_Y \Gamma^a_{bc} - U^a_{(b;c)} \tag{49b}$$

then for either $U_{ab} \neq 0$ or $V_{abc} \neq 0$ we have a non-degenerate 3-surface case for which $\left[\mathbf{Y}^{\mathbf{A}}, \mathbf{L}\right] \notin \text{span}\left\{\mathbf{Y}^{\mathbf{A}}, \mathbf{L}\right\}$. The definitions (49) show that in principle Y_a (or $\overline{Y}_a$) may be Killing with $U_{ab} \neq 0 \neq V_{abc}$. However, we were unable to prove that this is true in general, or indeed to make further progress in the general case.

We now examine the special sub-case $k = l = n = 0$ of $\gamma = 0$. Although $\mathbf{W}$ are now 2-surface forming and commuting, $\mathbf{Y^A}$ is not necessarily 2-surface forming with $\mathbf{L}$. (Note that the gauge freedom (43b) only preserves this sub-case if λi (47c) and (47e) reduce to

$$2A_{a(b;c)} - Y_{a;(bc)} - R_{a(bc)d}Y^d = 0 \tag{50a}$$

$$R_{a(bc|e|;d)}Y^e + 2R_{a(bc|e|}Y^e_{;d)} - R_{a(bc|e|}A^e_{d)} - A_{a(b;cd)} = 0 \tag{50b}$$

Equation (50a) implies that $Y_{(a;bc)} = 0$ which means that $Y_{a;b}$ is a Killing tensor. By (49) and (50)

$$V^a_{bc} = U^a_{(b;c)} = \tfrac{1}{2}\mathcal{L}_Y\Gamma^a, U_{a(b;cd)} = R_{a(bc|e|}U^e_{d)} \tag{51}$$

Even in this special sub-case we are unable to determine the general solution via (51) or otherwise. We would like to find an example where the matter symmetry does not reduce to a Killing symmetry. The integrability conditions (51) are identically satisfied if Y_a is homothetic (i.e. $U_{(ab)} = \psi g_{ab}, \psi_{;a} = 0$). However, it is not clear to us whether the remaining equations in (48), or the higher order counterparts of (47), (48), will force Y_a to be Killing. Note that we have not used any field equations. In summary:

We are unable to extend the Berezdivin and Sachs result to the 3-surface case - and clearly the more general cases will be yet more complex. In the 3-surface sub-case where $\mathbf{L}$ *commutes with* $\left[\mathbf{Y^A}, \mathbf{L}\right], Y_{(a;b)}$ *is a Killing tensor, regardless of the gravitational field equations.*

There may be another approach which bypasses the surface-forming conditions and allows for a definite answer. The indications from the 3-surface forming equations are that the matter symmetry is still likely to reduce to a geometrical symmetry, even if not necessarily an isometry.

6 Concluding Remarks

In the case of a macroscopic fluid model, Bonnor and Ellis [4] introduce an observationally and termodynamically based definition of homogeneity - but this dynamical homogeneity does *not* lead in general to a geometrical homogeneity. In the microscopic kinetic model, the dynamical matter symmetry appears to lead inevitably to a geometrical symmetry. At first sight, one may suspect that these contrasting results arise from the fact that the

microscopic dynamical symmetry is too detailed and stringent, whereas the macroscopic dynamical symmetry allows for more latitude.

However the problem goes deeper than this first impression. The fact is that the dynamical matter symmetries reduce to geometrical symmetries only when we impose *additional assumptions* about their surface-forming properties. Without these additional assumptions, it is unclear what happens. Even our attempt to relax the 2-surface forming assumption involves a 3-surface forming assumption.

These surface-forming assumptions are not merely technical. As we pointed out in the 2-surface case, the assumption amounts to *assuming that the dynamical matter symmetry is simultaneously a dynamical path symmetry* (or a modified type of path symmetry). Thus in fact we remain unclear about the *essential* nature of matter symmetries - because the "pure" matter symmetry case appears intractable without simplifying assumptions.

Path and matter symmetries are very different approaches to dynamical symmetries in kinetic theory. The path symmetry has no apparent observational basis and leads directly to a *geometrical symmetry (at least in the unsatisfactory concept of dynamical symmetry).* In contrast, the matter symmetry of Berezdivin and Sachs is observationally based - but appears to be too broad without further assumptions.

The implications of a "pure" matter symmetry remain unknown. There may be another approach, alternative to our simplification and generalisation of the Berezdivin and Sachs approach, which uncovers the consequences of a matter symmetry without surface-forming assumptions. Alternatively, there may be additional dynamical (as opposed to phase-space geometrical) aspects which could naturally be added to the matter symmetry definition, or used to modify it, and which would lead to answers about the nature of genuinely dynamical symmetries in kinetic theory. One possible approach may be to seek a kinetic foundation for the fluid postulate of uniform thermal histories of Bonnor and Ellis [4]. These issues are currently under investigation.

References

[1] Kramer D., Stephani, H., MacCallum, M. A. H., and Herlt, E. (1980). *Exact Solutions*

of Einstein's Field Equations, Cambridge University Press, London.

[2] Coley, A. A., and Tupper, B. O. J. (1990). *Classical and Quantum Gravity*, **7**, 1961.

[3] Maartens, R., and Maharaj, S. D. (1985). *Journal of Mathematical Physics*, **26**, 2869.

[4] Bonnor, W. B., and Ellis, G.F.R. (1986). *Monthly Notices of the Royal Astronomical Society*, **218**, 605.

[5] Maartens, R., and Taylor, D. R. (1993). *International Journal of Theoretical Physics*, **32**, 143.

[6] Berezdivin, R., and Sachs, R. K. (1973). *Journal of Mathematical Physics*, **14**, 1254.

[7] Oliver, D. R., and Davis, W. R. (1979). *Annals de l'Institut Henri Poincaré*, **30**, 339.

[8] Barrow, J. D., and Ottewill, A. (1983). *Journal of Physics A*, **16**, 2757.

[9] Misner, C. W., Thorne, K. S., and Wheeler, J. A. (1973). *Gravitation*, Freeman, New York.

[10] Ehlers, J., Geren P., and Sachs, R. K. (1968). *Journal of Mathematical Physics*, **9**, 1344.

[11] Ehlers, J. (1971). in *General Relativity and Gravitation*, edited by Sachs, R. K., Academic, New York, pp. 1-70.

[12] Maartens, R., Mason, D. P., and Tsamparlis, M. (1986). *Journal of Mathematical Physics*, **27**, 2987.

Anisotropic Cosmology with Conformal Symmetry

R. Maartens and C. M. Mellin
Department of Computational and Applied Mathematics and Centre for Nonlinear Studies, University of the Witwatersrand, Johannesburg, 2050, South Africa

Abstract

We show that Bianchi I spacetimes admit a conformal Killing vector under certain conditions. Using this additional symmetry we are able to find two new exact solutions to Einstein's equations which satisfy the necessary energy conditions. These solutions could model the early universe with a hot big bang. Only the one solution is however asymptotically a Friedmann-Robertson-Walker universe, i.e. includes the late universe as a limiting case.

1 Introduction

The early universe may have been highly anisotropic and inhomogeneous. In order to model this period of the universe, we can look at models which are anisotropic, viz. models in which all spatial directions are not equivalent. Furthermore, we would expect asymptotic dissipation of this anisotropy as the universe expands, so that for large time the model is nearly isotropic, and approaches a FRW form. The simplest anisotropic cosmology has the spatially homogeneous Bianchi I metric of the form

$$ds^2 = -dt^2 + X(t)^2dx^2 + Y(t)^2dy^2 + Z(t)^2dz^2 \tag{1.1}$$

(where $X = Y = Z$ is the FRW line element).
Given a metric one chooses a suitable fluid model and then attempts to solve Einstein's equations

$$G_{ab} = T_{ab} \tag{1.2}$$

where the curvature of spacetime is described by Einstein's tensor G_{ab} and the type of fluid is described by the energy-momentum tensor T_{ab}. Eq. (1.2) is in general ten second order differential equations and there is little hope of obtaining any solutions *unless* we impose symmetry on the geometry. For the symmetric geometry (1.1), many

exact solutions are known [1]. These solutions are obtained by assuming some form of equation of state amongst the fluid variables. Another approach is to assume that (1.1) admits in addition to its Killing symmetries a conformal symmetry. Our new solutions arise from this approach.

2 Conformal Symmetry

If $\mathcal{L}_\xi$ denotes the Lie derivative along ξ, then ξ is a Killing vector if and only if

$$\mathcal{L}_\xi g_{ab} = 0. \tag{2.1}$$

The natural generalisation of (2.1) is

$$\mathcal{L}_\xi g_{ab} = 2\psi g_{ab} \tag{2.2}$$

where $\psi(x^a)$ is the conformal factor and now ξ is a conformal Killing vector (CKV) [2-4]. The dynamical effects of ξ are based on the transformation of the fluid four-velocity [3]:

$$\mathcal{L}_\xi u^a = -\psi u^a + v^a \tag{2.3}$$

where $v^a u_a$=0. The CKV maps fluid flow-lines into each other if and only if v^a=0 [3]. This is the case of the "inheriting" CKV [4]:

$$\mathcal{L}_\xi u^a = -\psi u^a \tag{2.4}$$

It seems however that Eq. (2.4) is too restrictive, since Coley and Tupper proved the following theorem [4]: *Orthogonal synchronous perfect fluid spacetimes (including Bianchi spacetimes), other than FRW spacetimes, do not admit any inheriting proper CKV.*
Thus Coley and Tupper were led in [4] to conjecture that there exist no perfect fluid spacetimes admitting a proper inheriting CKV, except FRW specialisations and other very restrictive spacetimes.
Our results tend to support a generalisation of this claim to spacetimes in which v^a is not zero, i.e. to non-inheriting CKV. We weaken the inheriting condition (2.4) by assuming that ξ^a is two-surface-forming with u^a, i.e.

$$\mathcal{L}_\xi u^a = -\psi u^a + \lambda h^{ab}\xi_b \tag{2.5}$$

for some λ, where $h_{ab} = g_{ab} + u_a u_b$.

3 New Solutions

The Bianchi I metric (1.1) admits a two-surface-forming CKV of the form (2.5) in the (t,x) plane [5]

$$\xi = Ye^{bx}\partial_t + B(t)e^{bx}\partial_x \tag{3.1}$$

provided $Y = Z$ (i.e. axially symmetric Bianchi I), and

$$Y = X(C \sinh b\tau + D \cosh b\tau) \tag{3.2}$$

where b, C, D are constant and

$$\tau = \int \frac{dt}{X}. \tag{3.3}$$

For a cosmological solution of Einstein's equations (1.2) the type of fluid must be specified and be subject to the weak energy condition

$$\mu \geq 0, \tag{3.4}$$

where μ is the energy density, the dominant energy condition

$$\mu + p \geq 0, \tag{3.5}$$

where p is the isotropic pressure, and

$$0 \leq \left(\frac{dp}{d\mu}\right) \leq 1 \tag{3.6}$$

where the last equation ensures that locally the speed of sound is less than the speed of light and also that the fluid is stable against mechanical collapse.
We examined the following three types of fluid.

Type I

A perfect fluid in which the energy-momentum tensor takes the form

$$T_{ab} = \mu u_a u_b + p h_{ab}. \tag{3.7}$$

It is proved in [5] that in this case $\mu + p \leq 0$ so that the energy condition (3.5) is violated. However, note that unlike the inheriting case, a perfect fluid solution *does* exist for a two-surface-forming CKV.

Type II

Since the type I model did not have sufficient freedom to admit a physical solution, we considered an anisotropic fluid with unequal pressures $p_{\|}$ along the x-axis and $p_{\perp}$ perpendicular to the x-axis, so that the energy-momentum tensor has the form [3]

$$T_{ab} = \mu u_a u_b + p_{\|} n_a n_b + p_{\perp} p_{ab} \tag{3.8}$$

where $n_a u^a = 0$, $n_a n^a = 1$ and $p_{ab} = g_{ab} + u_a u_b - n_a n_b$. In this model the geometric anisotropy is accompanied by a dynamical anisotropy. Using (1.2) and (2.2) we get four differential equations in five unknowns and thus require an equation of state. Working with the radiation universe equation of state $p = \frac{1}{3}\mu$, where $p = \frac{1}{3}(p_{\|} + 2p_{\perp})$, and taking $C = D$ in Eq. (3.2) for simplicity, we obtain the solution [5]

$$X = B(\tau - A)e^{-b\tau}, \qquad Y = B(\tau - A) \tag{3.9}$$

5 Acknowledgements

CMM thanks the University of the Witwatersrand and the FRD of South Africa for support.

References

[1] D. Kramer, H. Stephani, E. Herlt and M. MacCallum, *Exact Solutions of Einstein's Field Equations* (Cambridge University Press, 1980).

[2] L. Herrera, J. Jimenez, L. Leal, J. Ponce de Leon, M. Esculpi and V. Galina, *J. Math. Phys.* **25** (1984) 3274.

[3] R. Maartens, D. P. Mason and M. Tsamparlis, *J. Math. Phys.* **27** (1986) 2987.

[4] A. Coley and B. Tupper, *Class. Quantum Grav.* **7** (1990) 1961.

[5] R. Maartens and C. M. Mellin, (1993) (in preparation).

[6] J. Peter Vajk and P. G. Eltgroth, *J. Math. Phys.* **11** (1970) 2212.

2 Emission Mechanisms

Before looking at the regions that produce the radio and IR emission, we will digress in order to discuss the physics of how the radiation is produced. We also address the question of why these two types of radiation are related.

Radio emission can be generated in a number of ways, the process that we are interested in is called a maser. To understand how a maser works we need to look at how radiation interacts with matter on the atomic level. An atom consists of a central nucleus made up of protons, which are positively charged, and neutrons, surrounded by orbiting negatively charged electrons. The electrons can only occupy certain energy states; in going from one energy state to another they either emit or absorb a photon. The electrons are like a ball on a flight of steps which represent the different energy levels, in this case gravitational potential energy.

Einstein identified three processes by which matter (atoms or molecules) interacts with radiation. Radiation is made up of bundles of energy called photons. Each photon has an energy that is directly proportional to its frequency. A beam of radiation with a specific frequency consists of a bunch of photons all travelling in the same direction and having the same energy.

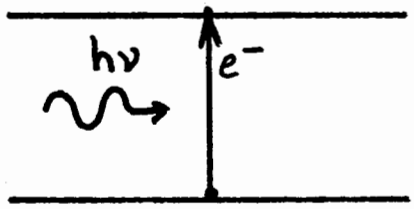

Absorption In this process an electron absorbs a photon of energy and moves from one level to a higher level.

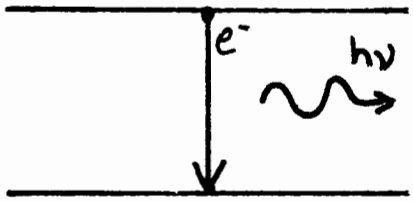

Spontaneous emission An electron initially in a level drops down to a lower level, emitting a photon in the process.

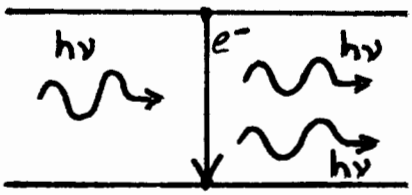

Stimulated emission In this case an electron in an upper level is stimulated to make a downward transition by a beam of radiation.

If a beam of radiation passes through a gas that absorbs photons, the intensity of that beam is reduced. In spontaneous emissions the photon is emitted in a random direction, whereas the photon emitted by the process of stimulated emission has the same frequency and direction of propagation as the incident beam. The intensity of the beam increases with each interaction and hence the initial signal is amplified. This mechanism, Microwave Amplification by Stimulated Emission of Radiation, is referred to by the acronym maser. This same process can work with shorter wavelength radiation such as visible light, in which case the mechanism is called a laser.

The frequency of the photon absorbed or emitted by these processes is unique for each transition of an atom or molecule. Hence, line emission or absorption can be used to identify the atom or molecule that is interacting with the radiation.

2.1 Infrared Emission

Any object that has a temperature above absolute zero emits radiation. In an ideal situation the object is called a blackbody and has an intensity distribution, i.e. brightness per unit area versus frequency, given by the Planck function which can be parameterized in terms of one quantity only, namely the temperature. It turns out that the hotter an object is the higher the frequency of its peak emission. This phenomenon can be demonstrated by sticking a poker into a fire - first it glows with a reddish hue, then passes through orange and yellow phases as it heats up, until finally it becomes white hot. Stars follow the same pattern. Red stars, whether they be giants or dwarfs, have a cool surface, whereas hot bodies such as O or B stars have a blue or white colour. Because giant stars have a larger surface area than dwarfs, they are more luminous than their smaller counterparts at the same temperatures and are more likely to be seen. For example, Antares and Betelgeuse are red supergiants at distances of approximately 400 and 600 lightyears respectively and are clearly visible, whereas Barnard's star is a red dwarf at a distance of 6 lightyears but cannot be seen without optical aids. Similarly, the B supergiant Rigel is the seventh brightest star in the sky even though it lies 900 lightyears away, while Sirius's companion, a white dwarf only 8,7 lightyears away, can only be detected using a reasonably sized telescope.

Clearly, as a body cools down, its peak emission will decrease in frequency, eventually dropping below the optical band and into the IR. Because we cannot detect this radiation we do not see the heat radiation associated with bodies at normal room temperatures. Using IR cameras, however, it is possible to photograph this radiation. The blackbody radiation associated with the Big Bang has cooled down to such a low temperature (about 2,73K) that the frequency of its peak emission occurs at a radio frequency. Although dust does not behave like an ideal blackbody radiator, it nevertheless produces its peak intensity at a frequency that is related to its temperature. By measuring the intensity of the radiation at a range of frequencies it is possible to estimate where the peak occurs and hence the temperature of the dust grains. Most of the dust in our galaxy is at temperatures of a few hundred degrees Kelvin and therefore emits mainly in IR bands.

Dust around stars absorbs UV and visible radiation and heats up. The warm dust reradiates, producing its strongest emission in the IR. The energy of UV photons is sufficient to dissociate molecules and, if their frequency is high enough, even to ionize

atoms. Thick dust clouds surrounding stars absorb most of the radiation that would destroy molecules, thereby providing a secure environment for them to exist in. The ozone layer in our atmosphere serves much the same function. Harmful UV radiation from the Sun is absorbed by ozone molecules which occur naturally at heights between 12 and 50 km in the stratosphere. Without this protection, life would not survive the Sun's harmful rays.

3 Star-forming regions

Stars are believed to form inside Giant Molecular Clouds (GMCs) when the material becomes gravitationally unstable and collapses under its own gravity. The GMC fragments into smaller clouds, each of which contracts and heats up to become a protostar. The protostars thus formed have different masses. Only about 1 to 10 percent of the mass of a cloud actually ends up forming the star, the rest of the material gets blown into the interstellar medium.

If the mass of the protostars is low, typically less than the Sun, these very young objects that have not yet started burning hydrogen in their cores are called T Tauri stars. Their magnitudes vary irregularly and they have high velocity infalling or outflowing gases. The outflowing gas often occurs in bipolar jets. This powerful, assymmetric wind from the star crashes into parts of the original cloud, producing small faintly luminous emission line nebulae which are irregular in outline and contain bright knots. Light from other parts of the dust cloud produces continuum emission. The young star is normally concealed by the dust clouds and can only be seen in the radio region. These objects, named after their discoverers, are called Herbig-Haro objects.

Larger mass stars form much deeper inside GMCs and are not visible optically until well after the star has evolved onto the main sequence. If a hot O or B star is formed, UV radiation from the stellar surface dissociates molecules and dust grains and ionizes the surrounding medium. Since hydrogen is the predominant component of the gas, these are known as H II regions. Initially the volume is very small or compact.

Maser emission from molecules of water (H_2O), hydroxyl (OH) and methanol (CH_3OH) have been discovered in the molecular clouds surrounding these compact H II regions. Water masers occur particularly in regions associated with outflows, while OH and methanol appear to come from regions with temperatures of $\sim$50 K. Water masers have been found in Herbig-Haro objects where the bipolar jets interact with the dust cloud. Empirically it has been found that methanol masers appear to be associated with very young star-forming regions; the stars are probably no more than $\sim$10000 - 100000 years old. By searching for radio emission from methanol masers, a number of probable new star-forming regions have been discovered.

The Omega nebula, M17, and the Orion nebula, M42, are examples of stellar nurseries at a slightly more advanced stage of evolution. The four stars making up the Trapezium in M42 are responsible for ionizing the medium and causing it to glow. The emission nebula forms a cavity inside a much larger dark nebula. The Rosette nebula provides an example of a star-forming region where the radiation pressure from the hot young stars has blown out a cavity in the centre. The Pleiades and the Jewel Box are examples of clusters of

stars that have blown away the clouds from which they formed. The Trifid Nebula is an example of an H II region (characterized by the red emission from Hα) interspersed with a network of dark bands of cool interstellar dust which are not yet ionized by the hot stars. Stars may still condense out of this material. To the north of the emission nebula there is a blue reflection nebula. This is material that is not ionized; its bluish colour is due to light from the bright central star being scattered off dust particles.

4 Late-type Stars

When a star has exhausted all the hydrogen in its core it evolves away from the main sequence and becomes a red giant. Hydrogen is still being converted into helium but the burning occurs in a shell surrounding the core.

Once a star has become a giant, its luminosity increases as it ages. This raises the radiation pressure on material in the outer layers and enhances the rate at which matter is driven off the star. As material is lost from the surface, deeper layers of the star are exposed. Eventually, the star has lost so much material that its very hot core is exposed. The radiation from the hot core ionizes the gas it has ejected, thereby causing it to glow in the same way that hot, young stars cause their progenitor clouds to glow. The ejected shell is seen as a ring around the central star and is known as a planetary nebula (PN). The Helix and Ring nebulae are spectacular examples of this stage of stellar evolution.

During the red giant phase and before it becomes a PN, the star may vanish optically. To see why this occurs we need to look at what is happening in the stellar interior. Elements such as carbon, nitrogen, oxygen and silicon are synthesized inside the star by nuclear fusion processes during its evolution. Atoms of these elements are brought to the surface by convective motions in the stellar envelope. The outer layers are then ejected and about one stellar radius above the surface the material has cooled sufficiently for atoms of carbon to condense into grains or combine with oxygen to form stable CO molecules. Likewise, SiO can form in this cool environment. The dust and molecules continue to cool as they move away from the star but also start to absorb optical and UV radiation from the star. Eventually the amount of dust produced is thick enough to block out most of the visible light from the star and a protected environment is produced in which more fragile molecules such as SiO, H_2O and OH can form. Once again during its evolution the conditions surrounding the star are right for the formation of masers.

Mira, a red giant also known as Omicron Ceti, was the first star to be discovered to vary periodically. It has a mean period of $\sim$330 days but it is subject to irregularities. It ranges in optical brightness between 2,0 and 10,1 magnitudes, but some maxima are brighter than others and some minima dimmer than others. In the IR the variation in brightness is much less, typically only about 1 magnitude. The star is losing mass via a stellar wind, the outflow velocity of this gas varying between 5 and 10 km/s.

Mira variables are pulsating stars similar to Mira. They are regularly variable red giants with periods in the range 100 to 1000 days. The mass of these stars is less than 3 $M_\odot$. Stars with masses greater than 3 $M_\odot$ have higher mass loss rates and longer periods than the Miras. Periods of up to 10 years have been found. Mass loss rates of up to 10^{-4} $M_\odot$ per year produce a thick circumstellar dust shell several stellar radii above the

surface that obscures these stars optically. However, they radiate strongly in the IR and were discovered to have associated OH masers. Although other types of masers have since been found in these stars, they are still known as OH/IR stars.

Because of a star's spherical structure, its outflow is symmetrical. Hence properties of its circumstellar material such as density, composition and temperature change as a function of the distance from the star. If the right conditions for masers to exist occur at some radius from the centre, maser emission will be produced from a shell. Because the emitting material is moving outwards, the wavelength of the radiation will be Doppler shifted. The material from the front of the shell is moving towards the observer and is hence blue-shifted, while the radiation from the back of the shell is moving away and therefore is red-shifted. The spectra of OH maser emission from OH/IR stars are typified by a double-peaked profile. The difference in wavelength between the two peaks can be used to determine the outflow velocity. Because maser lines are so narrow, the velocity of the radial component of the object can be measured to an accuracy of $\sim$1 km/s.

Because OH/IR stars pulsate, albeit with periods of years, the amount of radiation they emit varies. These changes cannot be seen in visible light, but the intensity of the IR and radio emissions is modulated by the stellar pulsations. The changes in the maser emission occur essentially simultaneously throughout the shell. However, because the maser region occurs a long way from the surface, the near and far side of the maser shell are separated by a vast distance. The light travel time across the shell can be from a few days to weeks or even months long. Because the signals take a finite time to transit the shell, an observer is going to see the change from the far side of the shell after the change from the near side. By measuring the phase lag between changes in the red- and blue-shifted peaks, it is possible to determine the light travel time across the shell, and therefore its size. Using VLBI techniques, a map of the shell can be obtained, from which the angular size of the shell can be measured. Comparing the angular size with the shell diameter it is possible to estimate a distance to these stars.

5 Conclusion

Because clouds of dust are far more transparent to long wavelength radiation than to optical emission, it is possible using radio and IR telescopes to study regions of our galaxy that are obscured to visible light. Grains of carbon, often referred to as dust, in molecular clouds or in circumstellar shells around evolved stars absorb UV and optical photons, obscuring stars embedded in the material. This causes the dust to heat up, attaining temperatures of up to a few hundred Kelvin so that it reradiates this thermal energy with peak emissions in the IR. This radiation can escape from the medium and can be detected.

Molecules of substances such as OH, H_2O, SiO and CH_3OH which are dissociated by UV radiation, are formed and can survive in the protected environment provided by the dust. Under the right conditions of density and temperature, the above mentioned molecules are able to amplify microwaves by the maser mechanism, producing intense beams of radio radiation at very specific wavelengths.

Star-forming regions can be identified by their IR radiation and by studying the maser

emission from them we can learn more about the conditions inside GMCs and hence the processes associated with stellar nurseries. By monitoring the maser emission from OH/IR stars we can determine their distance from us and trace how stars evolve from the giant phase to planetary nebulae.

Acknowledgments

Drs M.J. Gaylard and G.C. MacLeod are thanked for their helpful discussions and Peter and Helen Stocker for their comments and careful proof-reading.

The South African Large Telescope

R S Stobie
South African Astronomical Observatory
P O Box 9, Observatory, 7935, South Africa

Abstract

It is proposed that a 3.5 m telescope for optical / infrared astronomy be constructed and sited in southern Africa. With active and adaptive optics such a telescope will approach diffraction-limited performance and enable a wide range of new science not achievable with current facilities. The unique contribution that South Africa can make to astronomy, the advances in telescope technology that can be incorporated and the scientific impact of the South African Large Telescope are presented.

1 Introduction

Historically, observations of the Universe have contributed fundamentally to the development of mathematics and physical science. In the time of Babylon the solution of astronomical problems required new ways of doing mathematics, and in particular led to the development of geometry and trigonometry. Two thousand years later Newton's interpretation of the observations of planetary positions resulted in the laws of motion and mechanics, and inspired the development of the calculus. A further three hundred years lated the study of the Universe gave rise to relativity through Einstein and the concept of nuclear fusion to explain the energy source of stars through Eddington. Contemporary examples are: (1) The connection between cosmology and high energy particle physics by which the properties of the hypothesised elementary particles can be constrained from observations of the large scale structure of the Universe; (2) the inference, based on general relativity, that the binary pulsar orbit is decaying through the emission of gravitational radiation. It is absolutely clear that this process is not finished. For example, one of the major unsolved problems in modern astronomy is that the luminous matter in the Universe only accounts for ~10% of the mass. The remaining ~90% of the mass is in a form unknown, although we know that it is not made of atoms. Once the nature of this mass is discovered it seems very likely that this will lead to further fundamental advances in science. Time and time again astronomy has been responsible for generating advances in mathematics and science, and there is every reason to believe that it will continue to do so.

2 Importance of Astronomy to South Africa

South African astronomy has a long and distinguished history, with a renaissance of observational excellence in recent years arising from the creation of first rate national telescope facilities. Currently, the largest optical / infrared telescope is the 1.9 m telescope at the Sutherland outstation of the South African Astronomical Observatory (SAAO). This telescope was commissioned in 1948, demonstrating the long useful life that telescopes can have. During the last four decades the performance of the telescope has been successively improved, primarily through advances in the quality of the instrumentation. However, with the sensitivity of the detectors now approaching 100% quantum efficiency, further gains can be achieved only by increasing the light gathering capacity through the construction of a larger telescope.

The majority of optical / infrared telescopes are located in the northern hemisphere. Yet the southern sky is rich in objects which are of unique importance for modern astronomy and which can only be accessed easily from sites in the southern hemisphere. The centre of our own Galaxy, which may contain a black hole, passes almost overhead at the latitude of South Africa. The Galactic Centre also presents by far the nearest, and hence highest angular resolution, case for the study of unusual activity in the nuclei of some galaxies. Our two nearest extragalactic neighbours, the Large and Small Magellanic Clouds, are so far south that they can only be usefully observed from the southern hemisphere. They are laboratories of immense importance for the detailed study of stellar and galactic evolution. They also provide the basis for establishing the extragalactic distance scale on which estimates of the size and age of the Universe depend.

The unique geographical location of South Africa is crucial for many astronomical projects, particularly involving time-critical phenomena. Because of the distribution in longitude of the major land masses in the southern hemisphere, certain time-critical observations, which are not possible in South America or Australasia (because of daylight), can be obtained in southern Africa. Two examples when this was vital were when (1) the time of closest approach of the Giotto spacecraft to comet Halley was recorded by astronomers visiting South Africa and (2) the supernova 1987A (Figure 1), which was the brightest supernova for nearly 400 years (since Kepler's supernova of 1604), had its first spectrum taken at Sutherland. Furthermore, time series observations of astronomical objects sometimes require 24-hour coverage to understand the complex phenomena. Such coverage is only possible with astronomical sites in all three major continents of the southern hemisphere.

South Africa would not be able to make an important contribution to modern astronomy were it not for the excellence of its climate, and its clear and dark skies (well away from cities and light pollution). In this proposal two sites are considered for the location of the South African Large Telescope (SALT). One is the existing Sutherland outstation of the SAAO, which is a very good site, where the infrastructure already exists. The second possibility is the Gamsberg mountain in Namibia, which is an excellent site, but where the infrastructure would have to be developed. This second option would involve a tripartite agreement between the governments of South Africa and Namibia, and the Max Planck Institut für Astronomie, Heidelberg, Germany who own the top of the Gamsberg mountain.

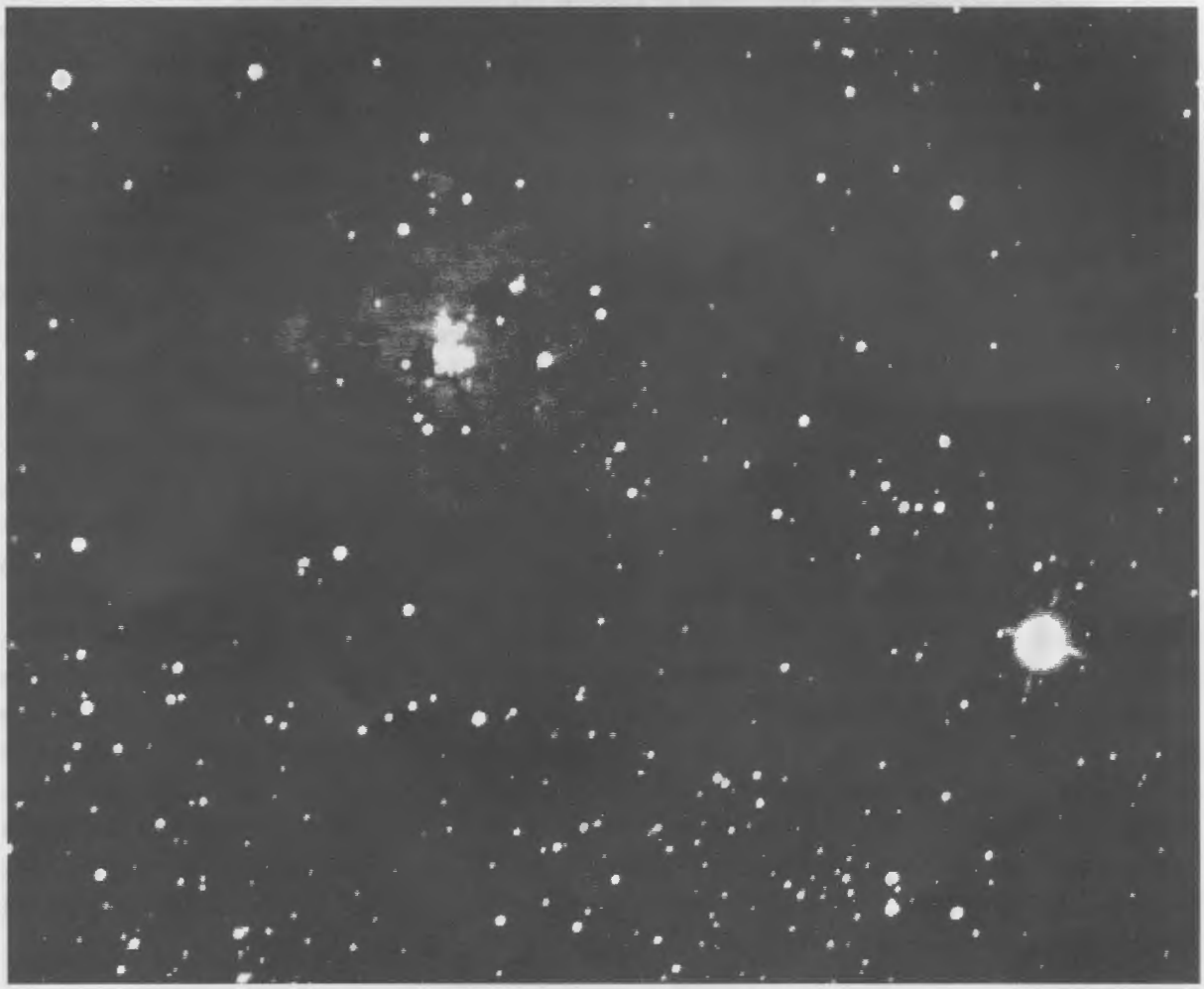

Figure 1: The supernova 1987A and the Tarantula Nebula in the Large Magellanic Cloud as photographed from Sutherland. It presented a major opportunity for southern hemisphere astronomers to study the physics of a supernova explosion and establish more accurately the distance scale of the Universe.

3 New Technology Telescope

Towards the end of the 1980s there were important developments in the technology of telescopes. First, the design of telescope mounting changed from equatorial to the much more compact alt-azimuth mounting, requiring sophisticated computer control. Second, thin mirror techonology took a quantum leap forward with active control of the shape of the primary and positional control of the secondary, together enabling better imaging performance. Third, developments in dome and building design and environmental control have improved the quality of the images. Fourth, major breakthroughs are taking place in adaptive optics, which effectively control flexible mirrors at rates of 10-20 Hz in order to remove the effects of the blurring of images caused by the passage of light through the Earth's atmosphere. The combination of these improvements means that a new technology telescope has the capability of approaching the ultimate in angular resolution, namely the diffraction limit of the telescope itself. This kind of performance is normally associated with telescopes in space, but now is becoming achievable with ground-base telescopes (at a fraction of the cost of a space mission).

Although there are a number of 4 m telescopes in the world, very few have this capability of approaching diffraction-limited performance. The first thin mirror telescope with active optics was the European Southern Observatory's New Technology Telescope, which was completed in 1988 and it dramatically demonstrated the improvement in imaging quality. The second telescope currently being built with this capability is the Osservatorio Astronomico di Padova's Telescopio Nazionale Galileo. Other large telescopes of 8 m class are being planned / built with a similar capability and are expected to come on-line towards the end of this decade. The ability to approach diffraction-limited performance makes a vast difference in the faintness of the object that can be recorded, enabling the study of the early Universe to become an observational reality, and is essential in the angular resolution improvements required for the study of crowded fields. Research proposals by South African astronomers to use SALT revealed that such a capability is essential for many of the projects. Such a capability would give the SALT 3.5 m telescope (Figure 2) a crucial competitive edge over most other 4 m class telescopes.

4 Scientific Impact of SALT

The new thin mirror technology, and the development of active and adaptive optics, enable major new scientific advances, of which most existing 4 m class telescopes are not capable. These advances relate primarily to the increase in angular resolution afforded by near-diffraction limited performance. To achieve this performance requires the telescope to be located at an excellent site where a substantial number of nights have sub-arcscond seeing and a reasonable fraction have sub-0.5 arcsecond seeing. Both sites, Sutherland and Gamsberg, have this high quality of seeing.

Increased angular resolution benefits many areas of astronomy. In the case of globular clusters it will permit the study of crowded stellar fields closer to the core of the cluster. In the study of star formation it will enable a more detailed study of regions close to the forming star, of the bi-polar flows that seem to be a common feature of star formation

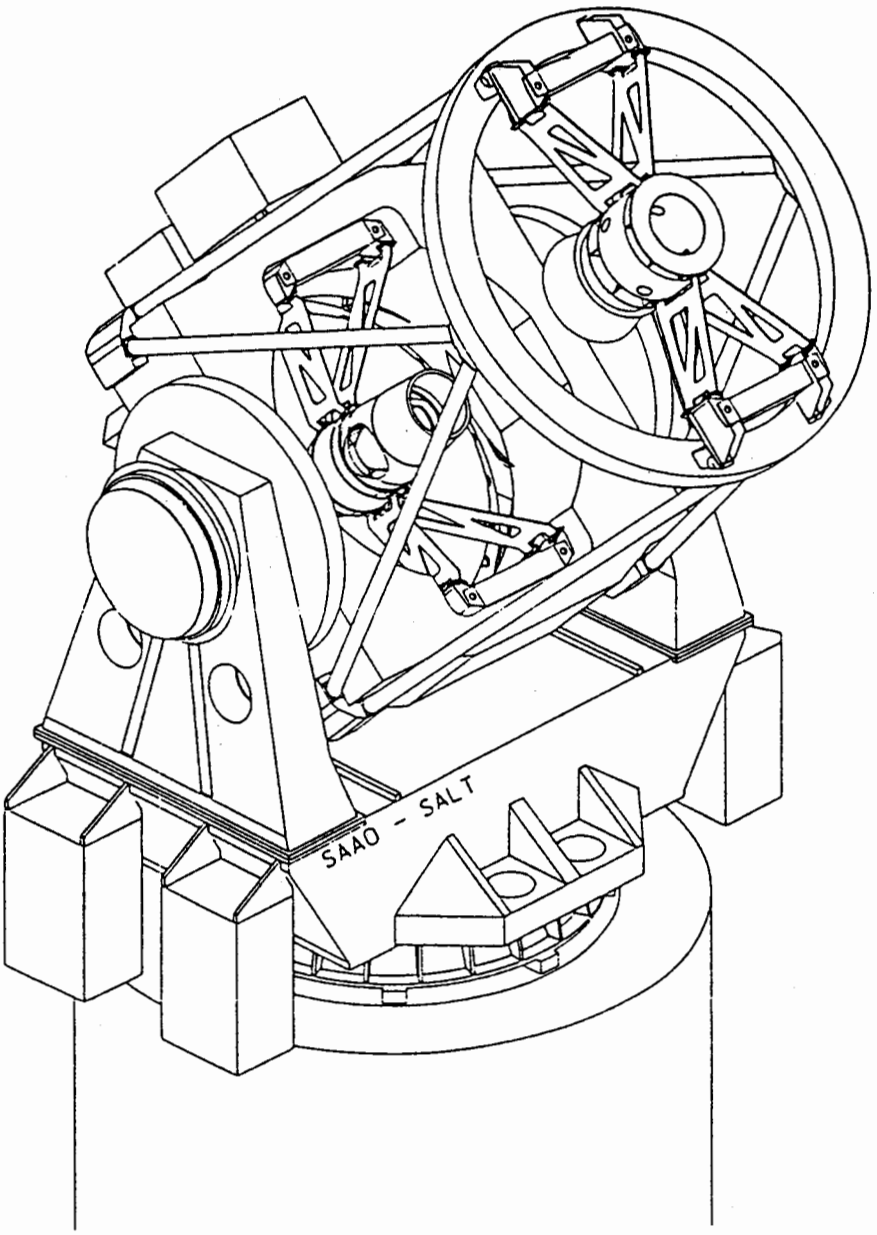

Figure 2: SALT 3D general assembly drawing, 45° elevation.

(Figure 3), of the dusty discs that surround some young stars and even of the possible existence of planets. Studies of the centre of our own Galaxy will benefit from high angular resolution enabling a linear resolution of 0.02 parsec at the very centre. The Magellanic Clouds are often difficult regions to study because of the crowded nature of the star fields - this situation will also be improved with better angular resolution. The same argument applies to other neighbouring galaxies; particularly in understanding the nature of active galactic nuclei where high angular resolution is essential.

One of the major motivations for the SALT 3.5 m telescope is the increased capability in cosmological studies. This arises from the increased light gathering capacity enabling both faint galaxies and the early evolution of the Universe to be studied. How galaxies formed, the early stages of evolution of galaxies and the discovery of proto-galaxies are areas of active research to which SALT can make major contributions.

The near diffraction-limited performance enables much fainter objects to be studied primarily because the concentration of light into a smaller image means that the sky background contribution is corrrespondingly reduced. This has a major impact especially on the study of faint point-source objects such as distant quasars. Quasars are known to be the very active nuclei of a small percentage of galaxies. As the most luminous objects in the Universe, they permit the study of the most distant and early stages in the evolution of the Universe.

A further factor which will enable SALT to make a substantial impact in the time when larger 8 m telescopes are coming on-line is the policy of telescope time allocation. During the last two decades, when 4 m telescopes were already in operation, the 1.9 m telescope at Sutherland remained internationally competitive partly because the policy of time allocation enabled longer-term projects to be pursued. This was not possible on most 4 m telescopes, where typically a few nights per annum were scheduled for specific projects. With future 8 m telescopes the pressure on time will increase and the amount allocated will be even shorter. Holding to the same policy of time allocation as with the 1.9 m telescope will enable the SALT 3.5 m telescope to remain internationally competitive even with 8 m telescopes in existence. In practice, 4 m class telescopes will be the work horses of the next 30-40 years and very few countries will have access to 8 m class telescopes.

5 Feasibility Study

In 1992 a feasibility study was initiated and carried out jointly by SAAO staff and the firm of consulting engineers, Liebenberg & Stander. This feasibility study determined the cost of constructing a 3.5 m telescope based on the Galileo design, the design and cost of a building to house the telescope, an assessment of the capability of South African industry to construct components, the infrastructure development cost associated with both the Sutherland and Gamsberg site options, and the breakdown of the project into its major components, the procurement plan and the project management.

The results of this feasibility study are being incorporated into a document "SALT - A Proposal for Funding". This document presents the complete case for SALT including the scientific case, the importance of astronomy to South Africa, the unique contribution

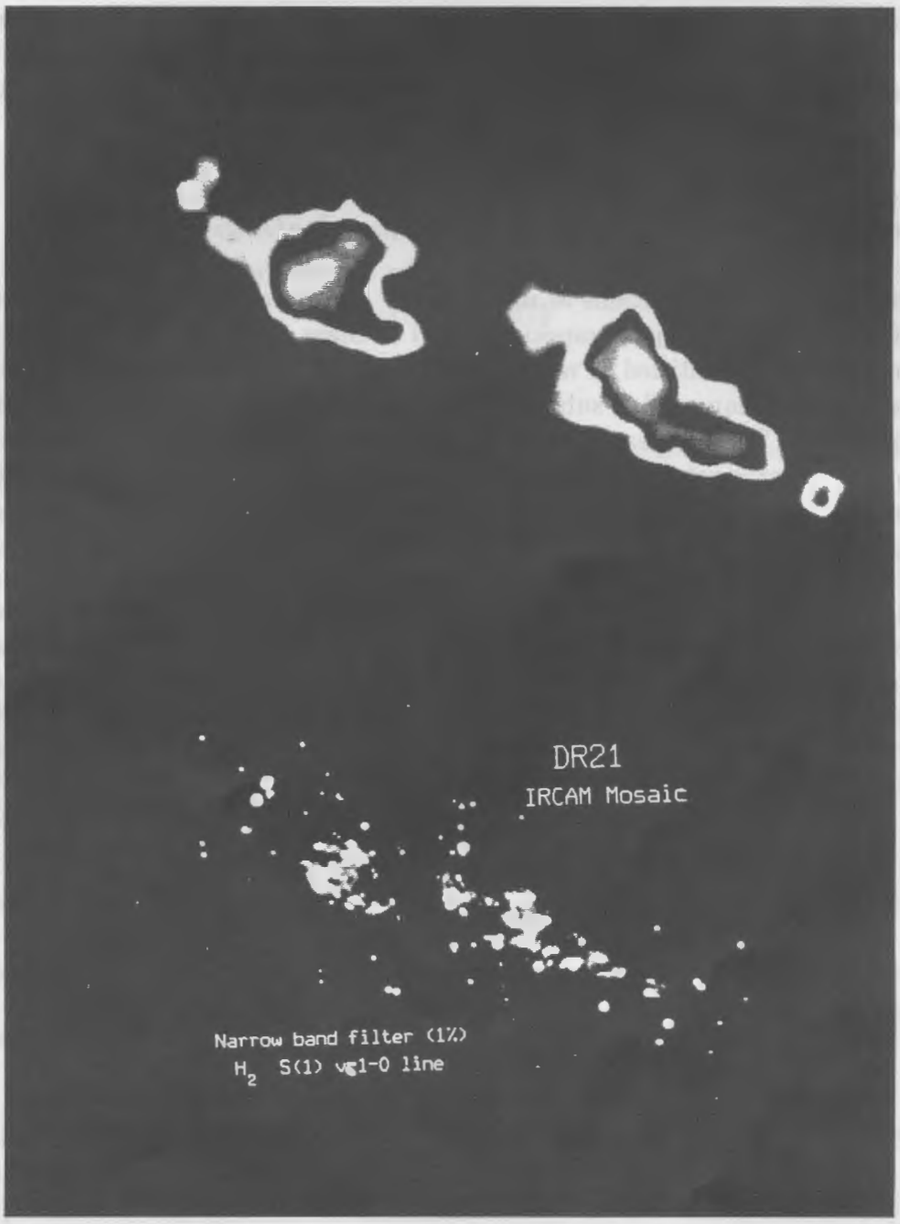

Figure 3: The star formation region DR21. These infrared pictures show the bi-polar flow as traced out by shocked molecular hydrogen emitting at 2.12 μm. The top picture was obtained by a single element detector with angular resolution 20 arcsecond, scanning across the field. The bottom picture, with angular resolution 1 arcsecond demonstrates the dramatic increase in resolution afforded by the development of infrared arrays. (UK Infrared Telescope, Royal Observatory, Edinburgh). SALT using adaptive optics techniques at 2 μm will provide a similar gain in resolution (i.e. to 0.1 arcsecond at $\lambda = 2\ \mu m$).

that South Africa can make, an intercomparison of the astronomical quality of the two sites, an evaluation of telescope design options, the requirements for the day 1 instrumentation, the control system and computing requirements, the steady state operations staff and cost implications, and the opportunities for international collaboration. This will be the main document in support of funding.

Acknowledgements

I acknowledge the contributions of many South African astronomers towards the development of the SALT project, especially Dr I S Glass of SAAO who in 1990 produced an influential report entitled "Proposal for a Large Telescope". In 1992 South African astronomers were requested to submit research proposals that required SALT and I thank all who replied. These research proposals form part of the detailed scientific case. Although the project is not funded yet it has received considerable support from the National Astronomy Facilities Board, the FRD Executive and the FRD Council.

Metallicity in Globular Clusters

V Pieters and W F Wargau
Department of Mathematics, Applied Mathematics and Astronomy, University of South Africa, P.O. Box 392, Pretoria, 0001

Abstract

The metallicities of most globular clusters must be found from indirect measures, calibrated by comparison with direct measures of metallicity obtained for nearby clusters. The quality of this calibration is therefore crucial. The calibration of Zinn and West has for more than a decade been used as the basis for most other calibrations. However, it may be that the alternative calibration by Pilachowski is more correct. Metallicities for 35 galactic globulars were redetermined using the Pilachowski calibration. Contrary to expectation, the metallicities of more metal rich clusters were not found to be reduced relative to the Zinn and West values. Rather, higher values were found for globular clusters in the middle range of Fe/H. Applied to M31 globulars, the Pilachowski calibration did not yield a lower mean metallicity as had been expected, nor did it eliminate the slight indication of a radial metallicity gradient.

1 Introduction

The subject of this talk formed part of a BSc Honours research project conducted during 1991. No new data were acquired for purposes of the study, but existing data was recalibrated.

2 Distinguishing characteristics of globular clusters

2.1 Spherical shape

Globular clusters are star clusters which are distinguished from open or galactic clusters by their spherical shape. This may not be their most important characteristic, but it is the first one which springs to mind and it is certainly no coincidence that it is also the characteristic from which this type of cluster takes its name.

2.2 Increasing density towards the centre

When viewed through a small telescope, another characteristic which is immediately noticeable is the increasing density towards the centre. Typically one sees a filamentary

galactocentric distance were to be confirmed, this would constitute supporting evidence for the above proposition.

3 Measurement of metallicity

3.1 Definition and measurement

The metallicity of an object is formally defined as

$$[Fe/H] = \log [Fe/H]_* - \log [Fe/H]_\odot$$

where Fe/H represents the number density of all the ions of iron, over the number density of hydrogen. Clearly this will always be a small fraction, making the logarithms negative. Anything which equals the solar metallicity will have a metallicity of 0,0 and progressively lower metallicities will be indicated by progressively more negative numbers.

Metallicities for close globulars are found from high dispersion spectroscopy of individual stars, followed by curve of growth analysis which gives n_r/n_H, in other words, the number density of the r-th ion of the element in question, over the number density of hydrogen.

However, high dispersion spectroscopy is only feasible in the case of globular clusters which are so close that individual stars may be studied with confidence. In order to determine the metallicity of clusters at greater distances, indirect indices - spectroscopic of photometric - must be found which can (1) be measured at these large distances and (2) be related to the results of the direct techniques in such a manner that a calibration relation is obtained. This then enables the metallicities of far-off clusters to be found. Of course the correctness of these findings depends critically on the quality of the calibration.

3.2 The scale of Zinn and West

Zinn (1980) used photoelectric photometry of the integral light of globular clusters in specific filter passbands to derive estimates of their metal abundance. Zinn's Q39 index was based on the argument that globular clusters can be ranked by metallicity on the basis of the amount of line blocking in the blue spectral region of their integrated spectra. The amount of line blocking in a particular wavelength interval can be measured photometrically by comparison with the continuum light from adjacent wavelength regions. For this purpose the light loss in the region around the strong H and K lines of CaII was chosen by Zinn. The success of the calibration of Q39 with [Fe/H] of course depends on the coupling of the abundances of Ca, etc, to the iron abundance. Q39 was calibrated by a linear least squares fit to smoothed values of [Fe/H], obtained from high-dispersion work. Twenty-five galactic globulars were used in this calibration which extended only to [Fe/H] = -0.36, the values for more metal-rich clusters being found from extrapolation of the line.

In a later paper Zinn and West (1984) used spectroscopy rather than photometry and found that the pseudo-equivalent widths of the CaI K line, G band and Mg1b lines correlated very well with each other and with Q39. So the relationships between Q39 and

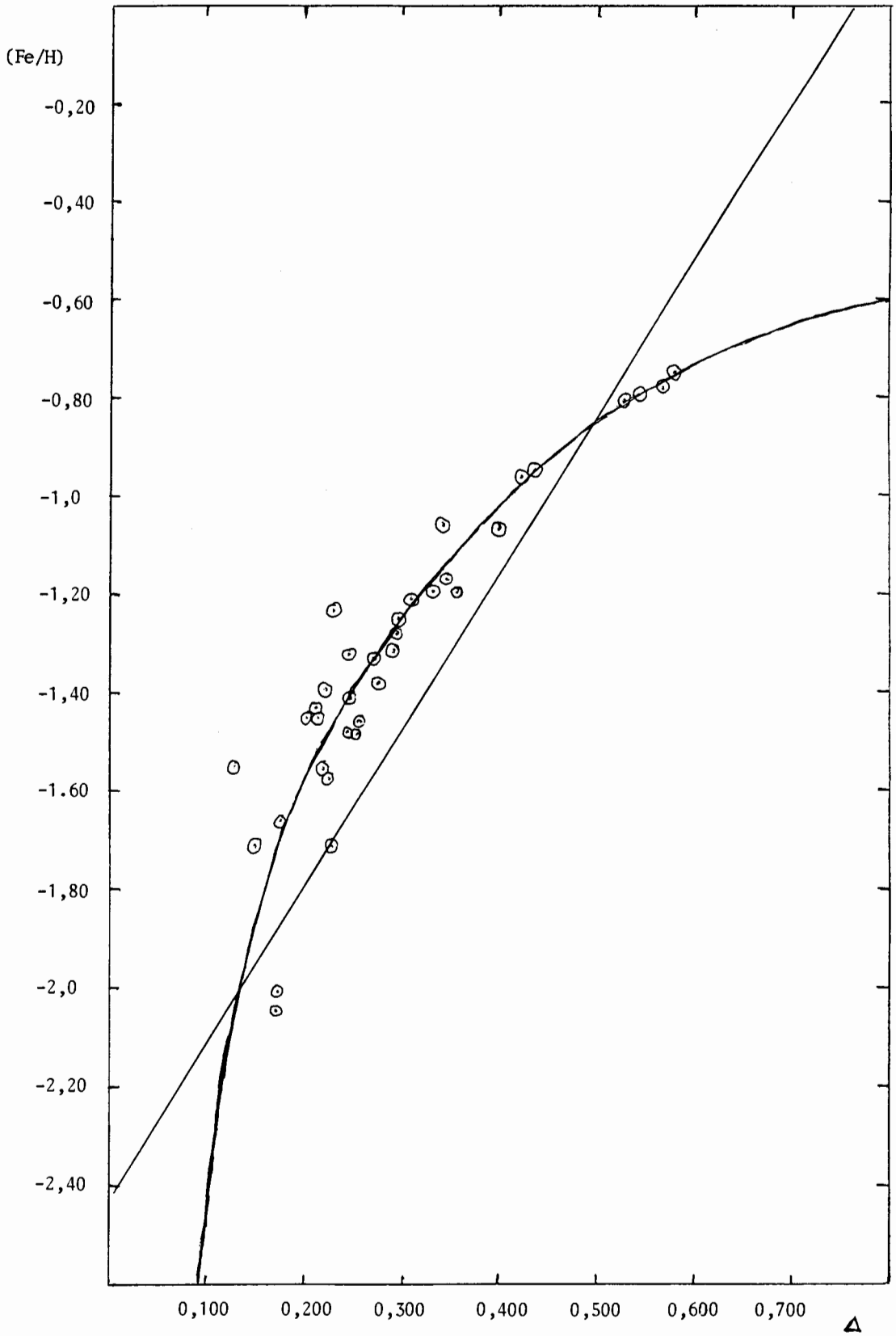

Figure 1: Calibration of [Fe/H] versus Δ using Pilachowski values, compared with the linear calibration relation of Zinn and West.

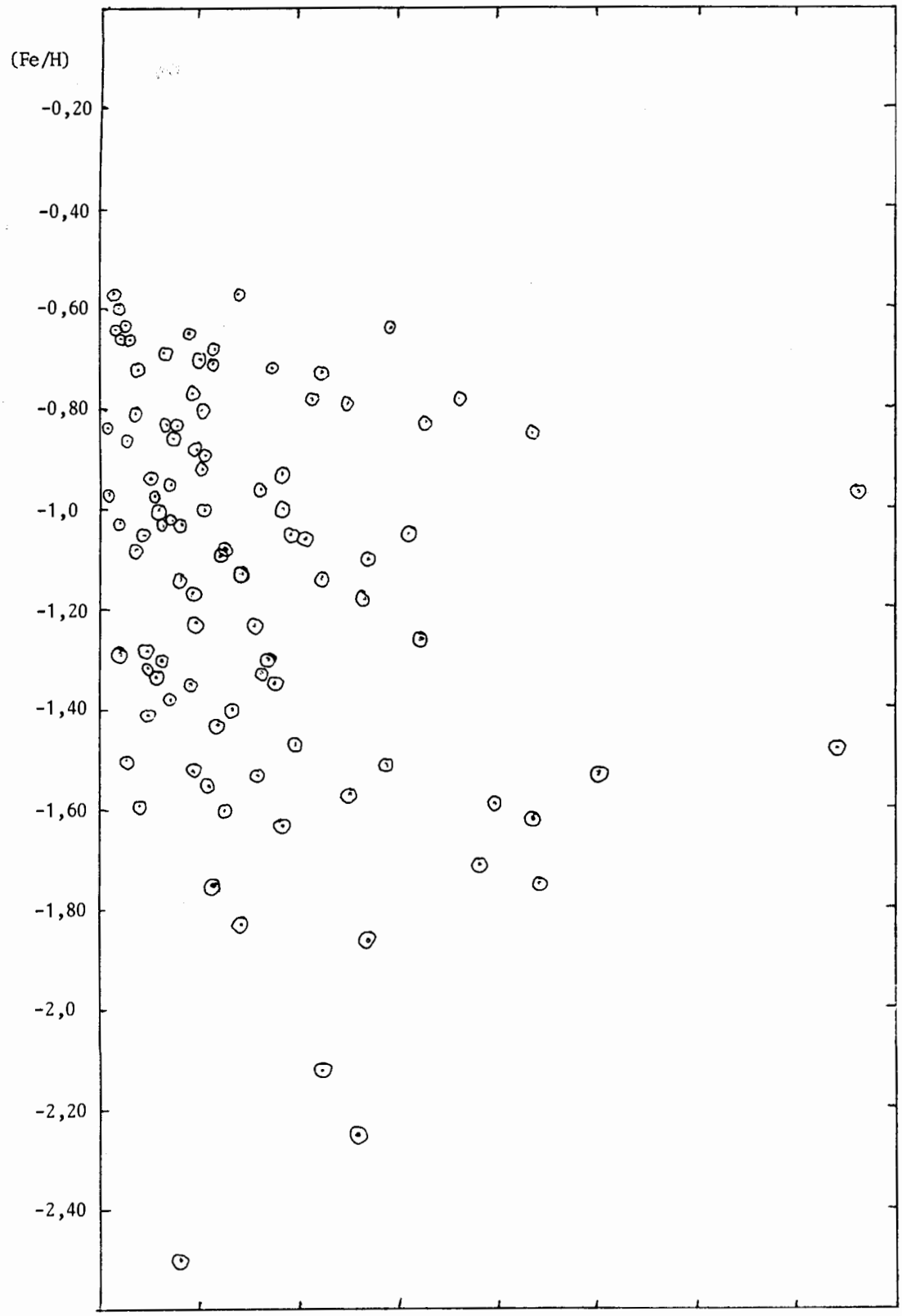

Figure 2: [Fe/H] versus galactocentric distance for M31 globular clusters.

the extreme values of metallicity were maintained, while the intermediate values were increased.

As the Δ index measurements for most of the M31 globular clusters had not been published, the two calibration curves were plotted on the same set of axes and the values of [Fe/H] according to the present calibration read off against the published values of [Fe/H] from Huchra et al. (1991), based on the Brodie and Huchra (1990) linear calibration relation.

The mean metallicity for M31 clusters was found to be [Fe/H] = -1.15 $\pm$ 0.39, which is in fact a slightly higher mean metallicity than found by Brodie and Huchra (1991) - because of the elevation in intermediate metallicity values.

The new metallicity values found for M31 globulars were also plotted against galactocentric distance (see Figure 2). It had been expected that the slight radial metallicity gradient found previously might disappear completely when the Pilachowski rather than the Zinn and West calibration was used. Although it was reduced, the indication for a metallicity gradient with galactocentric distance, did not disappear entirely. Thus the question of free-fall collapse of galaxies versus collapse in quasistatic equilibrium also still remains open from the point of view of metallicities of globular clusters.

Acknowledgments

We are grateful to Dr T Richtler of the University of Bonn, Germany, for his generous advice and many helpful discussions.

References

[1] Brodie, J. & Huchra, J., 1990, *Ap. J.*, **362**, 503.

[2] Brodie, J. & Huchra, J., 1991, *Ap.J.*, **379**, 157.

[3] Huchra, J., Brodie, J. & Kent, S., 1991, *Ap. J.*, **370**, 495.

[4] Pilachowski, C., 1984, *Ap. J.*, **281**, 614.

[5] Zinn, R., 1980, *Ap. J. S.*, **42**, 19.

[6] Zinn, R. & West, M., 1984, *Ap. J. S.*, **55**, 45.

The Solar Eclipse of June 1992 – what did we do? The Solar Eclipse of November 1994 – what will we do?

Jim Knight
Director, ASSA Solar Section

Abstract

We discuss the solar eclipse of the 30th June 1992 and the solar eclipse of the 3rd November 1994.

1 Introduction

This paper briefly looks at the following topics:
a) the Solar Eclipse of the 30th June 1992
- What did we do?
- What did we learn?
b) the Solar Eclipse of the 3rd November 1994
- What are its circumstances?

2 The Solar Eclipse of the 30th June 1992

2.1 What did we do before the eclipse?

Our first task, long before the eclipse, was to obtain the circumstances of the eclipse. With the aid of local astronomers and especially my counterpart in the United States, Peter Taylor, the details were assembled. The relevant details of this offshore event were then relayed to members of the Society via a paper presented at the first ASSA symposium held in Cape Town [1] and article in MNASSA[2].

We then had a dual task to tackle, first, that of organising an expedition and as the path of totality was off the Cape West coast, the only way to do this was by plane or boat. Unfortunately the necessary arrangements could not been made.

The second task was to organise events for the good partial eclipse that would be visible throughout Southern Africa. Each of the Society centres had some form of function or event planned. The Cape was the most favourably placed and the Planetarium there was in full swing. They prepared a special programme, an eclipse booklet and viewing sessions.

The Transvaal centre put on public viewing session at the City Hall and elsewhere. Many members also planned to have public and private viewing parties.

Due to the expected demand for Mylar the Solar Section contacted Roger Tuthill in the United States. Roger conducts expeditions to every Solar eclipse and had a large stock of Mylar for eclipse viewing that was left over from the previous eclipse over Hawaii, California and Mexico. We could obtain this Mylar in sufficient quantities and at a reduced price. Roger sent us samples, a video of the eclipse and a set of slides to use for our promotion of this event.

2.2 What did we do during the eclipse.

So, what did we do? Well, the ASSA centres did their thing, as did the Planetariums and several society members. The press and the TV had their usual field day and the eclipse was on the TV and in the papers.

Whilst little science could be done, it is of great interest and most encouraging to note that ASSA members were not prepared to just sit back, watch the show and say "gee - look at that!" Of their own initiative, a handful of members went ahead and did their own "science". A call was made to ASSA members after the eclipse and the following responded with reports. There were others, but they did not submit any details of their activities.

Sean Stanley Adams – Sean set up a camera at the Atlasville Observatory and photographed the eclipse every five minutes. These photos were to be used by the press and by HartRAO, who were doing radio maps and they wanted visual and photographic observations to supplement their data.

Tim Cooper – Tim set up a device at his office in Kempton Park to measure Solar Irradiance during the eclipse and to compare these results with those taken before the eclipse. Figure 1 illustrates the graph Tim obtained.

Mauritz Geyser – Mauritz also took photographs of the Sun and used these to calculate the percentage obstruction as observed in Pretoria. Figure 2 illustrates the graph Mauritz obtained.

Jim Knight – Visual observations, contact timings and Sunspot occultation timings were undertaken at the Atlasville Observatory.

Nico Kriek – Nico lives in Britstown and he submitted a useful set of accurate drawings, thus providing us with a detailed record of the eclipse as seen from deep in the Karoo.

Greg Roberts – Greg and two colleagues from SAAO took video recordings of the total eclipse from an aircraft over the South Atlantic[3].

Cliff Turk – Cliff took a very nice set of high quality photographs and these were later published by an overseas astronomy magazine.

HartRAO – The HartRAO/ASSA Solar section effort resulted in a set of correlated radio maps of the Sun during the partial eclipse.

The ASSA Transvaal Centre – The Transvaal centre had a large viewing session for the public in the middle of Johannesburg. The event attracted the press and got front page coverage together with one of the photographs taken by Sean Stanley Adams.

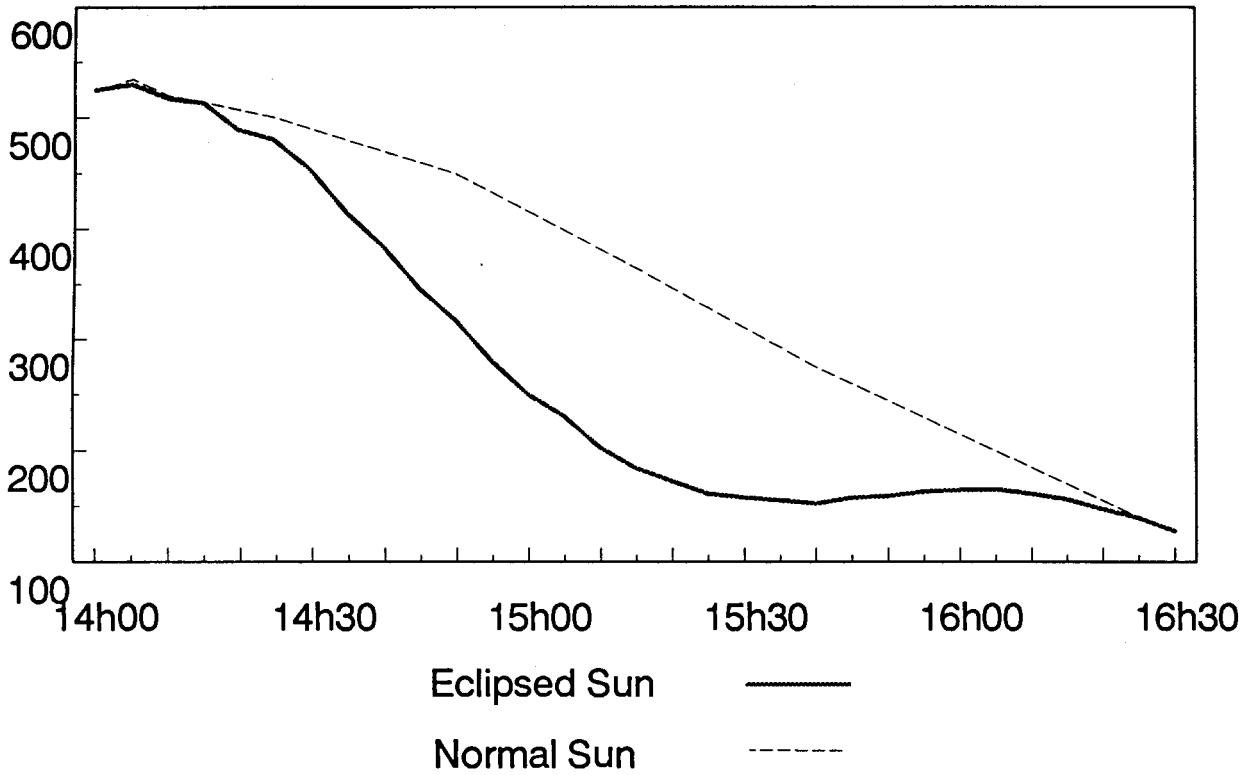

Figure 1: Solar Irradiance in W/m^2.

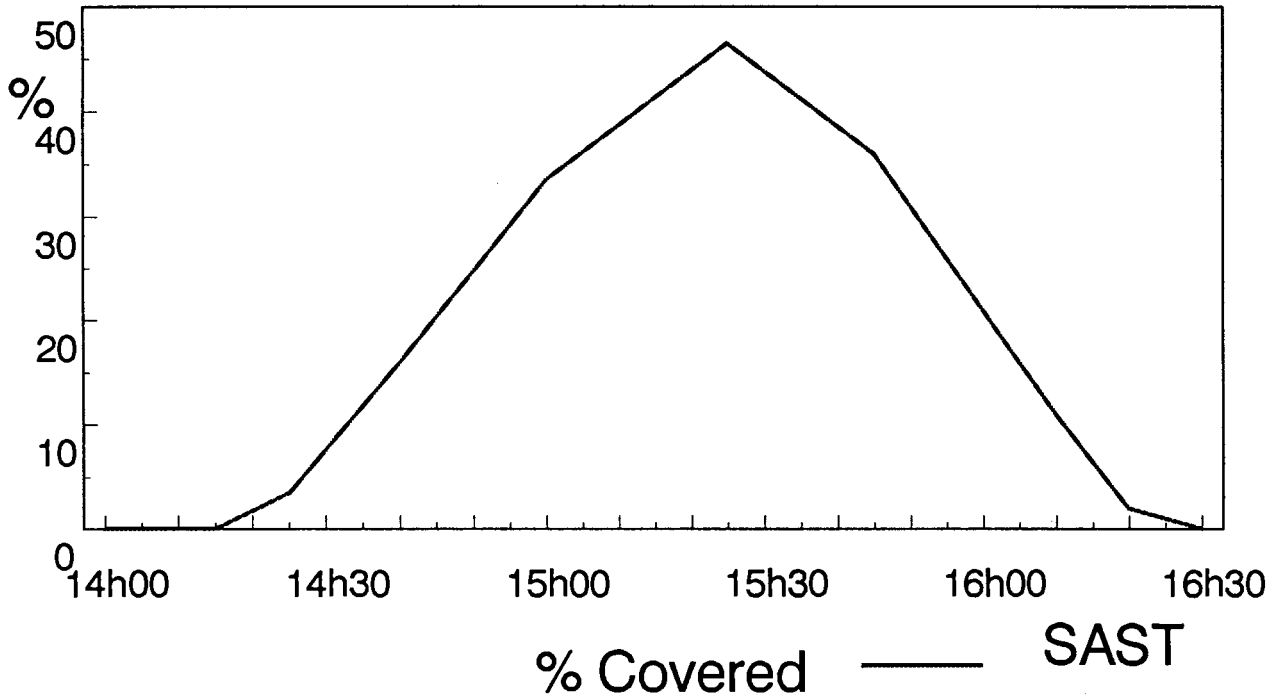

Figure 2: % Obstruction.

2.3 What did we learn?

a) The most stunning thing we learnt was that hardly anybody outside the amateur fraternity really took us seriously.
b) My plea at the ASSA conference in Cape Town for a co-ordinated effort did not succeed.
c) The society and the planetariums had no idea of the numbers involved. As a result, a week before the event we were inundated with requests for Mylar which was not available in sufficient quantities.

3 The Solar Eclipse of the 3rd of November 1994

3.1 What are its circumstances?

This will be the first eclipse since July 1991 to cross over land and passes over Central South America, the South Atlantic and ends off the Southern part of South Africa. Again, the eclipse is off shore for us – about 350 kilometres off the coast, where the path of totality will be about 130 km wide. The only other land that lies in the path of totality is Gough Island[4, 5]. Figure 3 illustrates the path of totality for this eclipse event.

Again the whole of Southern Africa will see a good partial eclipse. The best place to go will be Port Elizabeth which will have a spectacular 92% obstructed sun! Maximum eclipse will take place at about 17.15 SAST for Southern African stations.

The table below gives the obstruction figures for various centres.

Place	% Obstructed
Bloemfontein	74
Cape Town	88
Durban	81
Harare	36
Johannesburg	64
Kimberley	71
Port Elizabeth	92
Windhoek	42

November appears to offer reasonable weather prospects, at least in some areas. Offshore weather at this time has a mean cloud cover of 60%, but such clouds tend to have breaks, making a ship expedition promising, but wave heights could be a problem. The interior of South Africa has a mean cloud cover of 40 to 50% and the coastal areas between 50 and 60% at this time

This eclipse like the 1992 event, occurs in the afternoon, but it is going to take place later in the day and as a result, the sun will be much lower in the sky. Distant cloud will therefore play an important role in observing this eclipse. The duration of totality is also shorter than the last event. At $-40°$ latitude and $0°$ longitude for example, the Sun will be at an altitude of 43 degrees and totality will last for just over three and a half minutes at 16.45 SAST. At 17.45 SAST, at $-33°$ latitude and $41°$ E longitude, the sun will only be at an altitude of 5 degrees and totality will last just over two minutes.

Figure 3: The path of totality, eclipse of November 3, 1994.

3.2 What will we do for this eclipse?

As this eclipse crosses South America, we can anticipate that eclipse chasers and observers will flock to that part of the world and that they will ignore any ship or plane expeditions from South Africa. Most of us will not have the resources to travel to South America, so we need to organise expeditions for our people. We need to try to get both ship and air expeditions on the go and to get all the centres and planetariums to organise partial eclipse programmes. We need to build on the experiences and mistakes that we made with the 1992 eclipse!

The solar section's plan of action is as follows:

a) Convene a representative eclipse co-ordination and planning committee.

b) Both ship and plane expeditions will be considered.

c) Partial eclipse viewing programmes will be conducted by the various centres.

d) Members will continue their individual observation programmes.

e) Contact will be maintained with professional astronomers and the directors of the planetariums.

References

[1] "The Total Solar Eclipse of Tuesday 30 June 1992", MNASSA Vol. 51, No.'s 5 & 6, June 1992

[2] "Letter to the Editor," MNASSA, Vol. 52, No's 1 & 2, February 1993

[3] "The 30 June Eclipse viewed from a Boeing 707", MNASSA Vol. 51, No.'s 9 & 10, October 1992

[4] "Solar Eclipses, 1991 - 2000", United States Naval Observatory Circular No. 170, November 1986

[5] "Total Solar Eclipse of 3 November 1994", NASA Reference Publication 1318, October 1993